

National Institute of Technology Trichy
Department of Electrical and Electronics Engineering



A novel self-consistent model based filter design for the improved performance of 3-phase PLLs for phase tracking under grid imperfections

Project Thesis (B.Tech.)

Sambhav R Jain
Pradhyumna Ravikirthi



A novel self-consistent model based filter design for the improved performance of 3-phase PLLs for phase tracking under grid imperfections

Project Thesis (B.Tech.)

Sambhav R Jain ¹

Pradhyumna Ravikirthi ²

Supervising Professor: **Prof. Dr. C Nagamani**
Working period: **December 2011 - May 2012**

¹sambhav.eee@gmail.com

²pradhyumnarao@gmail.com

Abstract

Modern power system networks are highly interconnected for optimal use of the available resources such as thermal, hydro and nuclear, to serve the industrial and domestic loads located near or far. For the purpose of providing a reliable and controllable supply to the consumers, flexible ac transmission controllers (FACTS), which are essentially power electronic controllers, are also incorporated in strategic locations of the network. Further, the networks include distributed generation (DG) units based on local, renewable energy sources such as wind, solar, geothermal etc. In this scenario, continuous, accurate and dynamic synchronization of the FACTS controllers or the DG units with the overall complex network is of utmost importance for the smooth and stable operation of the overall system.

Synchronization is the process of tracking the grid frequency and phase dynamically with accuracy, irrespective of the changes in the grid voltage conditions. Ideally, the grid voltage can be considered to be purely sinusoidal in nature with a constant frequency and amplitude for all time. However, this is far from the existing situation, owing to the wide proliferation of power converters connected to the grid. The presence of harmonics, unbalanced voltages, frequency excursions, phase jumps and sags or swells of the voltage are some of the features of the increased burden on the grid. On the other hand, disconnection of any DG unit due to disturbed grid conditions is not acceptable from the point of view of stable network operation. Thus there is an urgent need for finding improved techniques for a stable, robust, fast and accurate phase lock loop (PLL) which can provide synchronization of the interfaced power converter under any grid condition.

A conventional PLL called the synchronous reference frame PLL (SRF PLL) forms the basis of the study of PLLs for tracking the 3-phase grid. SRF PLL can do what any basic PLL should do; track changes in frequency and phase. However, it requires ideal grid conditions for accurate tracking. Many PLL schemes have evolved since then, which can track even under imperfect grid conditions. The aim is to filter the unwanted components present in the grid voltage and utilize only the positive sequence component of the fundamental voltage for tracking. Hence most of these schemes are modifications or improvisations over SRF PLL. This along with three other PLL schemes, namely the Decoupled Double Synchronous Reference Frame (DDSRF) PLL [1], the Dual Second Order Generalized Integrator (DSOGI) based PLL [2] and the Multiple-Complex Coefficient-Filter (MCCF) based PLL [3] are studied in detail and modelled in Simulink[®]. A software tool is made to evaluate and compare the above PLLs and henceforth derive logical inferences.

Speed is an important parameter that can be used to measure PLL performance. The dynamic response of a PLL, to changes in the grid, needs to be optimized for reliable operation. In this work, a new self-consistent model based method is proposed, which is aimed at improving the design of the loop filter used in SRF PLL. It focuses on quantizing the error while optimizing the damping ratio, hence yielding an optimum dynamic performance which adheres

to the user criteria. Since many PLL schemes use SRF PLL as their fundamental block, this design method is applicable to those schemes as well. To enhance the feasibility of practical implementation, a comprehensive 3D lookup table is built which gives the optimized values of loop filter parameters for different sets of grid disturbances.

Finally, the operation of SRF PLL is experimentally verified using the MSP430TM by Texas Instruments. The implemented SRF PLL (designed for optimum dynamic performance) is subjected to a frequency excursion and its ability to track this disturbance is established.

Keywords: SRF PLL, grid imperfections, self-consistent model, loop filter design, 3D lookup table

Contents

1. Introduction to PLL	11
1.1. Need for Phase Tracking	11
1.2. Expectation of an ideal 3-phase PLL	11
1.3. Past developments and current trends	12
1.4. Scope of the present work	12
1.5. Contribution from our work	13
1.6. Organization of the report	13
2. Basics of Reference Frame Theory	15
2.1. Transformation to an Arbitrary Reference Frame	15
2.2. Transformation to a Stationary Reference Frame (Clarke Transformation)	16
2.3. Transformation to a Synchronous Reference Frame (Park Transformation)	17
2.4. Transformation between reference frames	18
2.5. Importance of Reference Frame Transformations	19
3. Conventional SRF PLL	20
3.1. Case 1: When the grid is balanced	20
3.1.1. The linear model	21
3.1.2. Modelling a voltage controlled oscillator (VCO)	22
3.1.3. When in lock	22
3.1.4. Importance of separate transformations	23
3.2. Case 2: When the grid voltage is unbalanced	23
3.2.1. The linear model	24
3.3. Case 3: When the grid is polluted with harmonics	25
3.3.1. The linear model	26
3.4. The two design aspects of a PLL	26
3.4.1. Filtering performance of the SRF PLL	27
3.4.2. Dynamic performance of the SRF PLL	34
3.5. Wiener optimization method	34
4. Design and Optimization of the SRF PLL	36
4.1. Input to the SRF PLL	38
4.1.1. Case 1: $\delta < 1$	39
4.1.2. Case 2: $\delta > 1$	42
4.1.3. Case 3: $\delta = 1$	47
4.2. Analytical proof for the sluggish response in the case $\delta > 1$	50
4.3. Analysis for a step change in frequency	53
4.3.1. Requirements to be met by the PI loop filter	53
4.3.2. Optimum design of δ and ω_n	54

Contents

4.4.	Analysis for a step change in frequency with phase jump	59
4.4.1.	Optimum design of δ and ω_n	60
4.4.2.	The Self-Consistent Model	71
4.4.3.	Loop Filter Parameters and the 3D Lookup Table	71
4.5.	Conclusions	75
5.	Other PLLs in literature	76
5.1.	Why go for other PLL schemes	76
5.2.	Decoupled Double Synchronous Reference Frame PLL (DDSRF PLL)	76
5.2.1.	Two separate Park transformations	77
5.2.2.	Decoupling network	78
5.3.	Dual Second Order Generalized Integrator based PLL (DSOGI PLL)	80
5.3.1.	Second Order Generalized Integrator for Quadrature Signals Generation (SOGI-QSG)	82
5.3.2.	Positive Sequence Detector using a dual SOGI-QSG	83
5.4.	Multiple-Complex Coefficient-Filter based PLL (MCCF PLL)	84
5.4.1.	A basic CCF	84
5.4.2.	Building a CCF	86
5.4.3.	MCCF structure	87
6.	Simulation Models	89
7.	Results and Discussions	95
7.1.	Results through the Wiener method	95
7.2.	Comparisons between the Wiener method and the proposed method	99
8.	Experimentation	104
8.1.	Implementation of Clarke and Park Transformations	105
8.2.	Implementation of the PI loop filter as a digital filter	106
8.3.	Implementation of VCO+Feedback	107
8.4.	Outputs using the PWM module	108
8.5.	Results	108
9.	Conclusions	113
10.	Acknowledgements	115
Bibliography		116
Appendices		
A. Mathematical concepts		118
A.1.	L' Hospital rule	118
A.2.	Properties of a cubic equation	118
A.3.	Newton Raphson iterative scheme	119
A.4.	Bilinear Transformation (BLT)	119

Contents

B. Hyperbolic functions	121
B.1. Properties	122
B.2. Identities	122
B.3. Inverse Hyperbolic Functions	123
C. Mathematical Simplifications	126
C.1. Section 2.1 Equation (2.4) to (2.5)	126
C.2. Section 3.3 Equation (3.24) to (3.25)	127
C.3. Section 3.4.1.1 Equation (3.50) to (3.51)	128
C.4. Section 4.1.2 Equation (4.79) to (4.80)	129
C.5. Section 4.1.3 Equation (4.103) to (4.104)	129
C.6. Section 4.3.2 Equation (4.136) to (4.137)	130
D. Error band as a function of Damping ratio	131
E. Nature of $f(\delta)$ in $(0,1)$ when $E'(0) > 0$	133
F. Cardan's analytical method to solve Cubic equations	136
G. Errata	145

List of Figures

2.1. 3-phase balanced grid voltages transformed to an arbitrary reference frame	16
2.2. 3-phase balanced grid voltages transformed to the stationary and synchronous reference frames	18
3.1. Conventional SRF PLL	20
3.2. Linearised model of SRF PLL in time domain	21
3.3. A simple VCO block	22
3.4. VCO equivalent model	22
3.5. SRF PLL linear model	27
3.6. Detailed Bode magnitude plot	30
3.7. Approximate Bode magnitude plot	32
3.8. The Bode magnitude plot for different ω_n	33
3.9. The Bode magnitude plot for different δ	34
4.1. Linearised model of SRF PLL in s-domain	36
4.2. Effect of frequency step	38
4.3. Effect of phase jump	38
4.4. Combined effect	38
4.5. Error w.r.t. time for the case $\delta < 1$	42
4.6. Error w.r.t. time for the case $\delta > 1$	46
4.7. Error w.r.t. time for the case $\delta = 1$	49
4.8. Sluggish response for the case $\delta \geq 1$	51
4.9. Design specifications	53
4.10. Lookup table for Approach 1	57
4.11. Lookup table for Approach 2	58
4.12. Error w.r.t. time for $\Delta\omega_{step} = 20\pi \text{ rad s}^{-1}$ and $\phi = 0.1 \text{ rad}$	60
4.13. Design specifications	61
4.14. Variation of error band with δ , sub-possibility 1	68
4.15. Variation of error band with δ , sub-possibility 2	69
4.16. Variation of error band with δ , possibility 2	70
4.17. The Self-Consistent Model	72
4.18. 3D lookup table for the optimised value of damping ratio, δ	73
4.19. 3D lookup table for the optimised value of natural frequency, ω_n	73
4.20. 3D lookup table for the optimised value of proportional gain, k_p	74
4.21. 3D lookup table for the optimised value of integral gain, k_i	74
4.22. 3D lookup table for the optimised value of time constant, τ	75
5.1. Decoupling cells used in the decoupling network	78
5.2. Decoupling network	79

List of Figures

5.3. SOGI - Quadrature Signals Generator	82
5.4. Bode plots for SOGI - QSG	83
5.5. DSOGI-QSG with Positive Sequence Calculator	83
5.6. Frequency response of Real and Complex Coefficient Filters	85
5.7. Complex coefficient filter	87
5.8. MCCF structure	88
6.1. Simulink model of SRF PLL	90
6.2. Simulink model of DDSRF PLL	90
6.3. Simulink model of DSOGI PLL	91
6.4. Simulink model of MCCF PLL	91
6.5. The grid simulator used to create grid imperfections	92
6.6. Complete Simulink model for all the PLL schemes	93
7.1. SRF PLL under frequency excursion	96
7.2. Phase error of the four PLLs	97
7.3. Comparison of error between the Wiener method and the proposed method . .	100
7.4. Comparison of the error bands for three cases of δ	100
7.5. Comparison of phase error in SRF PLL	101
7.6. Comparison between the Wiener method and the proposed method	102
8.1. MSP430 overview	105
8.2. Op-amp based positive clamper	106
8.3. PWM mode in the MSP430	108
8.4. SRF PLL tracking the 3-phase grid voltages at 50 Hz	109
8.5. SRF PLL during an LG fault	109
8.6. SRF PLL under frequency excursion with voltage swell	111
8.7. Experimental Setup	112
B.1. Hyperbolic sine and cosine functions	121
E.1. Variation of $f(\delta)$ with damping ratio in the interval $[0, 1]$	133
F.1. A cubic function $f(y)$ with three real roots	143

List of Tables

4.1. Comparison of error in the three cases of damping ratio δ	50
4.2. Comparison of the three approaches	56
4.3. Approaches 1 and 2 are not the best	59
4.4. Choice of an optimum damping ratio, δ	70
G.1. Choice of an optimum damping ratio, δ	145

1. Introduction to PLL

1.1. Need for Phase Tracking

In the past two decades, non-linear loads such as high voltage direct current transmission (HVDC) and variable speed ac drives which adopt six-pulse power converters cause significant power quality contamination of electrical distribution systems [4]. This is because these devices inject characteristic harmonics which pollute the grid.

There has been a rapid proliferation of DG units in electric networks [5]. A converter-interfaced DG unit, a wind generator unit or a photovoltaic (PV) unit for instance, requires accurate converter synchronization even under polluted environment. Moreover, DG units can have better ride-through capability (in case of faults) only if the fundamental voltage of the utility is tracked accurately.

Flexible ac transmission system (FACTS) devices are used to improve the energy transmission efficiency of transmission lines and the quality of voltage waveforms. There has been a lot of development in this field and many FACTS devices such as the static synchronous compensator (STATCOM), the thyristor controlled series capacitor (TCSC) and the unified power flow controller (UPFC) etc. have been practically implemented [6, 7, 8]. The stable performance of the FACTS devices necessitates proper synchronization of these power converters with the grid.

Other than DG units and FACTS devices, there are many electric systems which require grid synchronization and have not been discussed here. In general, synchronization with the grid is a necessity for the stable and smooth operation of an interfaced auxiliary source. The synchronization is done with respect to the phase angle of the voltage (or current) signals of the grid. But these signals used for synchronization are corrupted by harmonics, voltage unbalance, voltage sag/swells, phase angle jumps and frequency deviations [9, 10, 11]. Hence an efficient phase tracking algorithm is required which can track the phase angle of the grid even under polluted utility conditions.

1.2. Expectation of an ideal 3-phase PLL

Ideally, a phase lock loop must have the following two characteristics:

- (i) Ability to adaptively track the phase angle and frequency of the utility voltage even under

1. Introduction to PLL

- unbalanced and distorted conditions
- (ii) Ability to accurately measure the positive sequence fundamental component of the utility voltage

A lot of research is being done on PLLs to achieve a near ‘ideal’ PLL. The majority of 3-phase PLLs in literature [1, 2, 3, 12] are modifications or improvisations over a basic PLL scheme which is known as the synchronous reference frame PLL (SRF PLL). Hence the understanding of the conventional SRF PLL is necessary for the understanding of subsequent chapters on PLLs.

1.3. Past developments and current trends

The use of PLLs was seen as early as in the 1920s. However, the theoretical description of a PLL was well established only in the late 1970s. From then on, with the advent of integrated circuits (ICs), PLL became an indispensable part of any modern communication system [13]. In the field of power systems, where grid synchronization is a must for stability, SRF PLL was one of the important milestones in phase tracking, which stimulated (and is still stimulating) further developments in this field.

SRF PLL can track changes in frequency and phase as long as the voltage fed to it is devoid of harmonics and voltage unbalance. But as the grid voltages are compromised in the form of such imperfections, SRF PLL (as such) can no longer be used for reliable phase tracking. At present, there are improved PLLs, which can be viewed as modifications on SRF PLL, to deal with grid imperfections, such as DDSRF, DSOGI and MCCF PLL. The augmented stages in each of these aim at filtering out the positive sequence component of the fundamental grid voltage. At the same time, the dynamic performance is an important aspect that needs urgent attention.

1.4. Scope of the present work

In this work, the existing PLL schemes, namely SRF, DDSRF, DSOGI and MCCF PLL are analysed in depth. Each of these schemes are mathematically modelled on a common convention to enable comparison. These models are simulated for different grid disturbances such as harmonics, voltage unbalance, frequency excursion and phase jump. A software tool (applet) is developed which allows comparisons in an extensive manner. The applet is generalized to accommodate any number of additions of new PLL schemes. The design of loop filter parameters is identified as an important step for fast phase tracking, and the work is extended towards developing a novel technique to achieve this. Moreover, a working model of SRF PLL is implemented on a practical setup.

1. Introduction to PLL

1.5. Contribution from our work

A unique self-consistent model based loop filter design is proposed to enhance the dynamic performance of SRF PLL and the modified PLLs which are based on SRF PLL. A 3D lookup table that contains the optimized design of the loop filter parameters for all practical ranges of frequency excursion ($\Delta\omega_{step}$) and phase jump (ϕ), is obtained as an end-result of the self-consistent model.

1.6. Organization of the report

This report is organized in the following manner:

- a) Chapter 2 presents the basics of reference frame theory which is a pre-requisite to the understanding of SRF PLL and the modified PLLs. A common convention is established in this chapter for comparison.
- b) Chapter 3 contains an introduction to the fundamental SRF PLL followed by its detailed analysis. A linear model of SRF PLL is obtained under different grid conditions. The dynamic performance and filtering characteristic of SRF PLL is also discussed in this chapter. The present method of loop filter design, namely the Wiener optimization method is briefly explained here.
- c) Chapter 4 elaborates on the dynamic performance of SRF PLL for different cases of damping ratio. The proposed self-consistent model based technique to design the loop filter optimally is presented in this chapter. A 3D lookup table is obtained for the optimized design in a range of grid disturbances.
- d) Chapter 5 discusses three modified PLL schemes from literature, explaining the basis behind their development.
- e) Chapter 6 presents the simulation background that is used to support the analysis and study of the modified PLLs in literature.
- f) Chapter 7 contains the extensive plots for various comparisons that are made. The proposed design is compared with the existing design and light is shed on the significant improvement in the dynamic performance of SRF PLL through the proposed method.
- g) Chapter 8 explains the steps involved in implementing SRF PLL on a practical setup, and verifies the tracking capability of SRF PLL under certain imperfections.
- h) Chapter 9 concludes this report.

1. Introduction to PLL

At any juncture, if the mathematical steps involved in arriving at the result are complex, and if their absence does not hinder the coherence of this report, then a reference to the Appendices is cited and it is elaborately explained therein. Similarly, if certain mathematical background is required to understand a topic which does not fall in the scope of the chapter, it is explained in the Appendices and a reference is cited.

2. Basics of Reference Frame Theory

In this chapter, the basics of reference frame theory are presented, which are required to understand the further chapters on PLLs. Different conventions are adopted in literature for the explanation of reference frame theory. The convention that is followed throughout this report is presented in this chapter.

Reference frame theory is a general theory which is used to convert a set of quantities from its own frame to another reference frame of interest for easy mathematical manipulation. Since our objective is phase-locking for grid synchronization, the quantities of interest are the phase voltages of the grid. Hence in this chapter, reference frame theory specific to grid phase voltages is considered.

A balanced set of 3-phase grid voltages can be represented by

$$\begin{cases} v_a = V_m \cos \theta_{ef} \end{cases} \quad (2.1a)$$

$$\begin{cases} v_b = V_m \cos \left(\theta_{ef} - \frac{2\pi}{3} \right) \end{cases} \quad (2.1b)$$

$$\begin{cases} v_c = V_m \cos \left(\theta_{ef} + \frac{2\pi}{3} \right) \end{cases} \quad (2.1c)$$

where V_m is the peak value and θ_{ef} is the phase angle of the grid phase voltage.

2.1. Transformation to an Arbitrary Reference Frame

A transformation of 3-phase voltages to an arbitrary reference frame, rotating at an arbitrary angular speed ω , is given by

$$\begin{bmatrix} v_q \\ v_d \\ v_0 \end{bmatrix} = \frac{2}{3} \begin{bmatrix} \cos \theta & \cos(\theta - \frac{2\pi}{3}) & \cos(\theta + \frac{2\pi}{3}) \\ \sin \theta & \sin(\theta - \frac{2\pi}{3}) & \sin(\theta + \frac{2\pi}{3}) \\ \frac{1}{2} & \frac{1}{2} & \frac{1}{2} \end{bmatrix} \begin{bmatrix} v_a \\ v_b \\ v_c \end{bmatrix} \quad (2.2)$$

where v_q, v_d and v_0 are the transformed voltages in the arbitrary reference frame and

$$\omega = \frac{d\theta}{dt} \quad (2.3)$$

2. Basics of Reference Frame Theory

When the grid is perfectly balanced, $v_a + v_b + v_c = 0$; hence the v_0 component vanishes. The transformation in (2.2) thus reduces to

$$\begin{bmatrix} v_q \\ v_d \end{bmatrix} = \frac{2}{3} \begin{bmatrix} \cos \theta & \cos(\theta - \frac{2\pi}{3}) & \cos(\theta + \frac{2\pi}{3}) \\ \sin \theta & \sin(\theta - \frac{2\pi}{3}) & \sin(\theta + \frac{2\pi}{3}) \end{bmatrix} \begin{bmatrix} v_a \\ v_b \\ v_c \end{bmatrix} \quad (2.4)$$

On substituting the 3-phase grid voltages from (2.1) into (2.4) (see Appendix C.1), we get

$$\begin{bmatrix} v_q \\ v_d \end{bmatrix} = \begin{bmatrix} V_m \cos(\theta_{ef} - \theta) \\ -V_m \sin(\theta_{ef} - \theta) \end{bmatrix} \quad (2.5)$$

It can be noted that v_q and v_d are orthogonal to each other as is schematically represented in figure 2.1 showing the 3-phase balanced voltages (v_a, v_b and v_c) and the transformed voltages (v_q and v_d).

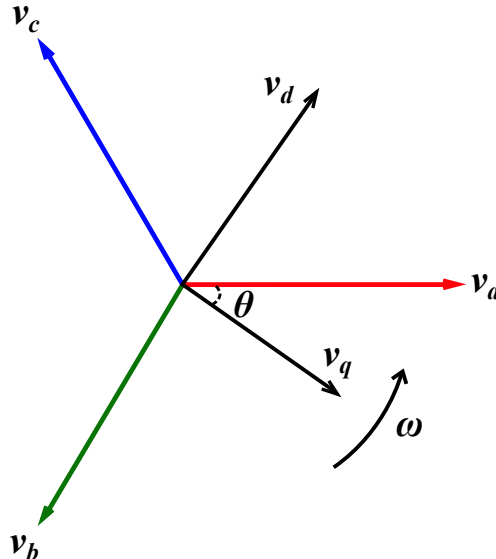


Figure 2.1.: 3-phase balanced grid voltages transformed to an arbitrary reference frame

2.2. Transformation to a Stationary Reference Frame (Clarke Transformation)

Let v_β, v_α and v_0 denote the transformed voltages in the stationary reference frame. Since transformation to a stationary reference frame is desired, the angular speed ω is zero. It follows from (2.3) that the phase angle θ is a constant. For mathematical simplicity, we choose θ to be zero; hence arriving at the Clarke Transformation. On substituting $\theta = 0$ in (2.2) to (2.5),

2. Basics of Reference Frame Theory

we obtain

$$\begin{bmatrix} v_\beta \\ v_\alpha \\ v_0 \end{bmatrix} = \frac{2}{3} \begin{bmatrix} 1 & -\frac{1}{2} & -\frac{1}{2} \\ 0 & -\frac{\sqrt{3}}{2} & \frac{\sqrt{3}}{2} \\ \frac{1}{2} & \frac{1}{2} & \frac{1}{2} \end{bmatrix} \begin{bmatrix} v_a \\ v_b \\ v_c \end{bmatrix} \quad (2.6)$$

In case of perfectly balanced 3-phase voltages, (2.6) reduces to

$$\begin{bmatrix} v_\beta \\ v_\alpha \end{bmatrix} = \frac{2}{3} \begin{bmatrix} 1 & -\frac{1}{2} & -\frac{1}{2} \\ 0 & -\frac{\sqrt{3}}{2} & \frac{\sqrt{3}}{2} \end{bmatrix} \begin{bmatrix} v_a \\ v_b \\ v_c \end{bmatrix} \quad (2.7)$$

$$= \begin{bmatrix} V_m \cos \theta_{ef} \\ -V_m \sin \theta_{ef} \end{bmatrix} \quad (2.8)$$

2.3. Transformation to a Synchronous Reference Frame (Park Transformation)

In this case the transformation is done to a reference frame which rotates at synchronous speed ($\omega = \omega_e$). i.e., $\theta = \theta_e$.

Let v_q^e , v_d^e and v_0^e denote the transformed voltages in the synchronous reference frame. Substituting $\theta = \theta_e$ in (2.2) to (2.5), we obtain

$$\begin{bmatrix} v_q^e \\ v_d^e \\ v_0^e \end{bmatrix} = \frac{2}{3} \begin{bmatrix} \cos \theta_e & \cos(\theta_e - \frac{2\pi}{3}) & \cos(\theta_e + \frac{2\pi}{3}) \\ \sin \theta_e & \sin(\theta_e - \frac{2\pi}{3}) & \sin(\theta_e + \frac{2\pi}{3}) \\ \frac{1}{2} & \frac{1}{2} & \frac{1}{2} \end{bmatrix} \begin{bmatrix} v_a \\ v_b \\ v_c \end{bmatrix} \quad (2.9)$$

Under balanced conditions of the grid, (2.9) reduces to

$$\begin{bmatrix} v_q^e \\ v_d^e \end{bmatrix} = \frac{2}{3} \begin{bmatrix} \cos \theta_e & \cos(\theta_e - \frac{2\pi}{3}) & \cos(\theta_e + \frac{2\pi}{3}) \\ \sin \theta_e & \sin(\theta_e - \frac{2\pi}{3}) & \sin(\theta_e + \frac{2\pi}{3}) \end{bmatrix} \begin{bmatrix} v_a \\ v_b \\ v_c \end{bmatrix} \quad (2.10)$$

$$= \begin{bmatrix} V_m \cos(\theta_{ef} - \theta_e) \\ -V_m \sin(\theta_{ef} - \theta_e) \end{bmatrix} \quad (2.11)$$

Figure 2.2 shows the 3-phase voltages (v_a , v_b and v_c) transformed to the stationary reference frame (v_β and v_α) and the synchronous reference frame (v_q^e and v_d^e) under balanced grid conditions.

2. Basics of Reference Frame Theory

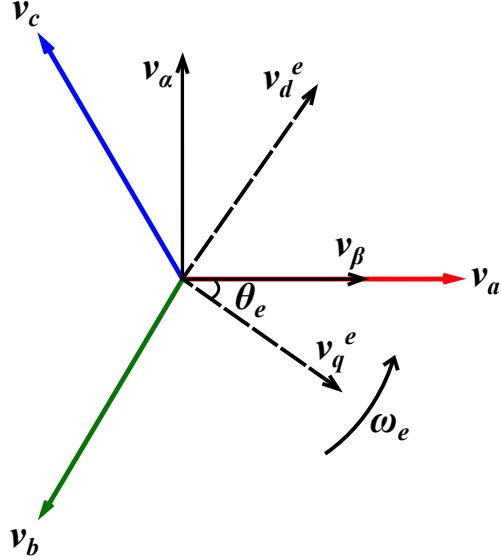


Figure 2.2.: 3-phase balanced grid voltages transformed to the stationary and synchronous reference frames

2.4. Transformation between reference frames

Consider a transformation of a set of voltages to an arbitrary reference frame x . Let the transformation matrix be denoted as \mathbf{K}^x . Thus we obtain

$$\mathbf{v}_{qd0}^x = \mathbf{K}^x \mathbf{v}_{abc} \quad (2.12)$$

Now consider a transformation to another arbitrary reference frame y , the transformation matrix for which is denoted as \mathbf{K}^y . Hence

$$\mathbf{v}_{qd0}^y = \mathbf{K}^y \mathbf{v}_{abc} \quad (2.13)$$

It is often useful to transform a set of quantities from one reference frame to another; for instance, transforming a set of voltages from a stationary reference frame to a synchronously rotating reference frame. In general, consider a transformation from reference frame x to reference frame y . From (2.12) we have

$$\mathbf{v}_{abc} = (\mathbf{K}^x)^{-1} \mathbf{v}_{qd0}^x \quad (2.14)$$

Substituting (2.14) into (2.13) yields

$$\mathbf{v}_{qd0}^y = \mathbf{K}^y (\mathbf{K}^x)^{-1} \mathbf{v}_{qd0}^x \quad (2.15)$$

Hence the final transformation can be expressed as

$$\mathbf{v}_{qd0}^y = {}^x \mathbf{K}^y \mathbf{v}_{qd0}^x \quad (2.16)$$

2. Basics of Reference Frame Theory

The transformation matrix ${}^x\mathbf{K}^y$ is called the ‘**vector rotator**’ and is given in (2.17).

$${}^x\mathbf{K}^y = \mathbf{K}^y(\mathbf{K}^x)^{-1} = \begin{bmatrix} \cos(\theta_y - \theta_x) & -\sin(\theta_y - \theta_x) & 0 \\ \sin(\theta_y - \theta_x) & \cos(\theta_y - \theta_x) & 0 \\ 0 & 0 & 1 \end{bmatrix} \quad (2.17)$$

2.5. Importance of Reference Frame Transformations

When a balanced set is considered, the 3-phase independent voltages v_a, v_b and v_c are under the constraint

$$v_a + v_b + v_c = 0 \quad (2.18)$$

However, it is clear that by applying either Clarke or Park transformation, we get **two** independent voltages (v_β and v_α) or (v_q^e and v_d^e). Since they are in quadrature phase relationship, they are independent, without any constraints. Hence it is easy to handle them in the further stages.

Moreover, it can be seen from (2.5) that just by choosing the speed of the reference frame according to our needs, it is possible to have a simplified form of the transformed voltages. For instance, if a stationary reference frame is chosen ($\omega = 0$), we would end up with transformed voltages having the same frequency as that of the grid. On the other hand, transforming to a synchronous reference frame ($\omega = \omega_e$), we would have the transformed voltages appearing as dc quantities. This choice can ease the mathematical complexity in the further stages.

3. Conventional SRF PLL

The basics of reference frame theory and the conventions to be followed were discussed in chapter 2. The conventional synchronous reference frame (SRF) PLL, which forms the basis of study of the other 3-phase PLLs, is analysed in depth in this chapter.

SRF PLL has two transformations on the grid phase voltages:

1. **Clarke transformation** from v_a, v_b, v_c to stationary reference frame v_β, v_α
2. **Park transformation** from v_β, v_α to synchronous reference frame v_q^e, v_d^e

Figure 3.1 shows the block diagram of SRF PLL. After Park transformation, the output v_d^e is fed to the PI loop filter whose task is to drive it to zero. The estimated frequency $\hat{\omega}$ is integrated and the resulting estimated angle $\hat{\theta}$ is fed back to the Park transformation block. Three cases are chosen to understand the behaviour of SRF PLL under different grid situations.

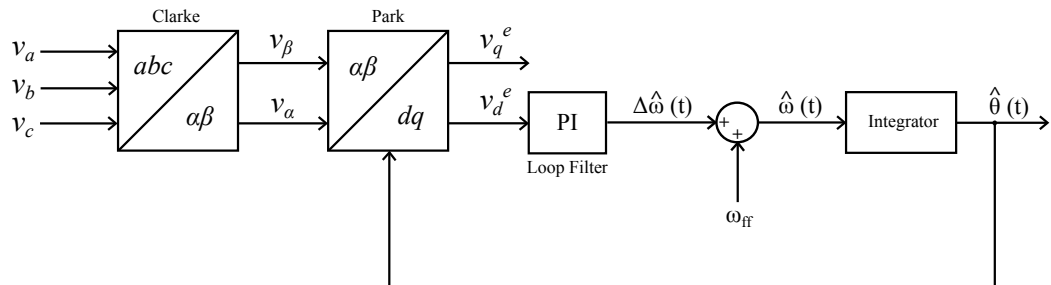


Figure 3.1.: Conventional SRF PLL

3.1. Case 1: When the grid is balanced

As discussed in section 2.2, in case of a balanced grid, the voltages v_β and v_α in the stationary reference frame are

$$\begin{bmatrix} v_\beta \\ v_\alpha \end{bmatrix} = \begin{bmatrix} V_m \cos \theta_{ef} \\ -V_m \sin \theta_{ef} \end{bmatrix} \quad (3.1)$$

The transformation from a stationary reference frame to a synchronously rotating reference frame can be done using the ‘vector rotator’ (as seen in section 2.4) and substituting the phase

3. Conventional SRF PLL

angles θ_x and θ_y corresponding to the stationary and synchronous reference frames respectively. i.e.,

$$\theta_x = 0 \quad (3.2)$$

$$\theta_y = \hat{\theta} \quad (3.3)$$

where $\hat{\theta}$ denotes the estimated phase angle that is fed back in figure 3.1. Hence the transformed voltages v_q^e and v_d^e become

$$\begin{bmatrix} v_q^e \\ v_d^e \end{bmatrix} = \begin{bmatrix} \cos \hat{\theta} & -\sin \hat{\theta} \\ \sin \hat{\theta} & \cos \hat{\theta} \end{bmatrix} \begin{bmatrix} v_\beta \\ v_\alpha \end{bmatrix} \quad (3.4)$$

Substituting (3.1) into (3.4), we get

$$\begin{bmatrix} v_q^e \\ v_d^e \end{bmatrix} = \begin{bmatrix} V_m \cos(\theta_{ef} - \hat{\theta}) \\ -V_m \sin(\theta_{ef} - \hat{\theta}) \end{bmatrix} \quad (3.5)$$

In general, when an error signal $e(t)$ is given to a PI controller in closed loop, the control action will be such that the error eventually becomes zero. In our case, the d-component of the transformed voltages, v_d^e , is fed to the PI loop filter because it contains the error information as shown in section 3.1.1.

3.1.1. The linear model

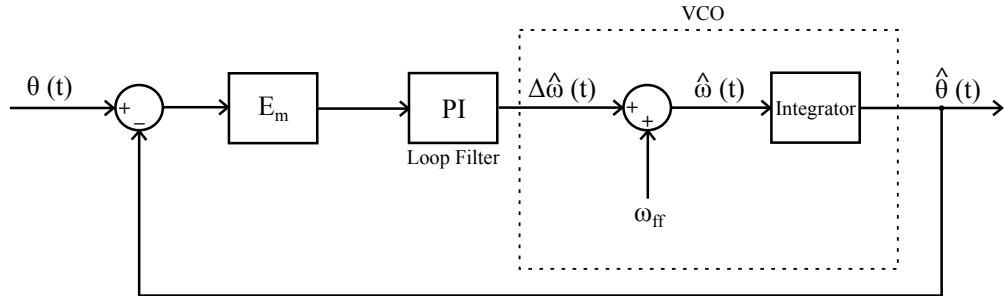


Figure 3.2.: Linearised model of SRF PLL in time domain

When the estimated angle, $\hat{\theta}$, is close to the grid phase angle, θ_{ef} , we may express the d-component of the transformed voltages, v_d^e , as the error component. i.e.,

$$v_d^e = -V_m \sin(\theta_{ef} - \hat{\theta}) \approx -V_m (\theta_{ef} - \hat{\theta}) \quad (3.6)$$

Equation (3.6) holds true as long as the PLL is in its lock-range. This approximation is of high significance because it allows us to obtain a linearised model of SRF PLL. Linear modelling

3. Conventional SRF PLL

in turn enables the design and optimization of the PI loop filter parameters. Figure 3.2 shows the linearised SRF PLL model where, in case of a balanced grid,

$$\theta(t) = \theta_{ef}(t) \quad (3.7)$$

and

$$E_m = -V_m \quad (3.8)$$

3.1.2. Modelling a voltage controlled oscillator (VCO)

A voltage controlled oscillator produces an output frequency which is proportional to the input voltage given to it.

$$\omega_{out} = \omega_{ff} + K_{vco} v_{in} \quad (3.9)$$

where ω_{ff} is the natural frequency of the VCO, or the output frequency of the VCO when the input voltage fed to it is zero.

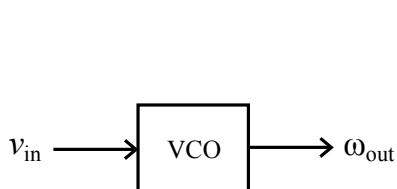


Figure 3.3.: A simple VCO block

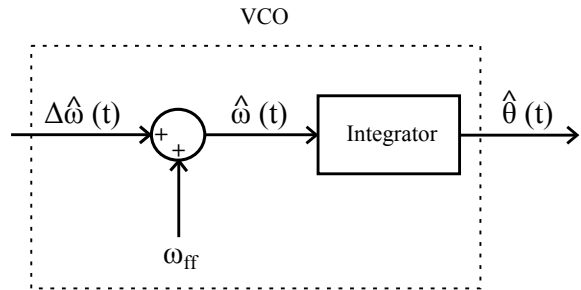


Figure 3.4.: VCO equivalent model

3.1.3. When in lock

When the PLL is in lock, $\theta_{ef} = \hat{\theta}$. Hence from (3.5), the error (d-)component,

$$v_d^e = 0 \quad (3.10)$$

and the q-component,

$$v_q^e = V_m \quad (3.11)$$

We see that the q-component of the transformed voltage gives the fundamental voltage magnitude and is called the '**space vector**'.

3. Conventional SRF PLL

3.1.4. Importance of separate transformations

Since the transformed voltages of interest are v_d^e and v_q^e in case of an SRF PLL, an obvious question that would arise is, why go for Clarke transformation followed by Park transformation? Why not do a direct transformation to the synchronous reference frame?

The answer is, a two step transformation, although not mandatory in the implementation of an SRF PLL, allows flexibility of innovating and adding further improvement stages on the conventional PLL scheme. Further stages, for instance, filters or decoupling networks may be added to the transformed voltages at the stationary reference frame itself, without having to deal with them in the synchronous reference frame. This reduces the complexity of analysis of a PLL in closed loop.

3.2. Case 2: When the grid voltage is unbalanced

The unbalanced grid voltages can be represented as

$$\left\{ \begin{array}{l} v_a = V_a \cos \theta_{ef} \\ v_b = V_b \cos \left(\theta_{ef} - \frac{2\pi}{3} \right) \\ v_c = V_c \cos \left(\theta_{ef} + \frac{2\pi}{3} \right) \end{array} \right. \quad (3.12a)$$

$$\left\{ \begin{array}{l} v_a = V_m^{+1} \left[\cos(\theta_{ef}) \right] \\ v_b = V_m^{-1} \left[\cos(\theta_{ef} - \frac{2\pi}{3}) \right] \\ v_c = V_m^0 \left[\cos(\theta_{ef} + \frac{2\pi}{3}) \right] \end{array} \right. \quad (3.12b)$$

$$\left\{ \begin{array}{l} v_a = V_m^{+1} \left[\cos(\theta_{ef}) \right] \\ v_b = V_m^{-1} \left[\cos(\theta_{ef} - \frac{2\pi}{3}) \right] \\ v_c = V_m^0 \left[\cos(\theta_{ef} + \frac{2\pi}{3}) \right] \end{array} \right. \quad (3.12c)$$

According to Charles L. Fortescue's theory, the 3-phase unbalanced voltages can be written as the sum of balanced positive, negative and zero sequence voltages. i.e.,

$$\begin{bmatrix} v_a \\ v_b \\ v_c \end{bmatrix} = V_m^{+1} \begin{bmatrix} \cos(\theta_{ef}) \\ \cos(\theta_{ef} - \frac{2\pi}{3}) \\ \cos(\theta_{ef} + \frac{2\pi}{3}) \end{bmatrix} + V_m^{-1} \begin{bmatrix} \cos(-\theta_{ef}) \\ \cos(-\theta_{ef} - \frac{2\pi}{3}) \\ \cos(-\theta_{ef} + \frac{2\pi}{3}) \end{bmatrix} + V_m^0 \begin{bmatrix} \cos(\theta_{ef}) \\ \cos(\theta_{ef}) \\ \cos(\theta_{ef}) \end{bmatrix} \quad (3.13)$$

The zero sequence current can flow only when (i) the neutral is grounded and (ii) a fourth wire wye is used [14]. Since the neutral is left unconnected, there is no path for the zero sequence current to flow, thus making $V_m^0 = 0$. Hence (3.13) reduces to

$$\begin{bmatrix} v_a \\ v_b \\ v_c \end{bmatrix} = V_m^{+1} \begin{bmatrix} \cos(\theta_{ef}) \\ \cos(\theta_{ef} - \frac{2\pi}{3}) \\ \cos(\theta_{ef} + \frac{2\pi}{3}) \end{bmatrix} + V_m^{-1} \begin{bmatrix} \cos(-\theta_{ef}) \\ \cos(-\theta_{ef} - \frac{2\pi}{3}) \\ \cos(-\theta_{ef} + \frac{2\pi}{3}) \end{bmatrix} \quad (3.14)$$

Now applying Clarke transformation from (2.7), to transform the grid phase voltages in (3.14)

3. Conventional SRF PLL

to the stationary reference frame,

$$\begin{bmatrix} v_\beta \\ v_\alpha \end{bmatrix} = V_m^{+1} \begin{bmatrix} \cos(\theta_{ef}) \\ -\sin(\theta_{ef}) \end{bmatrix} + V_m^{-1} \begin{bmatrix} \cos(-\theta_{ef}) \\ -\sin(-\theta_{ef}) \end{bmatrix} \quad (3.15)$$

Using vector rotator (section 2.4) to convert from stationary reference frame to synchronous reference frame,

$$\begin{bmatrix} v_q^e \\ v_d^e \end{bmatrix} = V_m^{+1} \begin{bmatrix} \cos(\theta_{ef} - \hat{\theta}) \\ -\sin(\theta_{ef} - \hat{\theta}) \end{bmatrix} + V_m^{-1} \begin{bmatrix} \cos(-\theta_{ef} - \hat{\theta}) \\ -\sin(-\theta_{ef} - \hat{\theta}) \end{bmatrix} \quad (3.16)$$

The d-component in (3.16) is fed to the loop filter, which is given by

$$v_d^e = -V_m^{+1} \sin(\theta_{ef} - \hat{\theta}) - V_m^{-1} \sin(-\theta_{ef} - \hat{\theta}) \quad (3.17)$$

3.2.1. The linear model

When the estimated angle follows the grid phase angle closely, we may say

$$\theta_{ef} \approx \hat{\theta} \quad (3.18)$$

Hence (3.17) becomes,

$$v_d^e = -V_m^{+1}(\theta_{ef} - \hat{\theta}) + V_m^{-1} \sin(2\theta_{ef}) \quad (3.19)$$

Rewriting (3.19),

$$\begin{aligned} v_d^e &= -V_m^{+1} \left(\theta_{ef} - \hat{\theta} - \frac{V_m^{-1}}{V_m^{+1}} \sin(2\theta_{ef}) \right) \\ &= \underbrace{-V_m^{+1}}_{E_m} \left(\underbrace{\theta_{ef} - \frac{V_m^{-1}}{V_m^{+1}} \sin(2\theta_{ef})}_{\theta} - \hat{\theta} \right) \end{aligned} \quad (3.20)$$

Hence the linearised SRF PLL model shown in figure 3.2 can still be used with

$$E_m = -V_m^{+1} \quad (3.21)$$

and

$$\theta = \theta_{ef} - K_{-1} \sin(2\theta_{ef}) \quad (3.22)$$

where

$$K_{-1} = \frac{V_m^{-1}}{V_m^{+1}} \quad (3.23)$$

3. Conventional SRF PLL

3.3. Case 3: When the grid is polluted with harmonics

In the presence of harmonics, the grid phase voltages can be expressed as

$$\begin{bmatrix} v_a \\ v_b \\ v_c \end{bmatrix} = V_m^{+1} \begin{bmatrix} \cos(\theta_{ef}) \\ \cos(\theta_{ef} - \frac{2\pi}{3}) \\ \cos(\theta_{ef} + \frac{2\pi}{3}) \end{bmatrix} + V_m^{+5} \begin{bmatrix} \cos 5(\theta_{ef}) \\ \cos 5(\theta_{ef} - \frac{2\pi}{3}) \\ \cos 5(\theta_{ef} + \frac{2\pi}{3}) \end{bmatrix} + V_m^{+7} \begin{bmatrix} \cos 7(\theta_{ef}) \\ \cos 7(\theta_{ef} - \frac{2\pi}{3}) \\ \cos 7(\theta_{ef} + \frac{2\pi}{3}) \end{bmatrix} + \dots \quad (3.24)$$

It is notable that the third harmonic and its multiples are absent. This is because the third harmonic frequency ($3 \times 120^\circ$) is in time phase and so flows like zero phase sequence quantities [14, page 38].

Now applying Clarke transformation from (2.7), to transform the grid phase voltages in (3.24) to the stationary reference frame, we obtain (see Appendix C.2)

$$\begin{bmatrix} v_\beta \\ v_\alpha \end{bmatrix} = V_m^{+1} \begin{bmatrix} \cos \theta_{ef} \\ -\sin \theta_{ef} \end{bmatrix} + V_m^{+5} \begin{bmatrix} \cos 5\theta_{ef} \\ +\sin 5\theta_{ef} \end{bmatrix} + V_m^{+7} \begin{bmatrix} \cos 7\theta_{ef} \\ -\sin 7\theta_{ef} \end{bmatrix} + \dots \quad (3.25)$$

Using vector rotator (section 2.4) to convert from stationary reference frame to synchronous reference frame,

$$\begin{bmatrix} v_q^e \\ v_d^e \end{bmatrix} = V_m^{+1} \begin{bmatrix} \cos(\theta_{ef} - \hat{\theta}) \\ -\sin(\theta_{ef} - \hat{\theta}) \end{bmatrix} + V_m^{+5} \begin{bmatrix} \cos(-5\theta_{ef} - \hat{\theta}) \\ -\sin(-5\theta_{ef} - \hat{\theta}) \end{bmatrix} + V_m^{+7} \begin{bmatrix} \cos(7\theta_{ef} - \hat{\theta}) \\ -\sin(7\theta_{ef} - \hat{\theta}) \end{bmatrix} + \dots \quad (3.26)$$

It is important to note that on comparing (3.16) and (3.26), it is verified that fifth harmonic frequency ($5 \times 120^\circ$) is similar to negative sequence and seventh harmonic frequency ($7 \times 120^\circ$) is similar to positive sequence [14, page 38]. In general,

- 3^{rd} harmonic, 9^{th} harmonic, 15^{th} harmonic, ... are similar to zero sequence
- 5^{th} harmonic, 11^{th} harmonic, 17^{th} harmonic, ... are similar to negative sequence
- 7^{th} harmonic, 13^{th} harmonic, 19^{th} harmonic, ... are similar to positive sequence

The d-component in (3.26) is fed to the loop filter, which is given by

$$\begin{aligned} v_d^e &= -V_m^{+1} \sin(\theta_{ef} - \hat{\theta}) \\ &\quad - V_m^{+5} \sin(-5\theta_{ef} - \hat{\theta}) - V_m^{+7} \sin(7\theta_{ef} - \hat{\theta}) \\ &\quad - V_m^{+11} \sin(-11\theta_{ef} - \hat{\theta}) - V_m^{+13} \sin(13\theta_{ef} - \hat{\theta}) - \dots \end{aligned} \quad (3.27)$$

3. Conventional SRF PLL

3.3.1. The linear model

When the estimated angle follows the grid phase angle closely, we may say

$$\theta_{ef} \approx \hat{\theta} \quad (3.28)$$

Hence (3.27) becomes,

$$\begin{aligned} v_d^e &= -V_m^{+1} (\theta_{ef} - \hat{\theta}) \\ &\quad + \left\{ V_m^{+5} - V_m^{+7} \right\} \sin(6\theta_{ef}) \\ &\quad + \left\{ V_m^{+11} - V_m^{+13} \right\} \sin(12\theta_{ef}) + \dots \end{aligned} \quad (3.29)$$

Thus we notice that frequencies which are multiples of six times the grid frequency also appear prominently in the error component, v_d^e . Rewriting (3.29), we get

$$\begin{aligned} v_d^e &= -V_m^{+1} \left(\theta_{ef} - \hat{\theta} - \left\{ \frac{V_m^{+5} - V_m^{+7}}{V_m^{+1}} \right\} \sin(6\theta_{ef}) - \left\{ \frac{V_m^{+11} - V_m^{+13}}{V_m^{+1}} \right\} \sin(12\theta_{ef}) - \dots \right) \\ &= \underbrace{-V_m^{+1}}_{E_m} \left(\underbrace{\theta_{ef} - \left\{ \frac{V_m^{+5} - V_m^{+7}}{V_m^{+1}} \right\} \sin(6\theta_{ef}) - \left\{ \frac{V_m^{+11} - V_m^{+13}}{V_m^{+1}} \right\} \sin(12\theta_{ef}) - \dots}_{\theta} - \hat{\theta} \right) \end{aligned} \quad (3.30)$$

Thus the linearised SRF PLL model shown in figure 3.2 can still be used with

$$E_m = -V_m^{+1} \quad (3.31)$$

and

$$\theta = \theta_{ef} - K_{+6} \sin(6\theta_{ef}) - K_{+12} \sin(12\theta_{ef}) - \dots \quad (3.32)$$

where

$$K_{+6} = \left\{ \frac{V_m^{+5} - V_m^{+7}}{V_m^{+1}} \right\}, K_{+12} = \left\{ \frac{V_m^{+11} - V_m^{+13}}{V_m^{+1}} \right\}, \dots \quad (3.33)$$

3.4. The two design aspects of a PLL

When the grid voltages experience a sudden change in frequency, it is required that a PLL be able to track this change with minimum transients. The **dynamic performance** or the transient response of a PLL is primarily described by its settling time. Hence the design of a PLL should be done with the objective that the settling time be under the control of the

3. Conventional SRF PLL

designer. By ‘design of a PLL’ we mean the choice of the loop filter parameters, namely, the proportional gain, k_p , and the integral gain, k_i . These loop filter parameters should be designed such that they satisfy the dynamic performance specifications given by the user. In short, the transients involved should be precisely under our control, for a faster dynamic response.

Another design aspect is the **filtering characteristic** of the closed loop PLL. Filtering characteristic is primarily dependent on the bandwidth of the closed loop system. Hence, ideally, it is required that the bandwidth be under the control of the designer.

But it will be shown in the subsequent sections that filtering performance and fast tracking are an inconsistency, and the final design is usually expected to be a trade-off between the two.

3.4.1. Filtering performance of the SRF PLL

As discussed in section 3.1.1, a linearised model of SRF PLL will be used for all further analysis.

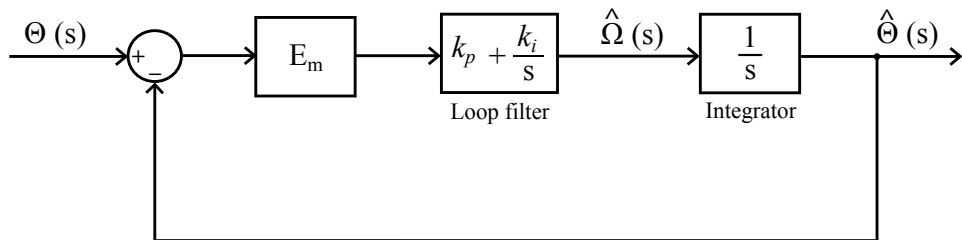


Figure 3.5.: SRF PLL linear model

The natural frequency ω_{ff} of the VCO is chosen as zero for mathematical simplicity. The closed loop transfer function can be derived to be of the form:

$$H_c(s) = \frac{\hat{\Theta}(s)}{\Theta(s)} = \frac{2\delta\omega_n s + \omega_n^2}{s^2 + 2\delta\omega_n s + \omega_n^2} \quad (3.34)$$

where

$$\omega_n = \sqrt{E_m k_i} \quad (3.35)$$

and

$$\delta = \frac{E_m k_p}{2\omega_n} \quad (3.36)$$

3.4.1.1. A detailed Bode magnitude plot

In case of a polluted grid environment, the input θ to the SRF PLL model will be of the form given by (3.22) or (3.32) as the case may be. To analyse the effect of the oscillating components

3. Conventional SRF PLL

in the input θ , a Bode magnitude plot of the closed loop system in figure 3.5 is necessary. This is obtained by substituting $s = j\omega$ in (3.34), thus giving

$$H_c(j\omega) = \frac{2\delta\omega_n(j\omega) + \omega_n^2}{(j\omega)^2 + 2\delta\omega_n(j\omega) + \omega_n^2} \quad (3.37)$$

$$= \frac{\omega_n^2 + j2\delta\omega_n\omega}{(\omega_n^2 - \omega^2) + j2\delta\omega_n\omega} \quad (3.38)$$

$$M = |H_c(j\omega)| = \sqrt{\frac{\omega_n^4 + 4\delta^2\omega_n^2\omega^2}{(\omega_n^2 - \omega^2)^2 + 4\delta^2\omega_n^2\omega^2}} \quad (3.39)$$

The magnitude of the closed loop transfer function is given by (3.39). This can be plotted by considering the following cases.

3.4.1.1.1. When $\omega \ll \omega_n$

In this case,

$$\omega_n^4 + 4\delta^2\omega_n^2\omega^2 \approx \omega_n^4 \quad (3.40)$$

and

$$(\omega_n^2 - \omega^2)^2 + 4\delta^2\omega_n^2\omega^2 \approx \omega_n^4 \quad (3.41)$$

This implies

$$M = 1 \quad (3.42)$$

$$M_{dB} = 20 \log_{10} M = 0 \quad (\text{in log scale}) \quad (3.43)$$

3.4.1.1.2. When $\omega \gg \omega_n$

In this case,

$$\omega_n^4 + 4\delta^2\omega_n^2\omega^2 \approx 4\delta^2\omega_n^2\omega^2 \quad (3.44)$$

and

$$(\omega_n^2 - \omega^2)^2 + 4\delta^2\omega_n^2\omega^2 \approx \omega^4 \quad (3.45)$$

This implies

$$M = \sqrt{\frac{4\delta^2\omega_n^2\omega^2}{\omega^4}} \quad (3.46)$$

$$= \frac{2\delta\omega_n}{\omega} \quad (3.47)$$

$$M_{dB} = 20 \log_{10} M \quad (3.48)$$

$$= 20 \log(2\delta\omega_n) - 20 \log \omega \quad (3.49)$$

which is a straight line (in a semi-log scale) with a slope of $-20dB/decade$.

3. Conventional SRF PLL

3.4.1.1.3. When ω is comparable to ω_n In this case, the expression for M as given in (3.39) cannot be approximated. However, certain features like the point of ω at maximum gain, the point of unity crossover, and the gain at ω_n helps us to plot (3.39) in this region.

3.4.1.1.3.1. Point of maxima (ω_{max}) and the maximum gain (M_{max}) To get the point of maxima, differentiate the magnitude M with respect to ω and equate it to zero. i.e.,

$$\frac{dM}{d\omega} = 0 \quad (3.50)$$

Substituting for M from (3.39) and simplifying (see Appendix C.3), we get the point of maxima as

$$\omega_{max} = \frac{\omega_n}{2\delta} \left[-1 + \sqrt{1 + 8\delta^2} \right]^{\frac{1}{2}} \quad (3.51)$$

Substituting (3.51) in (3.39) and simplifying, the maximum gain is given by

$$M_{max} = \sqrt{\frac{8\delta^2}{(8\delta^4 - 4\delta^2 - 1) + \sqrt{8\delta^2 + 1}}} \quad (3.52)$$

$$M_{max(dB)} = 20 \log_{10} M_{max} \quad (3.53)$$

$$= 10 \log \left[\frac{8\delta^2}{(8\delta^4 - 4\delta^2 - 1) + \sqrt{8\delta^2 + 1}} \right] \quad (3.54)$$

3.4.1.1.3.2. Point of unity gain crossover (ω_c) Equating the magnitude M given by (3.39) to unity, we get the point of unity crossover. i.e.,

$$M = 1 \implies M^2 = 1 \quad (3.55)$$

On substituting from (3.39),

$$\frac{\omega_n^4 + 4\delta^2\omega_n^2\omega^2}{(\omega_n^2 - \omega^2)^2 + 4\delta^2\omega_n^2\omega^2} = 1 \quad (3.56)$$

$$\omega_n^4 = (\omega_n^2 - \omega^2)^2 \quad (3.57)$$

$$\omega_n^2 = \pm (\omega_n^2 - \omega^2) \quad (3.58)$$

$$\omega = 0 \quad \text{or} \quad \omega = \sqrt{2} \omega_n \quad (3.59)$$

Clearly, $\omega = \sqrt{2} \omega_n$ is the point of unity gain crossover.

3. Conventional SRF PLL

3.4.1.1.3.3. Gain at $\omega = \omega_n$ The gain at ω_n can be obtained by substituting $\omega = \omega_n$ in (3.39). i.e.,

$$M|_{\omega=\omega_n} = \sqrt{\frac{\omega_n^4 + 4\delta^2\omega_n^4}{4\delta^2\omega_n^4}} \quad (3.60)$$

$$= \sqrt{1 + \frac{1}{4\delta^2}} \quad (3.61)$$

$$M_{dB}|_{\omega=\omega_n} = 10 \log \left[1 + \frac{1}{4\delta^2} \right] \quad (3.62)$$

Equations (3.51), (3.54), (3.59) and (3.62) give us enough information to get a rough plot in the region when ω is comparable to ω_n .

From regions 3.4.1.1.1, 3.4.1.1.2 and 3.4.1.1.3, the Bode magnitude plot of (3.39) in semi-logarithmic scale is obtained, as shown in figure 3.6.

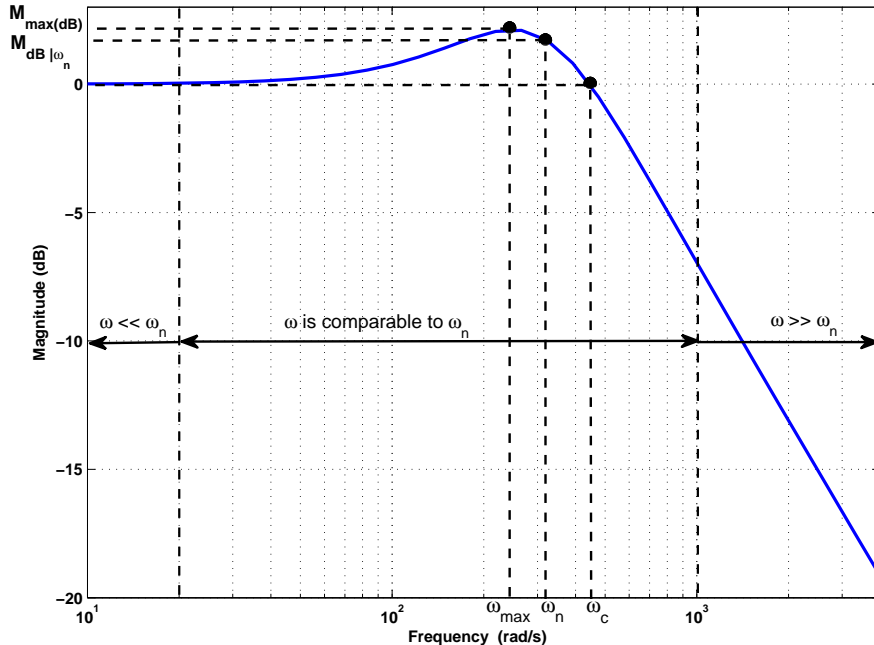


Figure 3.6.: Detailed Bode magnitude plot

3. Conventional SRF PLL

3.4.1.2. An approximate Bode magnitude plot

The closed loop transfer function of a 2^{nd} order system is given by

$$H(s) = \frac{2\delta\omega_n s + \omega_n^2}{s^2 + 2\delta\omega_n s + \omega_n^2} \quad (3.63)$$

To handle irreducible 2^{nd} order polynomials, $(ax^2 + bx + c)$ can, in many cases, be approximated as $(\sqrt{a}x + \sqrt{c})^2$ [15]. In this case, $(s^2 + 2\delta\omega_n s + \omega_n^2)$ can be approximated as $(s + \omega_n)^2$ for $2\delta \approx 1$. i.e., for values of damping ratio close to 0.5. Hence $H(s)$ becomes

$$H(s) = \frac{\omega_n(2\delta s + \omega_n)}{(s + \omega_n)^2} \quad (3.64)$$

$$= \frac{1 + \frac{2\delta s}{\omega_n}}{\left(1 + \frac{s}{\omega_n}\right)^2} \quad (3.65)$$

The corner frequencies of (3.65) are ω_n and $\frac{\omega_n}{2\delta}$

1. If $\delta > 0.5$, then the corner frequencies are located as $\omega_n > \frac{\omega_n}{2\delta}$
2. If $\delta = 0.5$, then the corner frequencies coincide at ω_n
3. If $\delta < 0.5$, then the corner frequencies are located as $\omega_n < \frac{\omega_n}{2\delta}$

The approximate Bode plots for three cases of δ close to 0.5 are shown in figure 3.7.

3.4.1.3. Significance of the Bode magnitude plot

A Bode magnitude plot gives the frequency response of a system. i.e., when a sinusoidal input of amplitude A and frequency ω is fed to a system, then the amplitude of the output gets multiplied by M (given by (3.39)). In other words, by knowing the Bode magnitude plot of a system, one can predict its output when a sinusoidal input is fed to it.

How does this concept help in understanding the filtering characteristic of a PLL? As discussed in sections 3.2 and 3.3, the input to the PLL can be expressed as (3.22) in the case of unbalanced grid voltages and (3.32) in the case of grid voltage having harmonics. They are rewritten below, for the sake of clarity.

3. Conventional SRF PLL

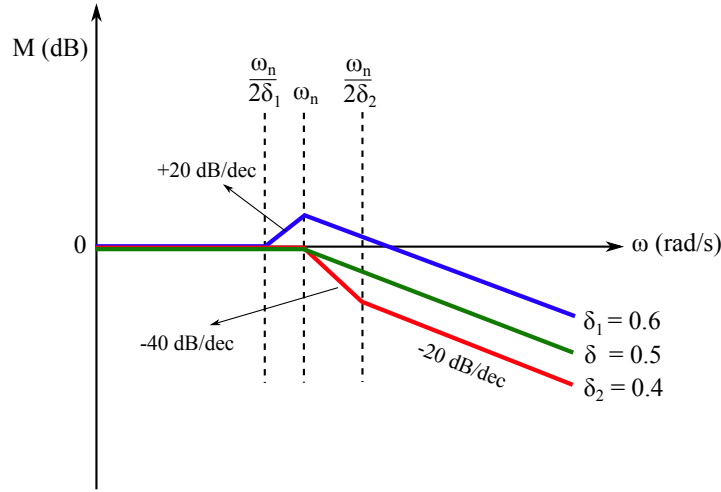


Figure 3.7.: Approximate Bode magnitude plot

In case of unbalanced grid:

$$\theta = \theta_{ef} - K_{-1} \sin(2\theta_{ef}) \quad (3.66)$$

In case of grid polluted with harmonics:

$$\theta = \theta_{ef} - K_{+6} \sin(6\theta_{ef}) - K_{+12} \sin(12\theta_{ef}) - \dots \quad (3.67)$$

When the oscillating components in the above equations are fed to the 2^{nd} order system, the output gets multiplied by M at the respective frequencies, as shown below:

$$\begin{aligned} K_{-1} &\text{ becomes } M \Big|_{2\omega} \times K_{-1} \\ K_{+6} &\text{ becomes } M \Big|_{6\omega} \times K_{+6} \\ K_{+12} &\text{ becomes } M \Big|_{12\omega} \times K_{+12} \end{aligned}$$

Clearly, the oscillating components get attenuated by a factor of M (at the respective frequencies). The amount of attenuation defines the filtering characteristic.

3.4.1.4. Measure of Bandwidth

How should the bandwidth of a PLL be defined? There is no one definition that applies to all. Some candidates are [16]:

1. natural frequency, ω_n

3. Conventional SRF PLL

2. loop gain, K defined as $K = 2\delta\omega_n$
3. noise bandwidth
4. 3dB bandwidth

It is discussed in [16] that noise bandwidth and 3dB bandwidth are not a good measure for a PLL and that natural frequency ω_n and loop gain $K = 2\delta\omega_n$ are often used to describe bandwidth. Moreover, according to [16], amongst natural frequency and loop gain, loop gain is a better measure of bandwidth. Although the reason as to why bandwidth must be defined as $2\delta\omega_n$ is beyond the scope of this report, a better understanding can be reached in the following way:

If bandwidth is defined as $2\delta\omega_n$, and since filtering is inversely proportional to bandwidth, we must expect filtering to be inversely proportional to both δ and ω_n . Figure 3.8 shows the filtering characteristic for three values of ω_n , namely $\omega_n = 100\pi \text{ rad s}^{-1}$, $\omega_n = 400\pi \text{ rad s}^{-1}$ and $\omega_n = 2000\pi \text{ rad s}^{-1}$, at a fixed $\delta = 0.1$. We can clearly see the inverse relationship of ω_n with filtering characteristic. Figure 3.9 shows the filtering characteristic for four values of δ , namely $\delta = 0.1$, $\delta = 0.5$, $\delta = 0.707$ and $\delta = 0.9$, at a fixed $\omega_n = 100\pi \text{ rad s}^{-1}$. We can see that smaller the δ , better is the filtering characteristic. Therefore filtering is inversely related to both δ and ω_n , which in turn implies, bandwidth is directly related to both δ and ω_n . Hence logically,

$$\text{Bandwidth} = 2\delta\omega_n \quad (3.68)$$

is a good measure.

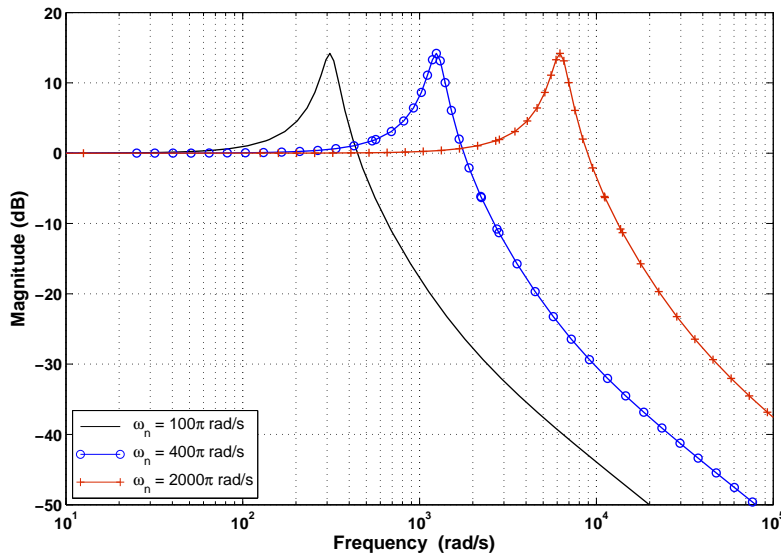


Figure 3.8.: The Bode magnitude plot for different ω_n

3. Conventional SRF PLL

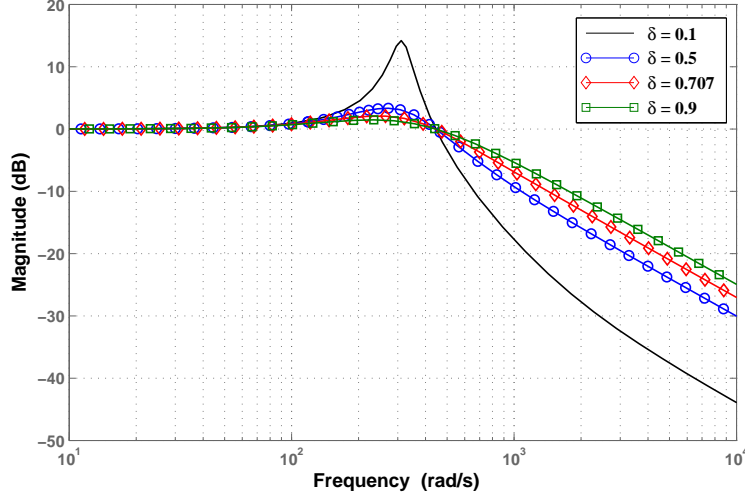


Figure 3.9.: The Bode magnitude plot for different δ

3.4.2. Dynamic performance of the SRF PLL

It can be shown that there exists an inverse relationship between the settling time and bandwidth (dealt in section 4.3.2, (4.135)). i.e., higher the bandwidth, lesser is the settling time, hence better dynamic performance.

But it was shown in the previous section that higher bandwidth causes poor filtering. Hence, usually, to get a good trade-off between the filtering characteristic and the dynamic performance of a PLL, the Wiener method [16] of optimization is commonly used.

3.5. Wiener optimization method

Here, the damping ratio δ is chosen as

$$\delta = \frac{1}{\sqrt{2}} \quad (3.69)$$

and ω_n is given by

$$\omega_n^2 = \Delta\omega\lambda\sqrt{\frac{2P_s}{\omega_0}} \quad (3.70)$$

where

- $\Delta\omega$: deviation in frequency
- P_s : input signal power
- ω_0 : input noise spectral density
- λ : Lagrangian multiplier which determines the relative proportions of noise and transient error

3. Conventional SRF PLL

However, it is very difficult to obtain the stochastic information of the noise and hence an empirical trade-off is used [17], where ω_n is determined by trial and error.

It is important to note that the Wiener method is aimed at getting a good trade-off between filtering and fast dynamic response. But in recent literature, filtering is taken care of by introducing various additional stages to the basic SRF PLL, as in [1, 2, 3]. Hence more emphasis can be given to the dynamic response of the respective PLL, leaving the burden of filtering to the augmented stages.

At this juncture, a novel optimization algorithm is proposed which allows the design of the loop filter parameters just by specifying the settling time, t_0 , and the maximum error band allowed at t_0 . As can be anticipated, this optimization algorithm is solely aimed at the dynamic performance of SRF PLL.

4. Design and Optimization of the SRF PLL

A linear model of the conventional SRF PLL was described in chapter 3. A novel optimization technique for the loop filter parameters is illustrated in this chapter. Figure 4.1 shows the SRF PLL model in s-domain.

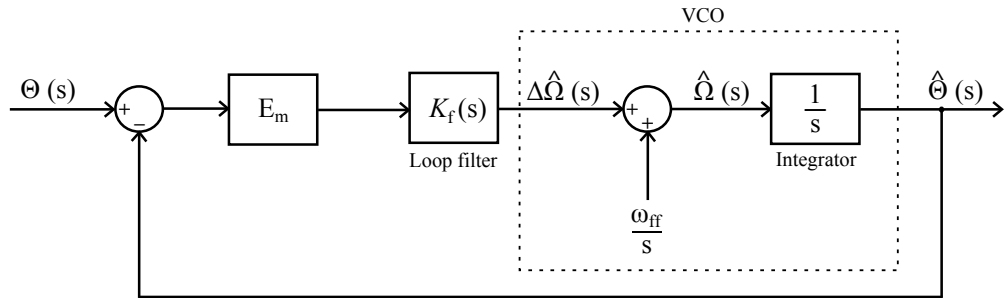


Figure 4.1.: Linearised model of SRF PLL in s-domain

Here, E_m is taken as

$$E_m = -V_m \quad (4.1)$$

and the transfer function of the PI loop filter in s-domain is

$$K_f(s) = \left(k_p + \frac{k_i}{s} \right) \quad (4.2)$$

where k_p is the proportional gain and k_i is the integral gain.

The output, $\hat{\Theta}(s)$, can be written as

$$\hat{\Theta}(s) = \frac{1}{s} \left\{ \frac{\omega_{ff}}{s} + E_m K_f(s) [\Theta(s) - \hat{\Theta}(s)] \right\} \quad (4.3)$$

On rearranging and simplifying, we obtain

$$\hat{\Theta}(s) = \left[\frac{E_m K_f(s) \Theta(s) + \frac{\omega_{ff}}{s}}{s + E_m K_f(s)} \right] \quad (4.4)$$

$$\hat{\Theta}(s) = \underbrace{\left[\frac{E_m K_f(s)}{s + E_m K_f(s)} \right]}_{G_c(s)} \Theta(s) + \underbrace{\left[\frac{1}{s(s + E_m K_f(s))} \right]}_{H_c(s)} \omega_{ff} \quad (4.5)$$

4. Design and Optimization of the SRF PLL

On substituting $K_f(s)$ from (4.2), the transfer function $G_c(s)$ can be expressed as

$$G_c(s) = \frac{E_m \left(k_p + \frac{k_i}{s} \right)}{s + E_m \left(k_p + \frac{k_i}{s} \right)} \quad (4.6)$$

$$= \frac{E_m k_p s + E_m k_i}{s^2 + E_m k_p s + E_m k_i} \quad (4.7)$$

and $H_c(s)$ can be expressed as

$$H_c(s) = \frac{1}{s^2 + E_m k_p s + E_m k_i} \quad (4.8)$$

On comparing $G_c(s)$ with the standard 2nd order transfer function, $G(s)$, which is

$$G(s) = \frac{2\delta\omega_n s + \omega_n^2}{s^2 + 2\delta\omega_n s + \omega_n^2} \quad (4.9)$$

we get

$$k_p = \frac{2\delta\omega_n}{E_m} \quad (4.10a)$$

$$k_i = \frac{\omega_n^2}{E_m} \quad (4.10b)$$

where δ is the damping ratio and ω_n is the natural frequency of the 2nd order system.

On comparing $H_c(s)$, with the standard 2nd order transfer function, $H(s)$, which is

$$H(s) = \frac{1}{s^2 + 2\delta\omega_n s + \omega_n^2} \quad (4.11)$$

we observe that the same relations of k_p and k_i hold true, as in (4.10).

In terms of the standard transfer functions, the output, $\hat{\Theta}(s)$, can be expressed as

$$\hat{\Theta}(s) = \underbrace{\left[\frac{2\delta\omega_n s + \omega_n^2}{s^2 + 2\delta\omega_n s + \omega_n^2} \right]}_{G(s)} \Theta(s) + \underbrace{\left[\frac{1}{s^2 + 2\delta\omega_n s + \omega_n^2} \right]}_{H(s)} \omega_{ff} \quad (4.12)$$

The time constant of such systems is given by

$$\tau = \frac{k_p}{k_i} = \frac{2\delta}{\omega_n} \quad (4.13)$$

4. Design and Optimization of the SRF PLL

4.1. Input to the SRF PLL

An SRF PLL tracks the input voltage (or current) signal correctly provided only the fundamental component of the positive sequence voltage (or current) is fed to it. Consider the input angle (fed to the linearised model of an SRF PLL) to be of the form

$$\theta(t) = \underbrace{\omega t}_{ramp} + \underbrace{\phi}_{step} \quad (4.14)$$

Consider a time instant $t = 0$, when the frequency steps from ω_{ff} to ω (figure 4.2) and the phase jumps from 0 to ϕ (figure 4.3). A combined effect of the frequency step and the phase jump is depicted in figure 4.4.

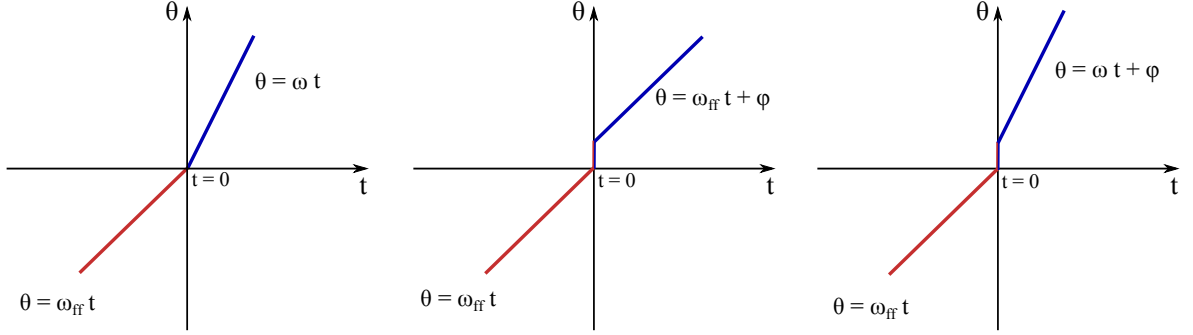


Figure 4.2.: Effect of frequency step

Figure 4.3.: Effect of phase jump

Figure 4.4.: Combined effect

Hence the analysis of the system response comprises of the study of a ramping input with a step offset. Each response shall be dealt with individually, and superposition shall be used to combine the effects of each. Taking the Laplace transform of (4.14),

$$\Theta(s) = \frac{\omega}{s^2} + \frac{\phi}{s} \quad (4.15)$$

On substituting (4.15) in (4.12),

$$\hat{\Theta}(s) = \left[\frac{2\delta\omega_n s + \omega_n^2}{s^2 + 2\delta\omega_n s + \omega_n^2} \right] \left(\frac{\omega}{s^2} + \frac{\phi}{s} \right) + \left[\frac{1}{s^2 + 2\delta\omega_n s + \omega_n^2} \right] \omega_{ff} \quad (4.16)$$

$$\hat{\Theta}(s) = \underbrace{\left[\frac{2\delta\omega_n s + \omega_n^2}{s^2 + 2\delta\omega_n s + \omega_n^2} \right]}_{A(s)} \frac{\omega}{s^2} + \underbrace{\left[\frac{2\delta\omega_n s + \omega_n^2}{s^2 + 2\delta\omega_n s + \omega_n^2} \right]}_{B(s)} \frac{\phi}{s} + \underbrace{\left[\frac{\omega_{ff}}{s^2 + 2\delta\omega_n s + \omega_n^2} \right]}_{C(s)} \quad (4.17)$$

4. Design and Optimization of the SRF PLL

Upon simplification,

$$A(s) = \omega \left\{ \frac{1}{s^2} - \frac{1}{s^2 + 2\delta\omega_n s + \omega_n^2} \right\} \quad (4.18)$$

$$B(s) = \phi \left\{ \frac{1}{s} - \frac{s}{s^2 + 2\delta\omega_n s + \omega_n^2} \right\} \quad (4.19)$$

$$C(s) = \frac{\omega_{ff}}{s^2 + 2\delta\omega_n s + \omega_n^2} \quad (4.20)$$

Taking the inverse Laplace transform on (4.17),

$$\hat{\theta}(t) = L^{-1} \{ A(s) + B(s) + C(s) \} \quad (4.21)$$

$$= \underbrace{L^{-1} \{ A(s) \}}_{a(t)} + \underbrace{L^{-1} \{ B(s) \}}_{b(t)} + \underbrace{L^{-1} \{ C(s) \}}_{c(t)} \quad (4.22)$$

4.1.1. Case 1: $\delta < 1$

On simplifying $A(s)$,

$$A(s) = \omega \left\{ \frac{1}{s^2} - \frac{1}{s^2 + 2\delta\omega_n s + \omega_n^2} \right\} \quad (4.23)$$

$$= \omega \left\{ \frac{1}{s^2} - \frac{1}{(s + \delta\omega_n)^2 + \omega_n^2 (1 - \delta^2)} \right\} \quad (4.24)$$

$$= \omega \left\{ \frac{1}{s^2} - \frac{1}{\omega_d} \times \frac{\omega_d}{(s + \delta\omega_n)^2 + \omega_d^2} \right\} \quad (4.25)$$

where ω_d is the damped natural frequency, given by

$$\omega_d = \omega_n \sqrt{1 - \delta^2} \quad (4.26)$$

Taking the inverse Laplace transform on $A(s)$,

$$a(t) = \omega t - \frac{\omega}{\omega_d} e^{-\delta\omega_n t} \sin(\omega_d t) \quad (4.27)$$

4. Design and Optimization of the SRF PLL

On simplifying $B(s)$,

$$B(s) = \phi \left\{ \frac{1}{s} - \frac{s}{s^2 + 2\delta\omega_n s + \omega_n^2} \right\} \quad (4.28)$$

$$= \phi \left\{ \frac{1}{s} - \frac{s + \delta\omega_n - \delta\omega_n}{(s + \delta\omega_n)^2 + \omega_n^2 (1 - \delta^2)} \right\} \quad (4.29)$$

$$= \phi \left\{ \frac{1}{s} - \frac{s + \delta\omega_n}{(s + \delta\omega_n)^2 + \omega_d^2} + \frac{\delta\omega_n}{\omega_d} \times \frac{\omega_d}{(s + \delta\omega_n)^2 + \omega_d^2} \right\} \quad (4.30)$$

Taking the inverse Laplace transform on $B(s)$,

$$b(t) = \phi \left[1 - e^{-\delta\omega_n t} \cos(\omega_d t) + \frac{\delta\omega_n}{\omega_d} e^{-\delta\omega_n t} \sin(\omega_d t) \right] \quad (4.31)$$

$$= \phi \left[1 - e^{-\delta\omega_n t} \cos(\omega_d t) + \frac{\delta}{\sqrt{1 - \delta^2}} e^{-\delta\omega_n t} \sin(\omega_d t) \right] \quad (4.32)$$

$$= \phi \left[1 - \frac{e^{-\delta\omega_n t}}{\sqrt{1 - \delta^2}} \left[\sqrt{1 - \delta^2} \cos(\omega_d t) - \delta \sin(\omega_d t) \right] \right] \quad (4.33)$$

Let us define the damping angle γ as

$$\cos \gamma = \delta \quad (4.34)$$

$$\sin \gamma = \sqrt{1 - \delta^2} \quad (4.35)$$

Hence

$$b(t) = \phi \left[1 - \frac{e^{-\delta\omega_n t}}{\sqrt{1 - \delta^2}} [\sin \gamma \cos(\omega_d t) - \cos \gamma \sin(\omega_d t)] \right] \quad (4.36)$$

$$= \phi \left[1 + \frac{e^{-\delta\omega_n t}}{\sqrt{1 - \delta^2}} \sin(\omega_d t - \gamma) \right] \quad (4.37)$$

$$= \phi \left[1 + e^{-\delta\omega_n t} \frac{\omega_n}{\omega_d} \sin(\omega_d t - \gamma) \right] \quad (4.38)$$

4. Design and Optimization of the SRF PLL

On simplifying $C(s)$,

$$C(s) = \frac{\omega_{\text{ff}}}{s^2 + 2\delta\omega_n s + \omega_n^2} \quad (4.39)$$

$$= \frac{\omega_{\text{ff}}}{(s + \delta\omega_n)^2 + \omega_n^2 (1 - \delta^2)} \quad (4.40)$$

$$= \frac{\omega_{\text{ff}}}{(s + \delta\omega_n)^2 + \omega_d^2} \quad (4.41)$$

$$= \frac{\omega_{\text{ff}}}{\omega_d} \left\{ \frac{\omega_d}{(s + \delta\omega_n)^2 + \omega_d^2} \right\} \quad (4.42)$$

Taking the inverse Laplace transform on $C(s)$,

$$c(t) = \frac{\omega_{\text{ff}}}{\omega_d} e^{-\delta\omega_n t} \sin(\omega_d t) \quad (4.43)$$

On substituting (4.27), (4.38) and (4.43) in (4.22), we obtain

$$\hat{\theta}(t) = (\omega t + \phi) - \frac{e^{-\delta\omega_n t}}{\omega_d} [(\omega - \omega_{\text{ff}}) \sin(\omega_d t) - \underbrace{\phi}_{2} \omega_n \sin(\omega_d t - \gamma)] \quad (4.44)$$

The error expression is,

$$e(t) = \theta(t) - \hat{\theta}(t) \quad (4.45)$$

On substituting $\theta(t)$ from (4.14) and $\hat{\theta}(t)$ from (4.44), (4.45) becomes

$$e(t) = \frac{e^{-\delta\omega_n t}}{\omega_d} \left[\underbrace{(\omega - \omega_{\text{ff}}) \sin(\omega_d t)}_{1} - \underbrace{\phi \omega_n \sin(\omega_d t - \gamma)}_{2} \right] \quad (4.46)$$

where

- 1 → step change in frequency
- 2 → phase jump, considering $\phi_{t=0^-} = 0$

From (4.46) it can be noted that both a step change in frequency and a phase jump are exponentially damped. This shows that an SRF PLL can track changes in both the frequency and the phase. Any basic PLL is supposed to do so by default, and hence it bears the name ‘Phase Lock Loop’.

To get a picture of the variation of the error with time, a specific case with zero phase jump ($\phi = 0$) is assumed. Thus the error in (4.46) becomes

$$e(t) = \frac{e^{-\delta\omega_n t}}{\omega_d} [(\omega - \omega_{\text{ff}}) \sin(\omega_d t)] \quad (4.47)$$

$$= \left\{ \frac{\Delta\omega_{\text{step}}}{\omega_d} e^{-\delta\omega_n t} \right\} \sin(\omega_d t) \quad (4.48)$$

4. Design and Optimization of the SRF PLL

where

$$\Delta\omega_{step} = (\omega - \omega_{ff}) \quad (4.49)$$

Numerical values of $\Delta\omega_{step} = 20\pi \text{ rad s}^{-1}$, $\omega_n = 100\pi \text{ rad s}^{-1}$ and $\delta = 0.1$ are chosen and (4.48) is plotted in figure 4.5. It can be seen that the error, $e(t)$, is contained in the envelope $\pm \left\{ \frac{\Delta\omega_{step}}{\omega_d} e^{-\delta\omega_n t} \right\}$.

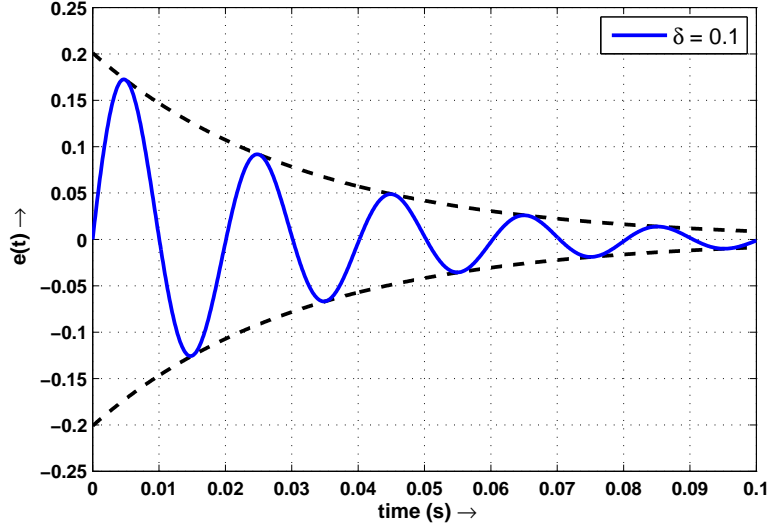


Figure 4.5.: Error w.r.t. time for the case $\delta < 1$

4.1.2. Case 2: $\delta > 1$

In this case, the roots of the polynomial $s^2 + 2\delta\omega_n s + \omega_n^2$ are real, and hence it can be factorized as

$$s^2 + 2\delta\omega_n s + \omega_n^2 = (s - p_1)(s - p_2) \quad (4.50)$$

where

$$p_1 = \left[-\delta + \sqrt{\delta^2 - 1} \right] \omega_n \quad (4.51a)$$

$$p_2 = \left[-\delta - \sqrt{\delta^2 - 1} \right] \omega_n \quad (4.51b)$$

4. Design and Optimization of the SRF PLL

Hence $A(s)$ of (4.18) becomes

$$A(s) = \omega \left\{ \frac{1}{s^2} - \frac{1}{(s - p_1)(s - p_2)} \right\} \quad (4.52)$$

$$= \omega \left\{ \frac{1}{s^2} - \frac{1}{(p_1 - p_2)} \left[\frac{1}{s - p_1} - \frac{1}{s - p_2} \right] \right\} \quad (4.53)$$

Taking the inverse Laplace transform on $A(s)$,

$$a(t) = \omega t - \frac{\omega}{(p_1 - p_2)} [e^{p_1 t} - e^{p_2 t}] \quad (4.54)$$

Substituting for p_1 and p_2 from (4.51) yields

$$a(t) = \omega t - \frac{\omega}{2\omega_n \sqrt{\delta^2 - 1}} (e^{\omega_n(-\delta + \sqrt{\delta^2 - 1})t} - e^{\omega_n(-\delta - \sqrt{\delta^2 - 1})t}) \quad (4.55)$$

$$= \omega t - \frac{\omega}{\omega_n \sqrt{\delta^2 - 1}} e^{-\delta \omega_n t} \underbrace{\left(\frac{e^{\omega_n \sqrt{\delta^2 - 1} t} - e^{-\omega_n \sqrt{\delta^2 - 1} t}}{2} \right)}_{\sinh(\omega_n \sqrt{\delta^2 - 1} t)} \quad (4.56)$$

$$= \omega t - \frac{\omega}{\omega_u} e^{-\delta \omega_n t} \sinh(\omega_u t) \quad (4.57)$$

where

$$\omega_u = \omega_n \sqrt{\delta^2 - 1} \quad (4.58)$$

Similarly, $B(s)$ from (4.19) becomes,

$$B(s) = \phi \left\{ \frac{1}{s} - \frac{s}{(s - p_1)(s - p_2)} \right\} \quad (4.59)$$

$$= \phi \left\{ \frac{1}{s} - \frac{1}{(p_1 - p_2)} \left[\frac{p_1}{s - p_1} - \frac{p_2}{s - p_2} \right] \right\} \quad (4.60)$$

Taking the inverse Laplace transform on $B(s)$,

$$b(t) = \phi - \frac{\phi}{(p_1 - p_2)} [p_1 e^{p_1 t} - p_2 e^{p_2 t}] \quad (4.61)$$

Substituting for p_1 and p_2 from (4.51), we get

$$b(t) = \phi - \frac{\phi}{2\omega_n \sqrt{\delta^2 - 1}} \left[(-\delta + \sqrt{\delta^2 - 1}) \omega_n e^{-\delta \omega_n t} e^{\sqrt{\delta^2 - 1} \omega_n t} - (-\delta - \sqrt{\delta^2 - 1}) \omega_n e^{-\delta \omega_n t} e^{-\sqrt{\delta^2 - 1} \omega_n t} \right] \quad (4.62)$$

4. Design and Optimization of the SRF PLL

$$= \phi - \frac{\phi e^{-\delta\omega_n t}}{2\sqrt{\delta^2 - 1}} \left[\sqrt{\delta^2 - 1} \left[e^{\sqrt{\delta^2 - 1}\omega_n t} + e^{-\sqrt{\delta^2 - 1}\omega_n t} \right] - \delta \left[e^{\sqrt{\delta^2 - 1}\omega_n t} - e^{-\sqrt{\delta^2 - 1}\omega_n t} \right] \right] \quad (4.63)$$

$$= \phi - \frac{\phi e^{-\delta\omega_n t}}{\sqrt{\delta^2 - 1}} \left[\sqrt{\delta^2 - 1} \cosh(\omega_u t) - \delta \sinh(\omega_u t) \right] \quad (4.64)$$

$$= \phi - \frac{\phi e^{-\delta\omega_n t}}{\sqrt{\delta^2 - 1}} [\sinh \gamma_u \cosh(\omega_u t) - \cosh \gamma_u \sinh(\omega_u t)] \quad (4.65)$$

$$= \phi + \frac{\phi e^{-\delta\omega_n t}}{\sqrt{\delta^2 - 1}} [\cosh \gamma_u \sinh(\omega_u t) - \sinh \gamma_u \cosh(\omega_u t)] \quad (4.66)$$

where

$$\cosh \gamma_u = \delta \quad (4.67)$$

$$\sinh \gamma_u = \sqrt{\delta^2 - 1} \quad (4.68)$$

Using the identity in (B.8), $b(t)$ can be written as

$$b(t) = \phi + \frac{\phi \omega_n}{\omega_u} e^{-\delta\omega_n t} \sinh(\omega_u t - \gamma_u) \quad (4.69)$$

where

$$\gamma_u = \cosh^{-1} \delta \quad (4.70)$$

$$= \log \left(\delta + \sqrt{\delta^2 - 1} \right) \quad (4.71)$$

(taking only the positive value of γ_u , as the value of $\sinh \gamma_u$ needs to be positive from (4.68); see Appendix B.3)

$C(s)$ from (4.20) may be written as

$$C(s) = \frac{\omega_{\text{ff}}}{(s - p_1)(s - p_2)} \quad (4.72)$$

$$= \frac{\omega_{\text{ff}}}{(p_1 - p_2)} \left\{ \frac{1}{s - p_1} - \frac{1}{s - p_2} \right\} \quad (4.73)$$

Taking the inverse Laplace transform on $C(s)$ and substituting for p_1 and p_2 from (4.51),

$$c(t) = \frac{\omega_{\text{ff}}}{\omega_u} e^{-\delta\omega_n t} \sinh(\omega_u t) \quad (4.74)$$

On substituting (4.57), (4.69) and (4.74) in (4.22), we obtain

$$\hat{\theta}(t) = (\omega t + \phi) - \frac{e^{-\delta\omega_n t}}{\omega_u} \left[(\omega - \omega_{\text{ff}}) \sinh(\omega_u t) - \phi \omega_n \sinh(\omega_u t - \gamma_u) \right] \quad (4.75)$$

4. Design and Optimization of the SRF PLL

The error expression is,

$$e(t) = \theta(t) - \hat{\theta}(t) \quad (4.76)$$

$$= \frac{e^{-\delta\omega_n t}}{\omega_u} \left[(\omega - \omega_{ff}) \sinh(\omega_u t) - \phi \omega_n \sinh(\omega_u t - \gamma_u) \right] \quad (4.77)$$

Consider a specific case with zero phase jump ($\phi = 0$). Thus the error from (4.77) becomes

$$e(t) = \frac{e^{-\delta\omega_n t}}{\omega_u} \left[\underbrace{(\omega - \omega_{ff})}_{\Delta\omega_{step}} \sinh(\omega_u t) \right] \quad (4.78)$$

The following points help in obtaining a rough sketch of the error in (4.78):

4.1.2.1. Maximum overshoot in error

The time at which maximum overshoot occurs ($t = t_{p1}$) is obtained by differentiating (4.78) and equating to zero. i.e.,

$$\frac{d}{dt} \left\{ \frac{e^{-\delta\omega_n t}}{\omega_u} \Delta\omega_{step} \sinh(\omega_u t) \right\} = 0 \quad (4.79)$$

Upon simplification (see Appendix C.4),

$$t_{p1} = \frac{\gamma_u}{\omega_u} \quad (4.80)$$

Substituting for γ_u from (4.71), we get

$$t_{p1} = \frac{\log(\delta + \sqrt{\delta^2 - 1})}{\omega_u} \quad (4.81)$$

The maximum overshoot is given by

$$e(t) \Big|_{t=t_{p1}} = \frac{e^{-\delta\omega_n t_{p1}}}{\omega_u} \Delta\omega_{step} \sinh \gamma_u \quad (4.82)$$

Now substituting for ω_u and $\sinh \gamma_u$ from (4.58) and (4.68) respectively, the maximum overshoot becomes

$$e_{max1} = e(t_{p1}) = \frac{e^{-\delta\omega_n t_{p1}}}{\omega_n \sqrt{\delta^2 - 1}} \Delta\omega_{step} \sqrt{\delta^2 - 1} \quad (4.83)$$

$$= \frac{e^{-\delta\omega_n t_{p1}}}{\omega_n} \Delta\omega_{step} \quad (4.84)$$

4. Design and Optimization of the SRF PLL

4.1.2.2. Error at $t \gg t_{p1}$

In this region,

$$\sinh(\omega_u t) = \frac{e^{\omega_u t} - e^{-\omega_u t}}{2} \quad (4.85)$$

$$\approx \frac{e^{\omega_u t}}{2} \quad (4.86)$$

Substituting this in (4.78), we obtain

$$e(t) = \frac{e^{-(\delta\omega_n - \sqrt{\delta^2 - 1}\omega_n)t}}{\omega_u} \Delta\omega_{step} \quad (4.87)$$

which is of the form $Ae^{-\alpha t}$, which is a decreasing exponential for a positive α .

4.1.2.3. Error at $t = 0$

Since at $t = 0$, the value of $\sinh(0) = 0$, thus the error $e(0) = 0$.

Hence points 4.1.2.1, 4.1.2.2 and 4.1.2.3 help us in roughly visualizing the error of (4.78). Figure 4.6 shows the error variation for two cases of damping ratio, $\delta = 2$ and $\delta = 4$, with values of $\omega_n = 100\pi \text{ rad s}^{-1}$ and $\omega_{step} = 20\pi \text{ rad s}^{-1}$. It is notable that the system is more sluggish for $\delta = 4$ than for $\delta = 2$.

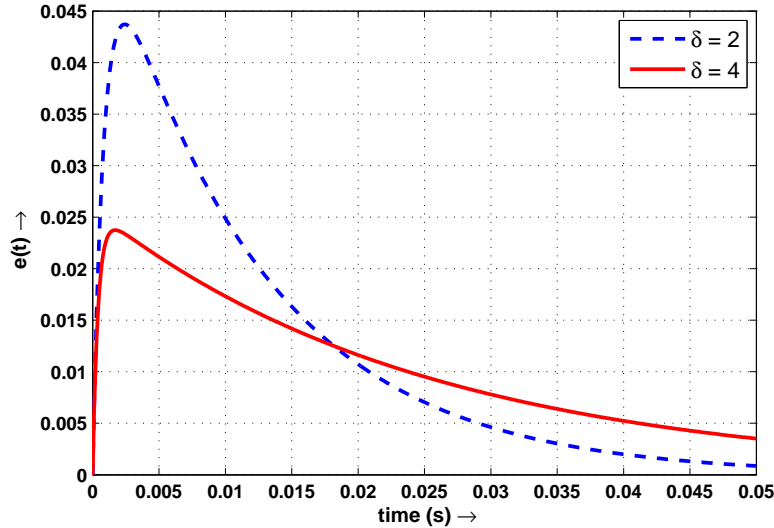


Figure 4.6.: Error w.r.t. time for the case $\delta > 1$

4. Design and Optimization of the SRF PLL

4.1.3. Case 3: $\delta = 1$

In this case, the roots of the polynomial $s^2 + 2\delta\omega_n s + \omega_n^2$ are real and equal, and can be written as

$$s^2 + 2\delta\omega_n s + \omega_n^2 = (s + \omega_n)^2 \quad (4.88)$$

Hence $A(s)$ of (4.18) becomes

$$A(s) = \omega \left\{ \frac{1}{s^2} - \frac{1}{(s + \omega_n)^2} \right\} \quad (4.89)$$

Taking the inverse Laplace transform on $A(s)$,

$$a(t) = \omega t - \omega t e^{-\omega_n t} \quad (4.90)$$

Similarly, $B(s)$ from (4.19) becomes,

$$B(s) = \phi \left\{ \frac{1}{s} - \frac{s}{(s + \omega_n)^2} \right\} \quad (4.91)$$

$$= \phi \left\{ \frac{1}{s} - \left[\frac{s + \omega_n}{(s + \omega_n)^2} - \frac{\omega_n}{(s + \omega_n)^2} \right] \right\} \quad (4.92)$$

$$= \phi \left\{ \frac{1}{s} - \left[\frac{1}{(s + \omega_n)} - \frac{\omega_n}{(s + \omega_n)^2} \right] \right\} \quad (4.93)$$

Taking the inverse Laplace transform on $B(s)$,

$$b(t) = \phi - \phi \left[e^{-\omega_n t} - \omega_n t e^{-\omega_n t} \right] \quad (4.94)$$

$$= \phi + \phi e^{-\omega_n t} (\omega_n t - 1) \quad (4.95)$$

$C(s)$ from (4.20) may be written as

$$C(s) = \frac{\omega_{ff}}{(s + \omega_n)^2} \quad (4.96)$$

Taking the inverse Laplace transform on $C(s)$,

$$c(t) = \omega_{ff} t e^{-\omega_n t} \quad (4.97)$$

4. Design and Optimization of the SRF PLL

Substituting (4.90), (4.95) and (4.97) in (4.22) yields

$$\hat{\theta}(t) = (\omega t + \phi) - \left[(\omega - \omega_{\text{ff}})t e^{-\omega_n t} - \phi e^{-\omega_n t}(\omega_n t - 1) \right] \quad (4.98)$$

$$= (\omega t + \phi) - e^{-\omega_n t} \left[(\omega - \omega_{\text{ff}})t - \phi(\omega_n t - 1) \right] \quad (4.99)$$

The error expression thus becomes

$$e(t) = \theta(t) - \hat{\theta}(t) \quad (4.100)$$

$$= e^{-\omega_n t} \left[(\omega - \omega_{\text{ff}})t - \phi(\omega_n t - 1) \right] \quad (4.101)$$

Consider a specific case with zero phase jump ($\phi = 0$). Thus the error from (4.101) becomes

$$e(t) = \Delta\omega_{\text{step}} t e^{-\omega_n t} \quad (4.102)$$

The following points help in obtaining a rough sketch of the error in (4.102):

4.1.3.1. Maximum overshoot in error

The time at which maximum overshoot occurs ($t = t_{p2}$) is obtained by differentiating (4.102) and equating it to zero. i.e.,

$$\frac{d}{dt} \left\{ \Delta\omega_{\text{step}} t e^{-\omega_n t} \right\} = 0 \quad (4.103)$$

Upon simplification (see Appendix C.5),

$$t_{p2} = \frac{1}{\omega_n} \quad (4.104)$$

The maximum overshoot is given by

$$e_{\text{max2}} = e(t) \Big|_{t=t_{p2}} = \Delta\omega_{\text{step}} t_{p2} e^{-\omega_n t_{p2}} \quad (4.105)$$

$$= e^{-1} \frac{\Delta\omega_{\text{step}}}{\omega_n} \quad (4.106)$$

4. Design and Optimization of the SRF PLL

4.1.3.2. Error at $t \rightarrow \infty$

In this case,

$$e(t) \Big|_{t \rightarrow \infty} = \lim_{t \rightarrow \infty} \Delta\omega_{step} t e^{-\omega_n t} \quad (4.107)$$

$$= \Delta\omega_{step} \lim_{t \rightarrow \infty} \left(\frac{t}{e^{\omega_n t}} \right) \quad (4.108)$$

Applying L' Hospital rule (see Appendix A.1) the error expression becomes

$$e(t) \Big|_{t \rightarrow \infty} = \Delta\omega_{step} \lim_{t \rightarrow \infty} \left(\frac{1}{\omega_n e^{\omega_n t}} \right) \quad (4.109)$$

$$= 0 \quad (4.110)$$

4.1.3.3. Error at $t = 0$

Clearly

$$e(t) \Big|_{t=0} = 0 \quad (4.111)$$

Hence points 4.1.3.1, 4.1.3.2 and 4.1.3.3 help us in roughly visualizing the error of (4.102). Figure 4.7 shows the error variation for the damping ratio $\delta = 1$, with values of $\omega_n = 100\pi \text{ rad s}^{-1}$ and $\omega_{step} = 20\pi \text{ rad s}^{-1}$.

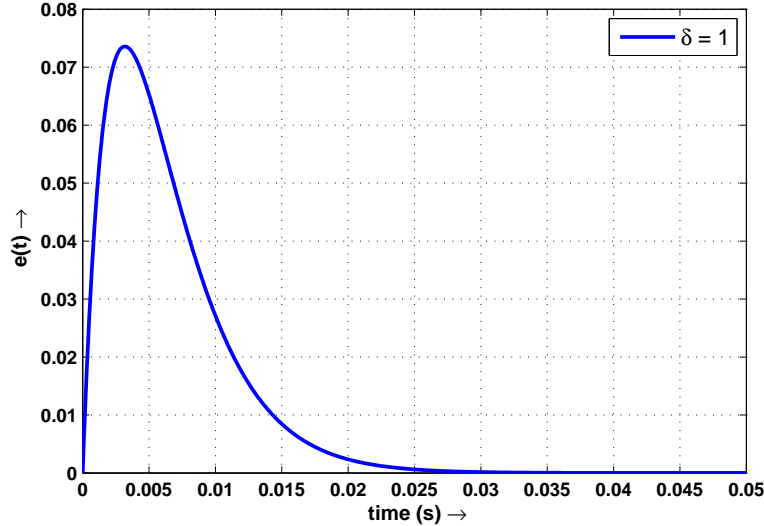


Figure 4.7.: Error w.r.t. time for the case $\delta = 1$

4. Design and Optimization of the SRF PLL

These three cases have been summarized in table 4.1

δ	$e(t)$
$\delta < 1$	$\frac{e^{-\delta\omega_n t}}{\omega_d} [\Delta\omega_{step} \sin(\omega_d t) - \phi \omega_n \sin(\omega_d t - \gamma)]$
$\delta > 1$	$\frac{e^{-\delta\omega_n t}}{\omega_u} [\Delta\omega_{step} \sinh(\omega_u t) - \phi \omega_n \sinh(\omega_u t - \gamma_u)]$
$\delta = 1$	$e^{-\omega_n t} [\Delta\omega_{step} t - \phi(\omega_n t - 1)]$

Table 4.1.: Comparison of error in the three cases of damping ratio δ

where

$$\omega_d = \omega_n \sqrt{1 - \delta^2} \quad (4.112)$$

$$\omega_u = \omega_n \sqrt{\delta^2 - 1} \quad (4.113)$$

$$\gamma = \cos^{-1} \delta \quad (4.114)$$

$$\gamma_u = \cosh^{-1} \delta \quad (4.115)$$

$$\Delta\omega_{step} = \omega - \omega_{ff} \quad (4.116)$$

To get a general idea about the dynamic response in these three cases of damping ratio, a specific case of $\phi = 0$, $\Delta\omega_{step} = 20\pi \text{ rad s}^{-1}$ and $\omega_n = 100\pi \text{ rad s}^{-1}$ is taken and the error, $e(t)$, is plotted for values of $\delta = 0.5$ (case 1), $\delta = 2$ (case 2) and $\delta = 1$ (case 3). The plot is as shown in figure 4.8. From the plot, it can be observed that the response for $\delta = 1$ and $\delta = 2$ is sluggish compared to $\delta = 0.5$.

4.2. Analytical proof for the sluggish response in the case $\delta > 1$

When can we call a response to be sluggish? Let the error at time $t = t_x$ be e_x and the error after time $t = kt_x$ (where $k > 1$), be e_y . The ratio of e_y to e_x is given by e_r . i.e.,

$$e_r = \frac{e_y}{e_x} \quad (4.117)$$

Equation (4.117) is a good indication of sluggishness. For instance, if $e_r \ll 1$, then the response

4. Design and Optimization of the SRF PLL

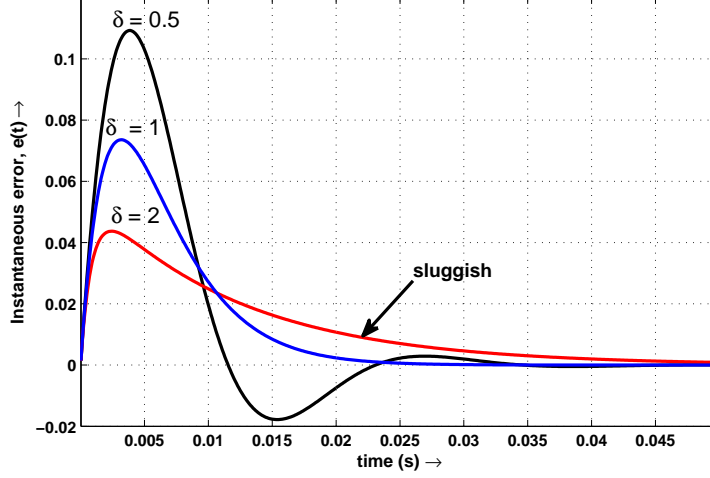


Figure 4.8.: Sluggish response for the case $\delta \geq 1$

is fast. And if e_r is close to 1, the response is sluggish. In general, greater the e_r , more sluggish is the response.

In case of $\delta < 1$ and $\phi = 0$ (for simplicity), the error $e(t)$ is given by

$$e(t) = \frac{e^{-\delta\omega_n t}}{\omega_d} \Delta\omega_{step} \sin(\omega_d t) \quad (4.118)$$

Since $\sin(\omega_d t)$ is contained in the interval $[-1, 1]$, the error $e(t)$ is contained in the interval

$$\left[-\frac{e^{-\delta\omega_n t}}{\omega_d} \Delta\omega_{step}, +\frac{e^{-\delta\omega_n t}}{\omega_d} \Delta\omega_{step} \right].$$

Hence the difference between the maximum and minimum limits of $e(t)$, given by

$$e_1 = \frac{2e^{-\delta\omega_n t}}{\omega_d} \Delta\omega_{step} \quad (4.119)$$

is a good indication of the maximum error possible at time ‘ t ’.

In case of $\delta > 1$ and $\phi = 0$ (for simplicity), the error $e(t)$ is given by

$$e(t) = \frac{e^{-\delta\omega_n t}}{\omega_u} \Delta\omega_{step} \sinh(\omega_u t) \quad (4.120)$$

Since the range of $\sinh(\omega_u t)$ is $[0, \infty]$, the error $e(t)$ itself is a good indication of the maximum error possible at time ‘ t ’. i.e.,

$$e_2 = \frac{e^{-\delta\omega_n t}}{\omega_u} \Delta\omega_{step} \sinh(\omega_u t) \quad (4.121)$$

4. Design and Optimization of the SRF PLL

The aim of this proof is to compare the *sluggishness* for $\delta > 1$ relative to the case when $\delta < 1$; in other words, to prove that the response is more sluggish for $\delta > 1$ compared to $\delta < 1$.

Let $e_1|_{t=t_x} = e_{x1}$ and $e_2|_{t=t_x} = e_{x2}$. Then, at $t = kt_x$, (4.119) becomes

$$e_1|_{t=kt_x} = \frac{2e^{-\delta\omega_n kt_x}}{\omega_d} \Delta\omega_{step} \quad (4.122)$$

$$= \underbrace{\left[\frac{2e^{-\delta\omega_n t_x}}{\omega_d} \Delta\omega_{step} \right]}_{e_{x1}} e^{-\delta\omega_n t_x(k-1)} \quad (4.123)$$

$$= e_{x1} e^{-\delta\omega_n t_x(k-1)} \quad (4.124)$$

Hence

$$\frac{e_1|_{t=kt_x}}{e_{x1}} = e^{-\delta\omega_n t_x(k-1)} = e_{r1} \quad (\text{say}) \quad (4.125)$$

Similarly, at $t = kt_x$, (4.121) becomes

$$e_2|_{t=kt_x} = \frac{e^{-\delta\omega_n kt_x}}{\omega_u} \Delta\omega_{step} \sinh(\omega_u kt_x) \quad (4.126)$$

$$= \underbrace{\left[\frac{e^{-\delta\omega_n t_x}}{\omega_u} \Delta\omega_{step} \sinh(\omega_u t_x) \right]}_{e_{x2}} \frac{\sinh(\omega_u kt_x)}{\sinh(\omega_u t_x)} e^{-\delta\omega_n t_x(k-1)} \quad (4.127)$$

$$= e_{x2} \frac{\sinh(\omega_u kt_x)}{\sinh(\omega_u t_x)} e^{-\delta\omega_n t_x(k-1)} \quad (4.128)$$

Hence

$$\frac{e_2|_{t=kt_x}}{e_{x2}} = \frac{\sinh(\omega_u kt_x)}{\sinh(\omega_u t_x)} e^{-\delta\omega_n t_x(k-1)} = e_{r2} \quad (\text{say}) \quad (4.129)$$

From (4.125) and (4.129), it is evident that

$$e_{r2} = e_{r1} \frac{\sinh(\omega_u kt_x)}{\sinh(\omega_u t_x)} \quad (4.130)$$

Since $\sinh(\omega_u kt_x) > \sinh(\omega_u t_x)$, ($\because \sinh x$ is an increasing function (see Appendix B.1))

$$e_{r2} > e_{r1} \quad (4.131)$$

As already discussed, e_r is a good measure of sluggishness; greater the e_r , more sluggish is the response. Hence from (4.131), it is obvious that the response in the case of $\delta > 1$ is more

4. Design and Optimization of the SRF PLL

sluggish compared to that of $\delta < 1$. An important inference that can be made from this discussion is that a better dynamic performance will be observed for values of damping ratio in the range $[0, 1]$. Hence all further discussions involving dynamic performance improvement will deal with values of damping ratio in the range $[0, 1]$.

4.3. Analysis for a step change in frequency

4.3.1. Requirements to be met by the PI loop filter

The PI loop filter must meet certain requirements specified by the user. They are

- (i) desired settling time, t_0
- (ii) maximum allowable frequency step, $\Delta\omega_{step}$
- (iii) maximum permissible error, E , at t_0 , for a frequency step of $\Delta\omega_{step}$

These design specifications are indicated in figure 4.9.

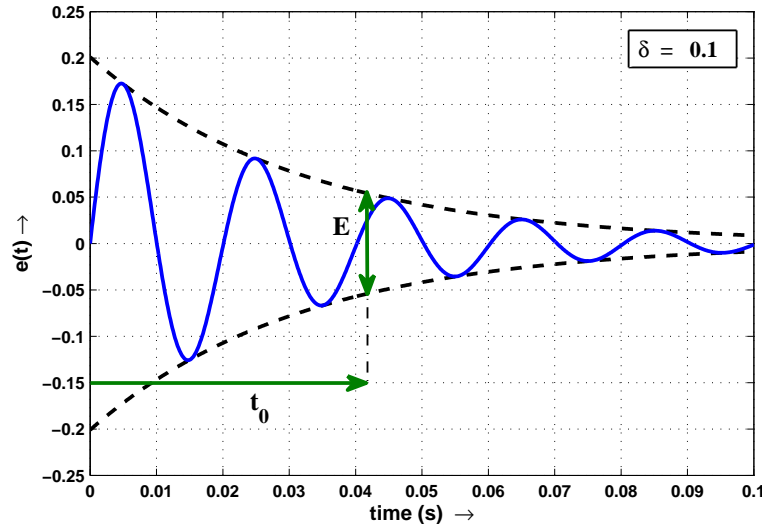


Figure 4.9.: Design specifications

4. Design and Optimization of the SRF PLL

4.3.2. Optimum design of δ and ω_n

Since the error is observed to be symmetrical in the positive and negative envelopes, it can be said that the error band is equal to twice the positive envelope at t_0 . Hence

$$E_{obs} = \frac{2 \Delta\omega_{obs}}{\omega_d} e^{-\delta\omega_n t_0} \quad (4.132)$$

$$= \frac{2 \Delta\omega_{obs}}{\omega_n \sqrt{1 - \delta^2}} e^{-\delta\omega_n t_0} \quad (4.133)$$

where E_{obs} is the observed error band for a frequency step of $\Delta\omega_{obs}$.

Note that designing the system for the worst case would ensure that the error at the current frequency step ($\Delta\omega_{obs}$) is less than the error at the maximum frequency step ($\Delta\omega_{step}$). Hence, designing for $\Delta\omega_{step}$,

$$E = \frac{2 \Delta\omega_{step}}{\omega_n \sqrt{1 - \delta^2}} e^{-\delta\omega_n t_0} \quad (4.134)$$

where E is the maximum error band for a frequency step of $\Delta\omega_{step}$.

The normalized error E_N , or, the error per unit frequency step can be expressed as

$$E_N = \frac{E}{\Delta\omega_{step}} = \frac{2 e^{-\delta\omega_n t_0}}{\omega_n \sqrt{1 - \delta^2}} \quad (4.135)$$

For the optimum performance at a fixed value of ω_n and t_0 , the damping ratio δ has to be designed such that E_N is minimum. Hence differentiating E_N with respect to δ and equating it to zero would yield the optimum δ . i.e.,

$$\frac{dE_N}{d\delta} = 0 \quad (4.136)$$

On solving, we get a quadratic equation in terms of δ (see Appendix C.6). i.e.,

$$\omega_n t_0 \delta^2 + \delta - \omega_n t_0 = 0 \quad (4.137)$$

The solution for δ is

$$\delta = \frac{-1 + \sqrt{1 + 4\omega_n^2 t_0^2}}{2\omega_n t_0} \quad (4.138)$$

The design of δ and ω_n can be done through the following three approaches:

4. Design and Optimization of the SRF PLL

4.3.2.1. Approach 1 - Error quantization

Step 1: Define the desired settling time, t_0 , and the maximum frequency step, $\Delta\omega_{step}$, for which the system is to be designed

Step 2: Specify the maximum error band, E , permitted at time t_0

Step 3: Compute E_N from (4.135)

Step 4: Assume a value of δ (say $\delta = 0.707$)

Step 5: Calculate ω_n from (4.135)

Although this approach meets the E specification at time t_0 , there may be more practical values of δ and ω_n which would satisfy the same requirement. This is simply because the assumed value of δ is not optimized for the specified error.

4.3.2.2. Approach 2 - Damping optimization

Step 1: Define the desired settling time, t_0

Step 2: Assume a value of ω_n (say $\omega_n = 100\pi \text{ rad s}^{-1}$)

Step 3: Calculate δ from (4.138)

Although this approach will yield the most optimum δ for a given ω_n and t_0 , it may or may not meet the error criterion as specified by the user, since error expression of (4.135) is not used.

4.3.2.3. Approach 3 - Damping optimization with Error quantization

For a given value of ω_n and t_0 , (4.138) yields a damping ratio δ at which the normalized error E_N is the least. However, if the error E_N is to be limited to a user-defined value, then (4.135) and (4.138) have to be solved iteratively, to obtain a consistent solution of ω_n and δ . Such equations are called *self-consistent equations*.

Step 1: Define the desired settling time, t_0 , and the maximum frequency step, $\Delta\omega_{step}$, for which the system is to be designed

Step 2: Specify the maximum error band, E , permitted at time t_0

4. Design and Optimization of the SRF PLL

Step 3: Compute E_N from (4.135)

Step 4: Assume an initial value of ω_n to start with (say $\omega_n = 100\pi \text{ rad s}^{-1}$)

Step 5: Calculate δ from (4.138)

Step 6: Use this value of δ in (4.135) to get the next iteration of ω_n

Step 7: Substitute the new ω_n in (4.138) to find the next iteration of δ

Step 8: Repeat until a consistent solution is reached

This approach is novel and it ensures that the design confines the envelope of error at time instant t_0 , to the user defined limit, and at the same time ensuring that physically realizable (or practical) values of δ and ω_n are chosen.

A fraction of the code segment to solve the two self consistent equations in approach 3 is given below.

Require: user to specify t_0 , $\Delta\omega_{step}$ and E

- 1: compute E_N from (4.135)
- 2: initialize $\omega_n^{(0)} = 100\pi \text{ rad s}^{-1}$
- 3: define the desired degree of accuracy, ϵ_{limit}
- 4: **while** $\epsilon \geq \epsilon_{limit}$ **do**
- 5: compute δ from (4.138)
- 6: solve (4.135) for ω_n
- 7: $\epsilon = \delta(i+1) - \delta(i)$
- 8: **end while**

Approach	E (rad)	δ	ω_n (rad s^{-1})	k_p ($\text{rad s}^{-1} \text{V}^{-1}$)	k_i ($\text{rad}^2 \text{s}^{-2} \text{V}^{-1}$)	τ (ms)
1 - Quantify error		0.5000	525.156	-1.6145	-847.88	1.90
	0.0200	0.7071	428.710	-1.8639	-565.04	3.30
2 - Optimize damping		0.9000	398.655	-2.2061	-488.60	4.51
	0.3718	0.7311	157.079	-0.7061	-75.86	9.31
3 - Optimize both	0.0526	0.8534	314.159	-1.6486	-303.42	5.43
	0.0088	0.8995	471.239	-2.6063	-682.71	3.82
3 - Optimize both	0.0200	0.8823	398.104	-2.1596	-487.25	4.43

Table 4.2.: Comparison of the three approaches

4. Design and Optimization of the SRF PLL

Table 4.2 compares the three approaches, for a settling time $t_0 = 0.01\text{ s}$ and a maximum frequency step $\Delta\omega_{step} = 10\text{ Hz}$. In the first approach, the maximum error is quantified to 0.02 rad. Three cases of δ are illustrated, for which the computed values of ω_n , k_p , k_i and τ are shown. All of the three cases limit the error band to 0.02 rad. However, there are infinitely many such cases which yield to the same error requirement. Hence it is very difficult to find out which set of loop parameters to take.

Figure 4.10 is a lookup table for Approach 1 where, for an assumed value of δ , the corresponding parameters ω_n , k_p , k_i and τ can be picked. A data-tip for the case of $\delta = 0.5$ is also shown in this figure.

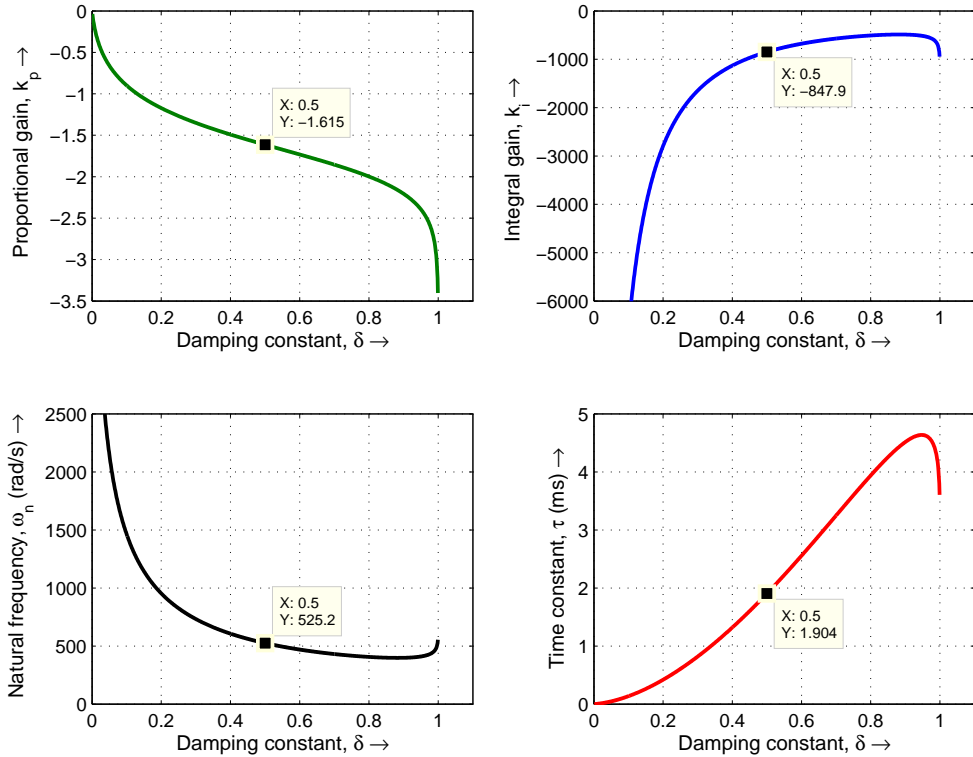


Figure 4.10.: Lookup table for Approach 1

The second approach purely concentrates on optimizing δ . We see that when the natural frequency, ω_n , is chosen to be $314.159\text{ rad s}^{-1}$, the optimum δ is computed as 0.8534. This means that for the chosen ω_n , this value of δ yields the lowest error band at t_0 . Any other choice of δ would result in an error band higher than 0.0526 rad. However, this optimization is of no use to us, as the error band is not within the maximum permissible error band (0.02 rad). Thus, although this approach optimizes the value of damping ratio, yet there are no error band constraints. A way to deal with this is by increasing ω_n . Table 4.2 shows a set of readings in approach 2, with increasing trend of ω_n . With increasing ω_n , the error band, E , reduces; this

4. Design and Optimization of the SRF PLL

can also be verified from (4.135). However, higher the ω_n , less relaxed is the time constant, τ , and more is the practical difficulty in implementing k_p and k_i of the loop filter.

Figure 4.11 is a lookup table for Approach 2 where, for an assumed value of ω_n , the corresponding parameters δ , k_p , k_i and τ can be picked. A data-tip for the case of $\omega_n = 314.1 \text{ rad s}^{-1}$ is also shown in this figure.

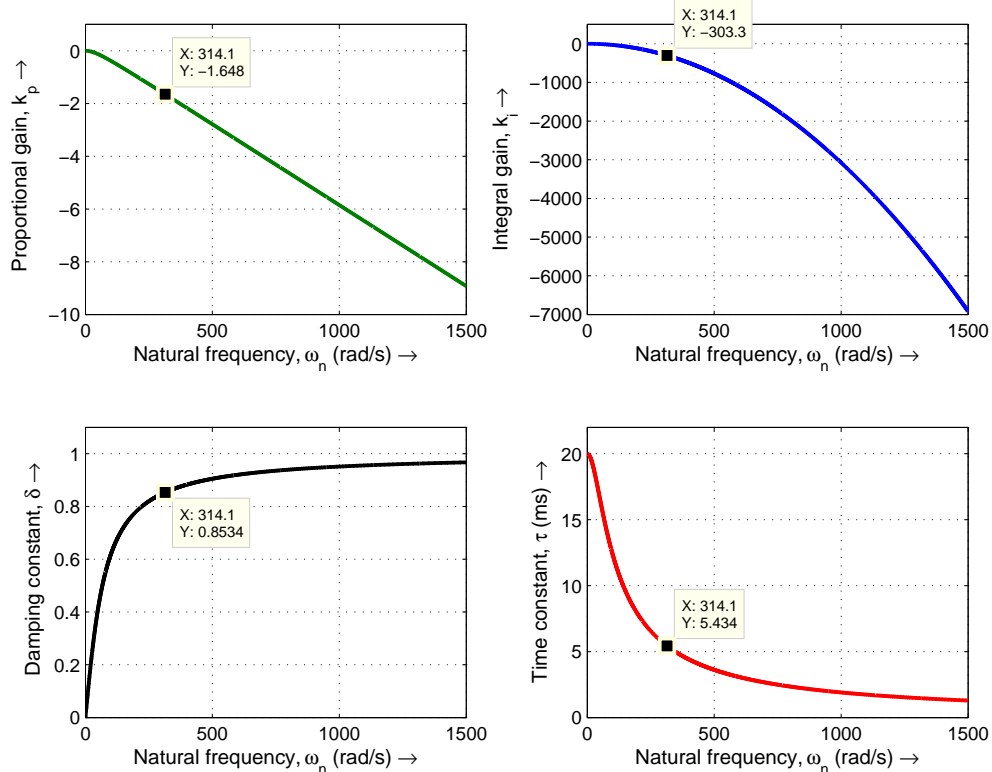


Figure 4.11.: Lookup table for Approach 2

Table 4.3 can be used to understand why both Approach 1 and 2 are not the best. At first, the natural frequency is chosen to be $314.159 \text{ rad s}^{-1}$. The optimum δ from Approach 2 gives an error band of 0.0526 rad. How can we say that this is the optimum value? It can be verified by using the same error band in Approach 1. For a damping ratio of 0.75 (which is lower than 0.8534), the natural frequency is computed as $322.23 \text{ rad s}^{-1}$. Also, for a damping ratio of 0.95 (which is higher than 0.8534), the natural frequency is computed as $330.679 \text{ rad s}^{-1}$. In both the cases, a natural frequency higher than $314.159 \text{ rad s}^{-1}$ is required to limit the maximum error to 0.0526 rad. But with Approach 2, a lower natural frequency does the job. Hence it is optimum. Yet, it still does not limit the error according to the specifications given by the user (0.02 rad). Thus it is not the best.

4. Design and Optimization of the SRF PLL

Approach	E (rad)	δ	ω_n (rad s^{-1})
1 - Error quantization	0.0526	0.7500	322.230
		0.9500	330.679
2 - Damping optimization	0.0526	0.8534	314.159

Table 4.3.: Approaches 1 and 2 are not the best

To conclude, Approach 3 has the following advantages over Approach 1 and Approach 2:

1. It both quantifies the error and optimizes the damping ratio, whereas Approach 1 and Approach 2 do only one of these.
2. It gives a unique set of loop filter parameters, whereas Approach 1 and Approach 2 give infinitely many such sets.

4.4. Analysis for a step change in frequency with phase jump

The generalized error equation for the case $\delta < 1$ is given by (4.46). i.e.,

$$e(t) = \frac{e^{-\delta\omega_n t}}{\omega_d} \left\{ \underbrace{(\omega - \omega_{ff})}_{\Delta\omega_{step}} \sin(\omega_d t) - \phi\omega_n \sin(\omega_d t - \gamma) \right\} \quad (4.139)$$

On expanding, we get

$$e(t) = \frac{e^{-\delta\omega_n t}}{\omega_d} \left\{ \Delta\omega_{step} \sin(\omega_d t) - \phi\omega_n [\sin(\omega_d t) \cos \gamma - \cos(\omega_d t) \sin \gamma] \right\} \quad (4.140)$$

$$= \frac{e^{-\delta\omega_n t}}{\omega_d} \left\{ (\Delta\omega_{step} - \phi\omega_n \delta) \sin(\omega_d t) + (\phi\omega_n \sqrt{1 - \delta^2}) \cos(\omega_d t) \right\} \quad (4.141)$$

(4.142)

This is of the form

$$e(t) = \frac{e^{-\delta\omega_n t}}{\omega_d} \{ A \sin(\omega_d t) + B \cos(\omega_d t) \} \quad (4.143)$$

where $A = \Delta\omega_{step} - \phi\omega_n \delta$ and $B = \phi\omega_n \sqrt{1 - \delta^2}$

4. Design and Optimization of the SRF PLL

We know that $A \sin(\omega_d t) + B \cos(\omega_d t)$ is contained in $[-\sqrt{A^2 + B^2}, +\sqrt{A^2 + B^2}]$, and hence we can see that $e(t)$ will be contained in the envelope

$$\pm \left[\frac{e^{-\delta\omega_n t}}{\omega_d} \sqrt{(\Delta\omega_{step} - \phi\omega_n\delta)^2 + (\phi\omega_n\sqrt{1-\delta^2})^2} \right] \quad (4.144)$$

i.e.,

$$\pm \left[\frac{e^{-\delta\omega_n t}}{\omega_d} \sqrt{\Delta\omega_{step}^2 + \phi^2\omega_n^2 - 2\Delta\omega_{step}\phi\omega_n\delta} \right] \quad (4.145)$$

The error given by (4.139) along with its envelope given by (4.145) for a phase jump $\phi = 0.1$ rad, frequency step $\Delta\omega_{step} = 20\pi$ rad s⁻¹, $\omega_n = 100\pi$ rad s⁻¹ and $\delta = 0.1$ is shown in figure 4.12

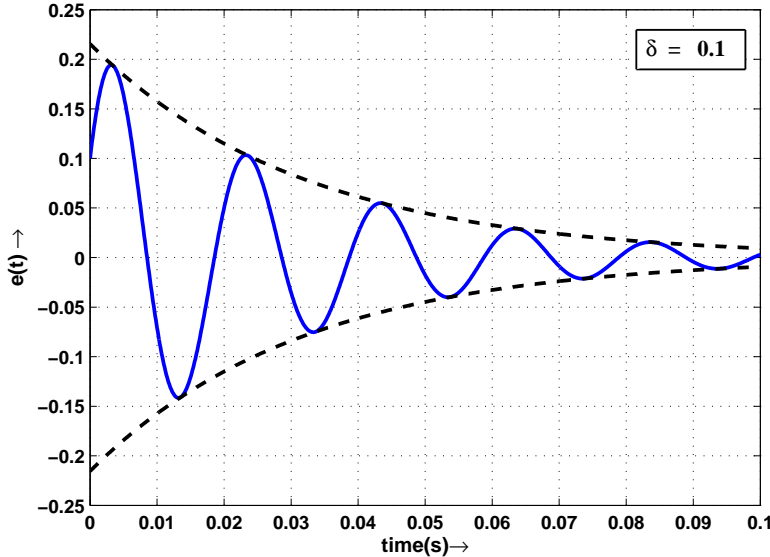


Figure 4.12.: Error w.r.t. time for $\Delta\omega_{step} = 20\pi$ rad s⁻¹ and $\phi = 0.1$ rad

4.4.1. Optimum design of δ and ω_n

The requirements to be met by the PI controller still remain the same, as discussed in section 4.3.1. The error band, E , and the settling time, t_0 , are as shown in figure 4.13.

Since the error $e(t)$ is contained in the envelope

$$\pm \left[\frac{e^{-\delta\omega_n t}}{\omega_d} \sqrt{\Delta\omega_{step}^2 + \phi^2\omega_n^2 - 2\Delta\omega_{step}\phi\omega_n\delta} \right] \quad (4.146)$$

4. Design and Optimization of the SRF PLL

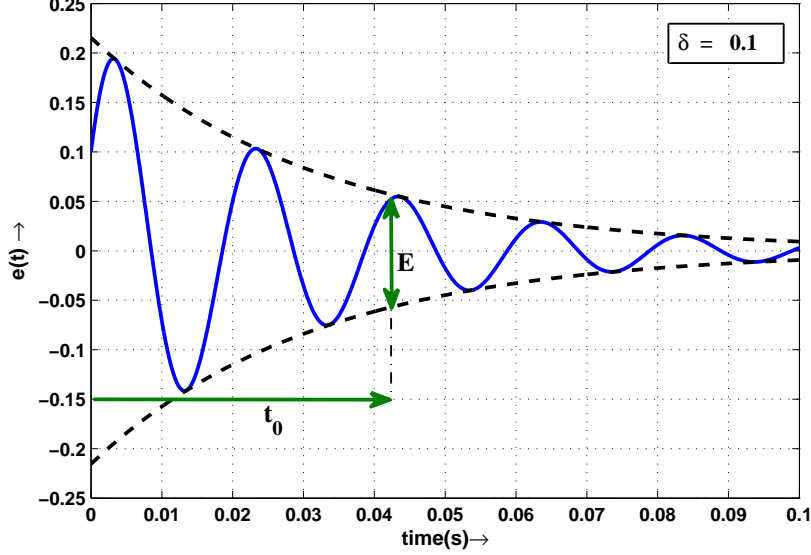


Figure 4.13.: Design specifications

the error band at settling time t_0 , E is given by

$$E = \frac{2e^{-\delta\omega_n t_0}}{\omega_d} \sqrt{c_1 - 2c_2\delta} \quad (4.147)$$

where

$$c_1 = \Delta\omega_{step}^2 + \phi^2\omega_n^2 \quad (4.148)$$

$$c_2 = \Delta\omega_{step}\phi\omega_n \quad (4.149)$$

The variables c_1 and c_2 are chosen as given by (4.148) and (4.149) to simply reduce the burden of mathematical simplifications in further steps.

For optimum dynamic performance, for a fixed natural frequency ω_n , the damping ratio δ has to be designed such that the error band E is minimum. Hence differentiating (4.147) with respect to δ and equating it to zero,

$$\frac{\partial E}{\partial \delta} = 0 \quad (4.150)$$

Simplifying (see Appendix D), we get the following cubic equation:

$$(-2\omega_n t_0 c_2)\delta^3 + (-c_2 + \omega_n t_0 c_1)\delta^2 + (c_1 + 2\omega_n t_0 c_2)\delta + (-c_2 - \omega_n t_0 c_1) = 0 \quad (4.151)$$

Equation (4.151) can be solved by considering the following two cases:

4. Design and Optimization of the SRF PLL

4.4.1.1. When $c_2 = 0$

When $c_2 = 0$, from (4.149), it is clear that either $\phi = 0$ or $\Delta\omega_{step} = 0$. Moreover, (4.151) reduces to

$$(\omega_n t_0)\delta^2 + \delta - \omega_n t_0 = 0 \quad (4.152)$$

which is exactly the same equation obtained in section 4.3.2 for the analysis of frequency step alone.

In this case, the optimum damping ratio is

$$\delta = \frac{-1 + \sqrt{1 + 4\omega_n^2 t_0^2}}{2\omega_n t_0} \quad (4.153)$$

4.4.1.2. When $c_2 \neq 0$

In this case, (4.151) cannot be simplified further. The analytical procedure to solve for the roots of a cubic equation is given by the Cardan's method. The procedure involved in this method is listed out below. It is important to note that Cardan's technique is an analytical method and not a numerical one. i.e., it does not involve iterations. A detailed explanation of this procedure is given in Appendix F.

1. Any cubic equation can be written as

$$ax^3 + bx^2 + cx + d = 0 \quad (4.154)$$

where $a \neq 0$.

2. The above expression is divided by a and written as

$$x^3 + lx^2 + mx + n = 0 \quad (4.155)$$

where $l = \frac{b}{a}$, $m = \frac{c}{a}$ and $n = \frac{d}{a}$

3. Put $y = x + \frac{l}{3}$ so that (4.155) reduces to the form

$$y^3 + py + q = 0 \quad (4.156)$$

where

$$p = m - \frac{l^2}{3} \quad (4.157)$$

$$q = \frac{2l^3}{27} - \frac{lm}{3} + n \quad (4.158)$$

4. Design and Optimization of the SRF PLL

4. If $\left(q^2 + \frac{4p^3}{27}\right) > 0$, then (4.155) has only one real root which is given by

$$x = \lambda - \frac{p}{3\lambda} - \frac{l}{3} \quad (4.159)$$

where

$$\lambda = \left[\frac{-q + \sqrt{q^2 + \frac{4p^3}{27}}}{2} \right]^{\frac{1}{3}} \quad (4.160)$$

5. If $\left(q^2 + \frac{4p^3}{27}\right) \leq 0$, then (4.155) has all real roots, and the solution set is given by

$$\left\{ \left[2r \cos \theta - \frac{l}{3} \right], \left[2r \cos \left(\theta + \frac{2\pi}{3} \right) - \frac{l}{3} \right], \left[2r \cos \left(\theta - \frac{2\pi}{3} \right) - \frac{l}{3} \right] \right\} \quad (4.161)$$

where

$$r = \left(\frac{-p}{3} \right)^{\frac{1}{2}} \quad (4.162)$$

$$\theta = \frac{1}{3} \tan^{-1} \left(\frac{\sqrt{-\left(q^2 + \frac{4p^3}{27}\right)}}{-q} \right) \quad (4.163)$$

6. Pick out the value of optimum δ in $[0, 1]$ from the solution set given in step 4 or step 5.

The steps 1 to 5 form a general procedure which can be used for solving any cubic equation. However, step 6 depends on the cubic equation of interest. i.e., (4.151). If there are multiple roots of the (4.151) in the region of interest $[0, 1]$, a question arises as to which δ should be chosen as the optimum one? Another concern is, what should the optimum δ be if there does not exist any root in $[0, 1]$? These questions will be explained in the following section.

4.4.1.3. Choosing an optimum damping ratio

Equation (4.151) is rewritten for clarity as shown below.

$$(-2\omega_n t_0 c_2)\delta^3 + (-c_2 + \omega_n t_0 c_1)\delta^2 + (c_1 + 2\omega_n t_0 c_2)\delta + (-c_2 - \omega_n t_0 c_1) = 0 \quad (4.164)$$

Dividing by $-2\omega_n t_0 c_2$, we have

$$\underbrace{\delta^3 + \left(\frac{-c_2 + \omega_n t_0 c_1}{-2\omega_n t_0 c_2} \right) \delta^2}_{l} + \underbrace{\left(\frac{c_1 + 2\omega_n t_0 c_2}{-2\omega_n t_0 c_2} \right) \delta}_{m} + \underbrace{\left(\frac{-c_2 - \omega_n t_0 c_1}{-2\omega_n t_0 c_2} \right)}_{n} = 0 \quad (4.165)$$

The following salient points help us in choosing an optimum δ :

4. Design and Optimization of the SRF PLL

4.4.1.3.1. Salient point 1: It is impossible to have all roots in [0, 1] This statement can be proved through contradiction. Let the three roots δ_1 , δ_2 and δ_3 be in $[0, 1]$. Then the sum and product of roots is given by (see Appendix A.2)

$$\delta_1 + \delta_2 + \delta_3 = -l \quad (4.166)$$

$$\delta_1\delta_2\delta_3 = -n \quad (4.167)$$

Since δ_1 , δ_2 , $\delta_3 \in [0, 1]$,

$$\delta_1 + \delta_2 + \delta_3 > 0 \quad \text{and} \quad \delta_1\delta_2\delta_3 > 0 \quad (4.168)$$

This implies

$$l < 0 \quad \text{and} \quad n < 0 \quad (4.169)$$

Or

$$l + n < 0 \quad (4.170)$$

But from (4.165), we have

$$l + n = \frac{-c_2 + \omega_n t_0 c_1}{-2\omega_n t_0 c_2} + \frac{-c_2 - \omega_n t_0 c_1}{-2\omega_n t_0 c_2} \quad (4.171)$$

$$= \frac{-2c_2}{-2\omega_n t_0 c_2} \quad (4.172)$$

$$= \frac{1}{\omega_n t_0} \quad (4.173)$$

which should always be positive. Clearly, (4.170) and (4.173) are an inconsistency. Hence the initial assumption is wrong. Therefore, it is impossible to have all real roots in $[0, 1]$.

4.4.1.3.2. Salient point 2: The error band tends to infinity when $\delta \rightarrow 1$ if $c_1 - 2c_2 \neq 0$
The expression for E is given by (4.147) and as $\delta \rightarrow 1$, the value of $E_{\delta \rightarrow 1}$ is given by

$$E_{\delta \rightarrow 1} = \lim_{\delta \rightarrow 1} \frac{2e^{-\delta \omega_n t_0}}{\omega_n \sqrt{1 - \delta^2}} \sqrt{c_1 - 2c_2 \delta} \quad (4.174)$$

Since $\sqrt{1 - \delta^2}$ is in the denominator, as $\delta \rightarrow 1$, $\sqrt{1 - \delta^2} \rightarrow 0$ and $\frac{1}{\sqrt{1 - \delta^2}} \rightarrow \infty$ and hence $E \rightarrow \infty$, provided $c_1 - 2c_2 \neq 0$.

4. Design and Optimization of the SRF PLL

4.4.1.3.3. Salient point 3: Special case - $E_{\delta \rightarrow 1}$ is finite if $c_1 - 2c_2 = 0$ From (4.174), it is clear that if the numerator does not approach zero as $\delta \rightarrow 1$, then $E_{\delta \rightarrow 1} \rightarrow \infty$. But if $c_1 - 2c_2 = 0$, then (4.174) has a $\frac{0}{0}$ form. Hence L' Hospital rule (see Appendix A.1) should be applied for evaluating it. i.e.,

$$E_{\delta \rightarrow 1} = \frac{2e^{-\omega_n t_0}}{\omega_n} \sqrt{\lim_{\delta \rightarrow 1} \frac{c_1 - 2c_2\delta}{1 - \delta^2}} \quad (4.175)$$

$$= \frac{2e^{-\omega_n t_0}}{\omega_n} \sqrt{\frac{-2c_2}{-2}} \quad (4.176)$$

$$= \frac{2e^{-\omega_n t_0}}{\omega_n} \sqrt{c_2} \quad (4.177)$$

which is finite.

This is a special case and can happen only if

$$c_1 - 2c_2 = 0 \quad (4.178)$$

i.e.,

$$\Delta\omega_{step}^2 + \phi^2\omega_n^2 - 2\Delta\omega_{step}\phi\omega_n = 0 \quad (4.179)$$

$$\implies (\Delta\omega_{step} - \phi\omega_n)^2 = 0 \quad (4.180)$$

$$\implies \omega_n = \frac{\Delta\omega_{step}}{\phi} \quad (4.181)$$

Moreover when $c_1 - 2c_2 = 0$, the error band, E , given by the (4.147) is continuously decreasing in the interval $[0, 1]$. This can be proved as follows:

The expression for error band given by (4.147) is rewritten for clarity. i.e.,

$$E = \frac{2e^{-\delta\omega_n t_0}}{\omega_n} \sqrt{\frac{c_1 - 2c_2\delta}{1 - \delta^2}} \quad (4.182)$$

Substituting $c_1 = 2c_2$,

$$E = \frac{2e^{-\delta\omega_n t_0}}{\omega_n} \sqrt{\frac{2c_2(1 - \delta)}{(1 - \delta)(1 + \delta)}} \quad (4.183)$$

$$= \frac{2\sqrt{2c_2}}{\omega_n} \underbrace{e^{-\delta\omega_n t_0}}_1 \underbrace{\frac{1}{\sqrt{1 + \delta}}}_2 \quad (4.184)$$

where '1' and '2' are decreasing functions. Hence E is a decreasing function and the minimum error band in this special case occurs as $\delta \rightarrow 1$, and is given as in (4.177). It is notable that $c_1 - 2c_2 = 0$ is valid only when c_2 is positive, since c_1 is always positive.

4. Design and Optimization of the SRF PLL

To sum up,

$$c_1 - 2c_2 = 0 \implies \begin{cases} c_2 > 0 \\ E_{\delta \rightarrow 1} = \text{finite} = \frac{2e^{-\omega_n t_0}}{\omega_n} \sqrt{c_2} \\ E \text{ is a decreasing function in } [0, 1] \\ \delta \rightarrow 1 \text{ is the optimum damping ratio} \end{cases} \quad (4.185)$$

4.4.1.3.4. Salient point 4: Slope of the error band at $\delta = 0$ for a fixed ω_n The error expression in (4.147) can be expressed as a function of δ as

$$E(\delta) = \frac{2e^{-\delta\omega_n t_0}}{\omega_n \sqrt{1-\delta^2}} \sqrt{c_1 - 2c_2\delta} \quad (4.186)$$

The slope at $\delta = 0$ is given by $E'(\delta)|_{\delta=0}$, where $E'(\delta)$ denotes the partial derivative of E with respect to δ . $E'(\delta)|_{\delta=0}$ can be written as (see Appendix D)

$$E'(\delta)|_{\delta=0} = E'(0) = \frac{2}{\omega_n \sqrt{c_1}} \{-(c_2 + \omega_n t_0 c_1)\} \quad (4.187)$$

4.4.1.3.4.1. Case 1: When $c_2 + \omega_n t_0 c_1 \leq 0$ In this case, from (4.187),

$$E'(0) \geq 0 \quad (4.188)$$

In other words, the slope at $\delta = 0$ is positive if $c_2 + \omega_n t_0 c_1 < 0$.

If $c_2 + \omega_n t_0 c_1 \leq 0$,

$$\implies \Delta\omega_{step} \phi \omega_n + \omega_n t_0 (\Delta\omega_{step}^2 + \phi^2 \omega_n^2) \leq 0 \quad (4.189)$$

$$\implies \Delta\omega_{step}^2 + \phi^2 \omega_n^2 + \frac{\Delta\omega_{step} \phi}{t_0} \leq 0 \quad (4.190)$$

Dividing by ϕ^2 on both sides of the inequality, and defining $\frac{\Delta\omega_{step}}{\phi} = x$,

$$x^2 + \frac{x}{t_0} + \omega_n^2 \leq 0 \quad (4.191)$$

$$t_0 x^2 + x + t_0 \omega_n^2 \leq 0 \quad (4.192)$$

4. Design and Optimization of the SRF PLL

For (4.192) to be satisfied, the discriminant of $t_0x^2 + x + t_0\omega_n^2$ must be positive; i.e., it should have real roots.

$$\implies 1 - 4\omega_n^2 t_0^2 \geq 0 \quad (4.193)$$

$$\implies \omega_n t_0 \leq \frac{1}{2} \quad (4.194)$$

Moreover, (4.192) can be rewritten as

$$(x - p_1)(x - p_2) \leq 0 \quad (4.195)$$

where

$$p_1 = \frac{-1 - \sqrt{1 - 4\omega_n^2 t_0^2}}{2t_0} \quad (4.196)$$

$$p_2 = \frac{-1 + \sqrt{1 - 4\omega_n^2 t_0^2}}{2t_0} \quad (4.197)$$

$$\implies x = \frac{\Delta\omega_{step}}{\phi} \in [p_1, p_2] \quad (4.198)$$

It is important to note that p_1 and p_2 are negative (from (4.196) and (4.197)) and therefore case 1 is true only when $\Delta\omega_{step}$ and ϕ are of opposite signs; or in other words, case 1 is true when c_2 is negative.

To summarize this case,

$$c_2 + \omega_n t_0 c_1 \leq 0 \implies \begin{cases} E'(0) \geq 0 \\ \omega_n t_0 \leq \frac{1}{2} \\ x = \frac{\Delta\omega_{step}}{\phi} \in [p_1, p_2] \end{cases} \quad (4.199)$$

4.4.1.3.4.2. Case 2: When $c_2 + \omega_n t_0 c_1 > 0$ Clearly, case 2 is the complement of case 1 and hence can be summarized as below.

$$c_2 + \omega_n t_0 c_1 > 0 \implies \begin{cases} E'(0) < 0 \\ \omega_n t_0 > \frac{1}{2} \\ x = \frac{\Delta\omega_{step}}{\phi} \in (-\infty, p_1) \cup (p_2, \infty) \end{cases} \quad (4.200)$$

The salient points discussed in sections 4.4.1.3.1 to 4.4.1.3.4 can be used to predict the behaviour of error band E with δ in the interval $[0, 1]$. The different possibilities are discussed in the next sub-sections.

4. Design and Optimization of the SRF PLL

4.4.1.3.5. Possibility 1: When $E'(0) < 0$: $E'(0) < 0$ physically means that the error band starts to decrease when δ starts increasing from zero. In this case there are two sub-possibilities:

4.4.1.3.5.1. Sub-possibility 1: When $E_{\delta \rightarrow 1} \rightarrow \infty$: From section 4.4.1.3.1, the condition of existence of three stationary points in $[0, 1]$ can be ruled out. Moreover it is physically impossible to have two stationary points in this interval, as the error band takes a *dip* at $\delta = 0$ ($E'(0) < 0$) and must reach infinity as $\delta \rightarrow 1$. Using exactly the same argument, the existence of no stationary point is also ruled out. Hence there has to be exactly one stationary point in $[0, 1]$. This is shown in the figure 4.14.

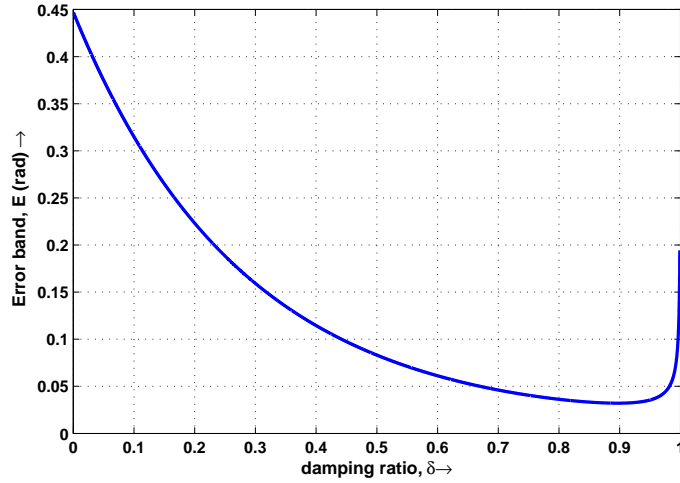


Figure 4.14.: Variation of error band with δ for $\Delta\omega_{step} = 20\pi \text{ rad s}^{-1}$, $\phi = 0.1 \text{ rad}$, $\omega_n = 100\pi \text{ rad s}^{-1}$ and $t_0 = 0.01 \text{ s}$

4.4.1.3.5.2. Sub-possibility 2: When $E_{\delta \rightarrow 1}$ is finite: From section 4.4.1.3.2, this corresponds to the case when $c_1 - 2c_2 = 0$ and from (4.185), we see that the error band is a decreasing function. Hence there is no stationary point in $[0, 1]$. Clearly, the minimum error band is observed as $\delta \rightarrow 1$. Hence a value close to 1 (say $\delta = 0.999$) should be chosen as the optimum damping ratio. This sub-possibility is shown in figure 4.15.

4.4.1.3.6. Possibility 2: When $E'(0) \geq 0$: $E'(0) \geq 0$ physically means that the error band starts to increase when δ starts increasing from zero. From section 4.4.1.3.4, this possibility happens when $c_2 + \omega_n t_0 c_1 < 0$.

$c_2 + \omega_n t_0 c_1 < 0$ implies $c_2 < 0$ which further implies $c_1 - 2c_2 > 0$. Therefore $c_1 - 2c_2$ can never

4. Design and Optimization of the SRF PLL

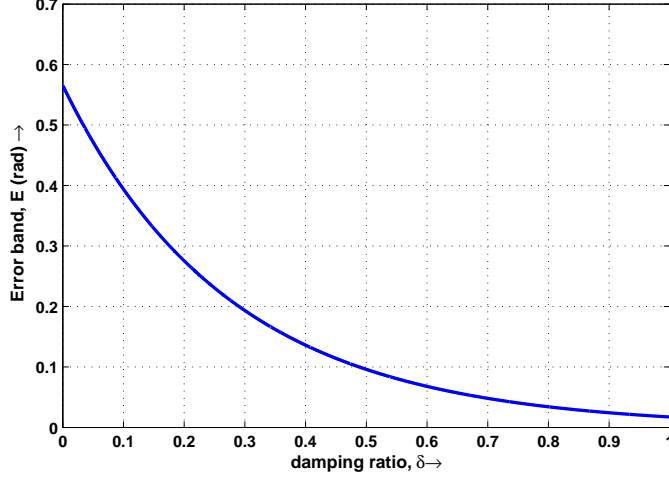


Figure 4.15.: Variation of error band with δ for $\Delta\omega_{step} = 20\pi \text{ rad s}^{-1}$, $\phi = 0.2 \text{ rad}$, $\omega_n = 100\pi \text{ rad s}^{-1}$ and $t_0 = 0.01 \text{ s}$

become zero, which in turn implies (from section 4.4.1.3.2) that

$$E_{\delta \rightarrow 1} \rightarrow \infty \quad (4.201)$$

Considering the expression for the slope of the error band, $E'(\delta)$, given by D.8,

$$E'(\delta) = \frac{2e^{-\delta\omega_n t_0}}{\omega_n (1 - \delta^2)^{\frac{3}{2}} \sqrt{c_1 - 2c_2\delta}} f(\delta) \quad (4.202)$$

In this case ($E'(0) \geq 0$), $f(\delta)$ is an increasing function in $[0, 1]$ (see Appendix E). Also, since $f(0)$ and $f(1)$ are positive (see Appendix D), no roots exist for $f(\delta) = 0$ in this interval. Therefore

$$f(\delta) > 0 \quad \forall \quad \delta \in [0, 1] \quad (4.203)$$

$$\implies E'(\delta) > 0 \quad (4.204)$$

Combining this result with (4.201), we can see that the error band $E(\delta)$ will be an increasing function in $[0, 1]$. This is shown in figure 4.16.

Section 4.4.1.3 can be concluded with table 4.4 showing the three different possibilities of the variation of error band with damping ratio.

4. Design and Optimization of the SRF PLL

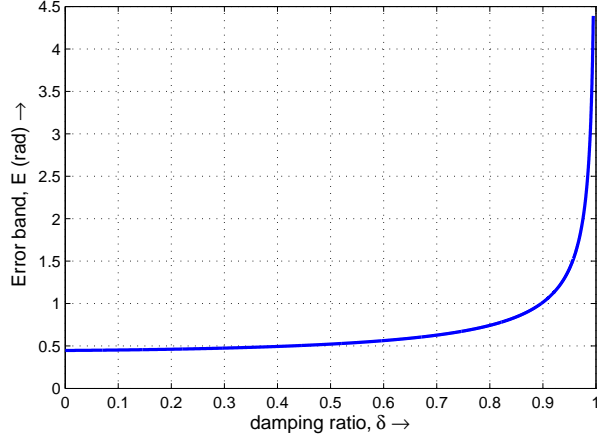


Figure 4.16.: Variation of error band with δ for $\Delta\omega_{step} = 20\pi \text{ rad s}^{-1}$, $\phi = -0.1 \text{ rad}$, $\omega_n = 100\pi \text{ rad s}^{-1}$ and $t_0 = 0.001 \text{ s}$

Possibility	Inference
1. $E'(0) < 0$ (or $c_2 + c_1\omega_n t_0 > 0$)	
(i) $c_1 - 2c_2 \neq 0$	Only one root exists in $[0, 1]$. Use Cardan's method to pick out this root.
(ii) $c_1 - 2c_2 = 0$	No root in $[0, 1]$; Optimum $\delta = 0.999$ i.e., $\delta \rightarrow 1$
2. $E'(0) \geq 0$ (or $c_2 + c_1\omega_n t_0 \leq 0$)	No root in $[0, 1]$; Optimum $\delta = 0$

Table 4.4.: Choice of an optimum damping ratio, δ

4. Design and Optimization of the SRF PLL

4.4.2. The Self-Consistent Model

The final objective is to find a single (δ, ω_n) pair that satisfies both (4.147) and (4.151). Rewriting both for clarity,

$$E = \frac{2e^{-\delta\omega_n t_0}}{\omega_n \sqrt{1 - \delta^2}} \sqrt{c_1 - 2c_2\delta} \quad (4.205)$$

$$(-2\omega_n t_0 c_2)\delta^3 + (-c_2 + \omega_n t_0 c_1)\delta^2 + (c_1 + 2\omega_n t_0 c_2)\delta + (-c_2 - \omega_n t_0 c_1) = 0 \quad (4.206)$$

where

$$c_1 = \Delta\omega_{step}^2 + \phi^2\omega_n^2 \quad (4.207)$$

$$c_2 = \Delta\omega_{step}\phi\omega_n \quad (4.208)$$

This can be solved iteratively as follows:

1) Assume: an initial value of ω_n .

2) Damping optimization: Solve for δ using (4.206). This is done using the Cardan's method as discussed in section 4.4.1. Choice of the optimum damping ratio should be done as discussed in section 4.4.1.3, summarized in table 4.4.

3) Error quantization: Solve for ω_n from (4.205), using the value of δ obtained from the previous step. This cannot be solved analytically, but can be solved iteratively using the Newton Raphson scheme (see Appendix A.3).

4) Repeat: The value of ω_n obtained in step 3 is fed to step 4 and the process is repeated till a unique (δ, ω_n) is obtained.

The scheme given above is symbolically represented in figure 4.17.

4.4.3. Loop Filter Parameters and the 3D Lookup Table

Once a unique set of damping ratio and natural frequency, (δ, ω_n) is obtained, the values of proportional gain k_p , integral gain k_i and time constant τ can be found using (4.10) and (4.13), which are rewritten for clarity, as follows:

$$k_p = \frac{2\delta\omega_n}{E_m} \quad (4.209a)$$

$$k_i = \frac{\omega_n^2}{E_m} \quad (4.209b)$$

$$\tau = \frac{k_p}{k_i} = \frac{2\delta}{\omega_n} \quad (4.209c)$$

4. Design and Optimization of the SRF PLL

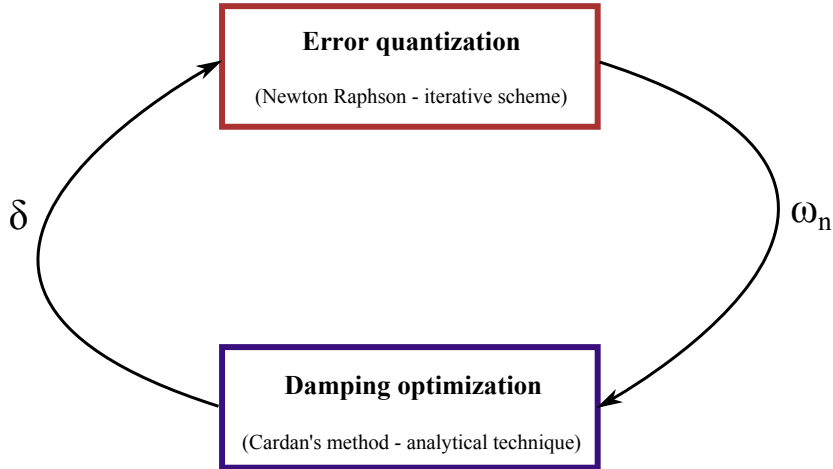


Figure 4.17.: The Self-Consistent Model

Equation (4.209) in turn yield a unique set of (k_p, k_i, τ) . From the user's point of view, this is extremely convenient because, just by specifying the settling time, error band at the settling time, the frequency excursion and the phase jump, the self-consistent model will generate this unique set. Moreover, this property can be made use of, by generating a $(\delta, \omega_n, k_p, k_i, \tau)$ set for every possible combination of frequency step $\Delta\omega_{step}$ and phase jump ϕ in the specified range.

For instance, $(\delta, \omega_n, k_p, k_i, \tau)$ can be calculated for a $\Delta\omega_{step}$ in the range $[-20, 20]$ Hz and a ϕ in the range $[-1, 1]$ rad. The number of data points in this range depends on the resolution required by the user (say increment of $\Delta\omega_{step}$ in 0.5 Hz and increment of ϕ in 0.025 rad). The resulting computation is done for $\frac{20-(-20)}{0.5} = 80$ values of $\Delta\omega_{step}$ and $\frac{1-(-1)}{0.025} = 80$ values of ϕ . i.e., the self-consistent model is solved for $80 \times 80 = 6400$ times. Hence we get 6400 unique sets of $(\delta, \omega_n, k_p, k_i, \tau)$ which correspond to 6400 unique values of $(\Delta\omega_{step}, \phi)$ in the specified range.

If $\Delta\omega_{step}$ is defined along the x -axis and ϕ along the y -axis, each parameter of $(\delta, \omega_n, k_p, k_i, \tau)$ can be plotted along the z -axis, to obtain a 3D lookup table for that parameter. This was done using MATLAB® and five lookup tables for each of $(\delta, \omega_n, k_p, k_i, \tau)$ with $E = 0.02$ rad, $t_0 = 0.01$ s, $\Delta\omega_{step} \in [-20, 20]$ Hz and $\phi \in [-1, 1]$ rad were obtained as shown in figures 4.18, 4.19, 4.20, 4.21 and 4.22.

Having a lookup table gives us the following advantages:

1. Theoretical perspective: It can be used as an educational tool. i.e., certain inferences can be made by looking at the 3D lookup table. A few inferences are:

- (i) Symmetry about the origin: The nature of variation of any of the parameters of the set $(\delta, \omega_n, k_p, k_i, \tau)$ in the 1^{st} quadrant ($\Delta\omega_{step} = +ve$, $\phi = +ve$) is similar to that in the 3^{rd} quadrant ($\Delta\omega_{step} = -ve$, $\phi = -ve$); this also applies to the variation in 2^{nd} and 4^{th} quadrant.

4. Design and Optimization of the SRF PLL

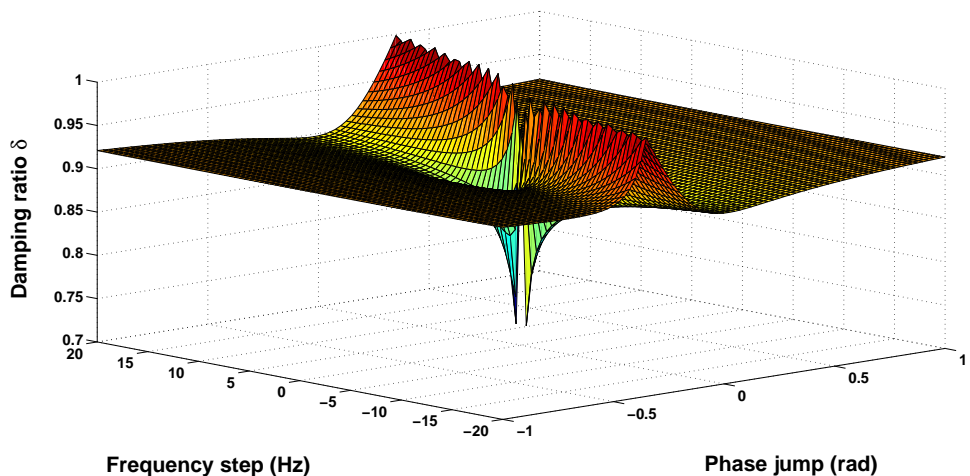


Figure 4.18.: 3D lookup table for the optimised value of damping ratio, δ

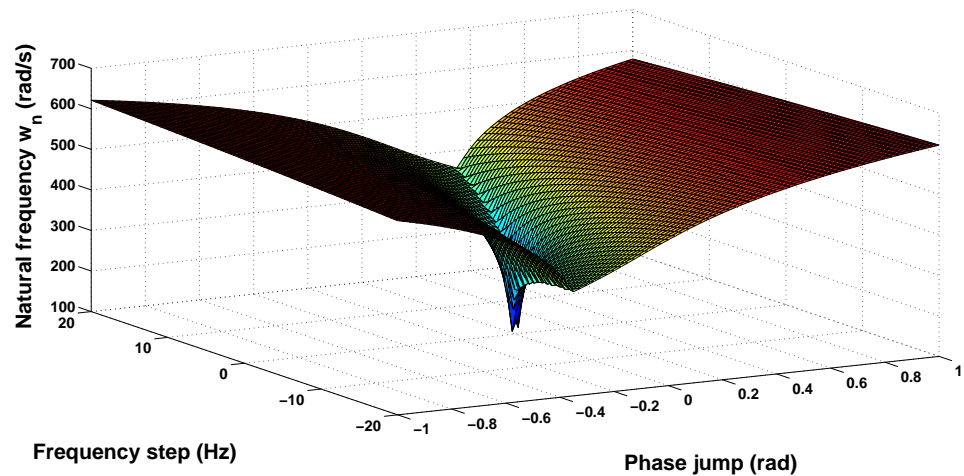


Figure 4.19.: 3D lookup table for the optimised value of natural frequency, ω_n

4. Design and Optimization of the SRF PLL

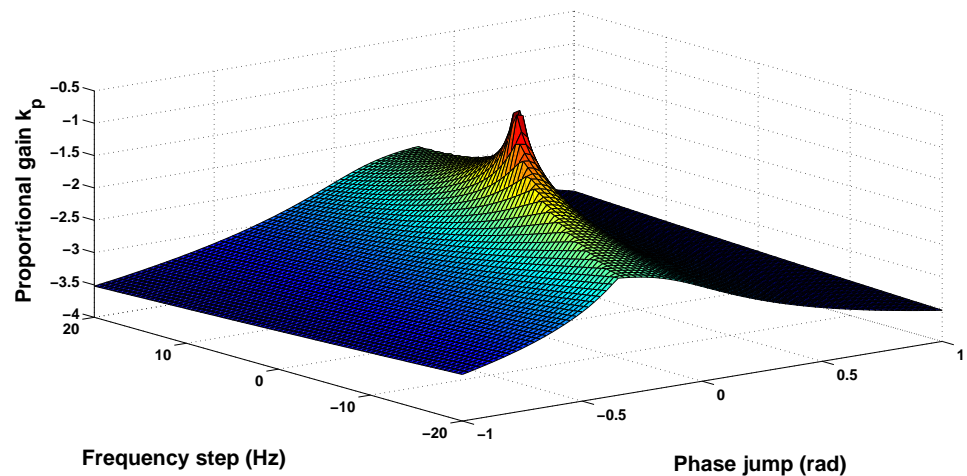


Figure 4.20.: 3D lookup table for the optimised value of proportional gain, k_p

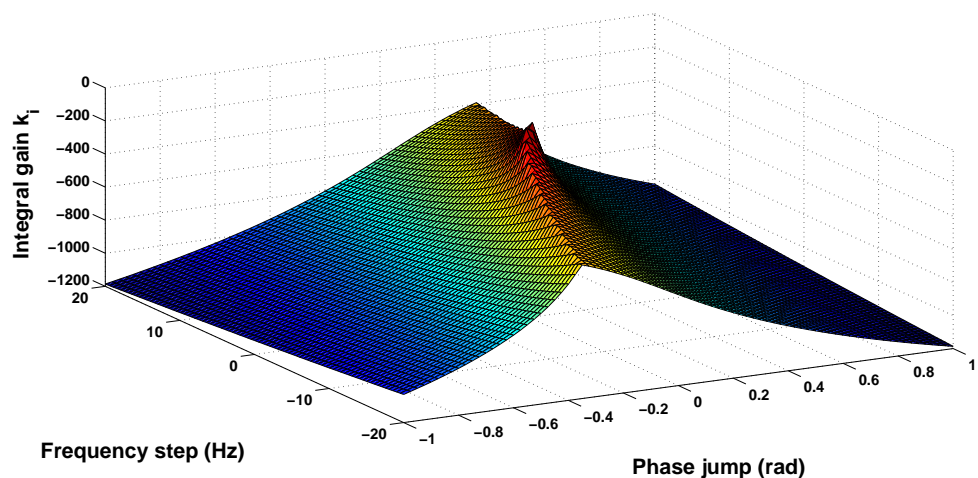


Figure 4.21.: 3D lookup table for the optimised value of integral gain, k_i

4. Design and Optimization of the SRF PLL

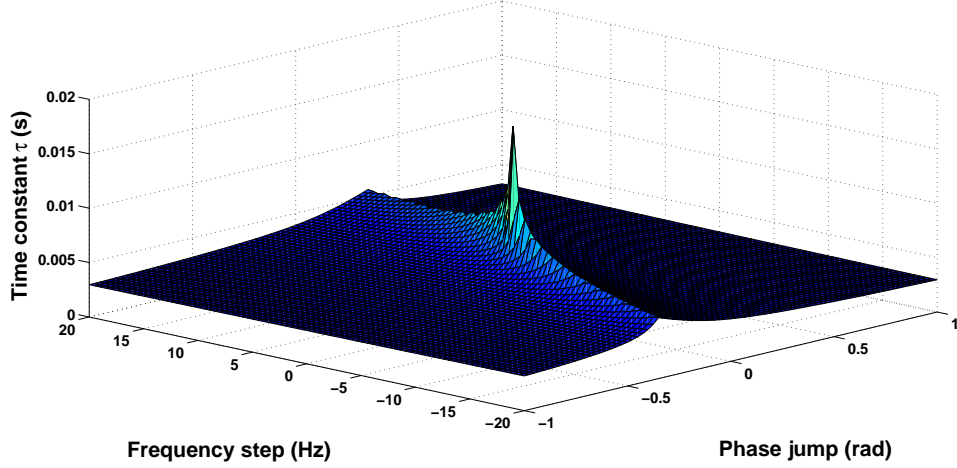


Figure 4.22.: 3D lookup table for the optimised value of time constant, τ

- (ii) One can expect less strained loop filter parameters (k_p, k_i) at lower values of $\Delta\omega_{step}$ and ϕ , through common sense. This can be verified from the 3D lookup tables.
- (iii) From figure 4.20 and 4.21, it can be inferred that the loop filter parameters have to be more stressed when $\Delta\omega_{step}$ and ϕ are of opposite signs (in 2nd and 4th quadrants) compared to when both are of the same signs (in 1st and 3rd quadrants). The mountain-like region in figure 4.20 and 4.21 show this aspect.

2. Practical perspective: To be able to design the loop filter parameters for the instantaneous occurrence of $\Delta\omega_{step}$ and ϕ in the grid, we may need to run the self-consistent model at regular intervals. Since the self-consistent model consists of iterative schemes and involves large computational complexity, it will be a burden on both the processor power and speed. However, *speed of tracking* is an important virtue of any PLL, which cannot be compromised.

Hence running the self-consistent model ‘once’ for the practical range of $\Delta\omega_{step}$ and ϕ in the grid, and storing the optimized values of the loop filter parameters in the form of a lookup table on the micro-controller (or DSP) would eliminate all the constraints on speed and computing power of the micro-controller (or DSP). In this way, depending on the grid situation ($\Delta\omega_{step}, \phi$), the corresponding optimized pair of (k_p, k_i) can be picked from the lookup table.

4.5. Conclusions

A comprehensive discussion on the design optimization of the loop filter is presented. Further, a novel technique for optimizing the filter parameters with a self-consistent set of δ and ω_n is proposed. The advantages of the new technique are illustrated.

5. Other PLLs in literature

The development of robust PLLs for phase tracking under grid imperfections has seen many improvisations over the conventional SRF PLL. Three of such schemes are introduced in this chapter.

5.1. Why go for other PLL schemes

While SRF PLL is capable of tracking the phase of the grid voltages during frequency changes and phase jumps, it loses track when the grid is polluted with unbalance and harmonics. This is because SRF PLL expects the positive sequence fundamental component of the grid voltage as its input. Hence, the need for better PLL schemes is clearly a must. The modified PLLs use different techniques to filter out the unwanted components from the polluted grid and allow only the positive sequence fundamental component to be fed to SRF PLL.

5.2. Decoupled Double Synchronous Reference Frame PLL (DDSRF PLL)

The DDSRF PLL is an improvisation over the conventional SRF PLL to cope with voltage unbalance. A detailed analysis of DDSRF PLL is available in [1]. The concept behind its working is presented in this section.

The positive sequence fundamental component of the error voltage (v_d) is extracted in the synchronously rotating reference frame before feeding it to the loop filter in DDSRF PLL. Once this is done, the working is similar to SRF PLL.

The extraction of the positive sequence fundamental component is done through the following two processes:

1. Two separate Park transformations
2. The development of a decoupling network

Hence the terms ‘decoupled’ (use of a decoupling network) and ‘double’ (two Park transformations) are used in naming DDSRF PLL.

5. Other PLLs in literature

5.2.1. Two separate Park transformations

A set of unbalanced grid voltages v_a , v_b and v_c can be expressed as

$$\begin{bmatrix} v_a \\ v_b \\ v_c \end{bmatrix} = V_m^{+1} \begin{bmatrix} \cos(\theta_{ef}^+) \\ \cos(\theta_{ef}^+ - \frac{2\pi}{3}) \\ \cos(\theta_{ef}^+ + \frac{2\pi}{3}) \end{bmatrix} + V_m^{-1} \begin{bmatrix} \cos(\theta_{ef}^-) \\ \cos(\theta_{ef}^- - \frac{2\pi}{3}) \\ \cos(\theta_{ef}^- + \frac{2\pi}{3}) \end{bmatrix} \quad (5.1)$$

where

$$\theta_{ef}^+ = \omega t + \phi^+ \quad (5.2)$$

$$\theta_{ef}^- = -\omega t + \phi^- \quad (5.3)$$

After Clarke transformation, v_β and v_α are given by (3.15). i.e.,

$$\begin{bmatrix} v_\beta \\ v_\alpha \end{bmatrix} = V_m^{+1} \begin{bmatrix} \cos(\theta_{ef}^+) \\ -\sin(\theta_{ef}^+) \end{bmatrix} + V_m^{-1} \begin{bmatrix} \cos(\theta_{ef}^-) \\ -\sin(\theta_{ef}^-) \end{bmatrix} \quad (5.4)$$

Two separate Park transformations (double SRF) are done on v_β and v_α ; i.e., one on a reference frame rotating in the positive direction, and other on a reference frame rotating in the negative direction. The respective d-q components are given by (3.16) as

$$\begin{bmatrix} v_q^{+1} \\ v_d^{+1} \end{bmatrix} = V_m^{+1} \begin{bmatrix} \cos(\theta_{ef}^+ - \hat{\theta}) \\ -\sin(\theta_{ef}^+ - \hat{\theta}) \end{bmatrix} + V_m^{-1} \begin{bmatrix} \cos(\theta_{ef}^- - \hat{\theta}) \\ -\sin(\theta_{ef}^- - \hat{\theta}) \end{bmatrix} \quad (5.5)$$

$$\begin{bmatrix} v_q^{-1} \\ v_d^{-1} \end{bmatrix} = V_m^{+1} \begin{bmatrix} \cos(\theta_{ef}^+ + \hat{\theta}) \\ -\sin(\theta_{ef}^+ + \hat{\theta}) \end{bmatrix} + V_m^{-1} \begin{bmatrix} \cos(\theta_{ef}^- + \hat{\theta}) \\ -\sin(\theta_{ef}^- + \hat{\theta}) \end{bmatrix} \quad (5.6)$$

When the estimated angle follows the grid phase angle closely,

$$\hat{\theta} = \omega t \quad (5.7)$$

Substituting (5.2), (5.3) and (5.7) in (5.5) and (5.6), we get

$$\begin{bmatrix} v_q^{+1} \\ v_d^{+1} \end{bmatrix} = V_m^{+1} \begin{bmatrix} \cos \phi^+ \\ -\sin \phi^+ \end{bmatrix} + V_m^{-1} \begin{bmatrix} \cos(-2\omega t + \phi^-) \\ -\sin(-2\omega t + \phi^-) \end{bmatrix} \quad (5.8)$$

$$= V_m^{+1} \begin{bmatrix} \cos \phi^+ \\ -\sin \phi^+ \end{bmatrix} + V_m^{-1} \cos \phi^- \begin{bmatrix} \cos(2\omega t) \\ \sin(2\omega t) \end{bmatrix} + V_m^{-1} \sin \phi^- \begin{bmatrix} \sin(2\omega t) \\ -\cos(2\omega t) \end{bmatrix} \quad (5.9)$$

5. Other PLLs in literature

$$\begin{bmatrix} v_q^{-1} \\ v_d^{-1} \end{bmatrix} = V_m^{+1} \begin{bmatrix} \cos(2\omega t + \phi^+) \\ -\sin(2\omega t + \phi^+) \end{bmatrix} + V_m^{-1} \begin{bmatrix} \cos \phi^- \\ -\sin \phi^- \end{bmatrix} \quad (5.10)$$

$$= V_m^{-1} \begin{bmatrix} \cos \phi^- \\ -\sin \phi^- \end{bmatrix} + V_m^{+1} \cos \phi^+ \begin{bmatrix} \cos(2\omega t) \\ -\sin(2\omega t) \end{bmatrix} + V_m^{+1} \sin \phi^+ \begin{bmatrix} -\sin(2\omega t) \\ -\cos(2\omega t) \end{bmatrix} \quad (5.11)$$

From (5.9) and (5.11), it is evident that both the voltage error (v_d) and space vector (v_q) are coupled with ' 2ω ' oscillations. The positive sequence fundamental component can be obtained from (5.9), if the ' 2ω ' oscillations are decoupled. This is done using the decoupling network.

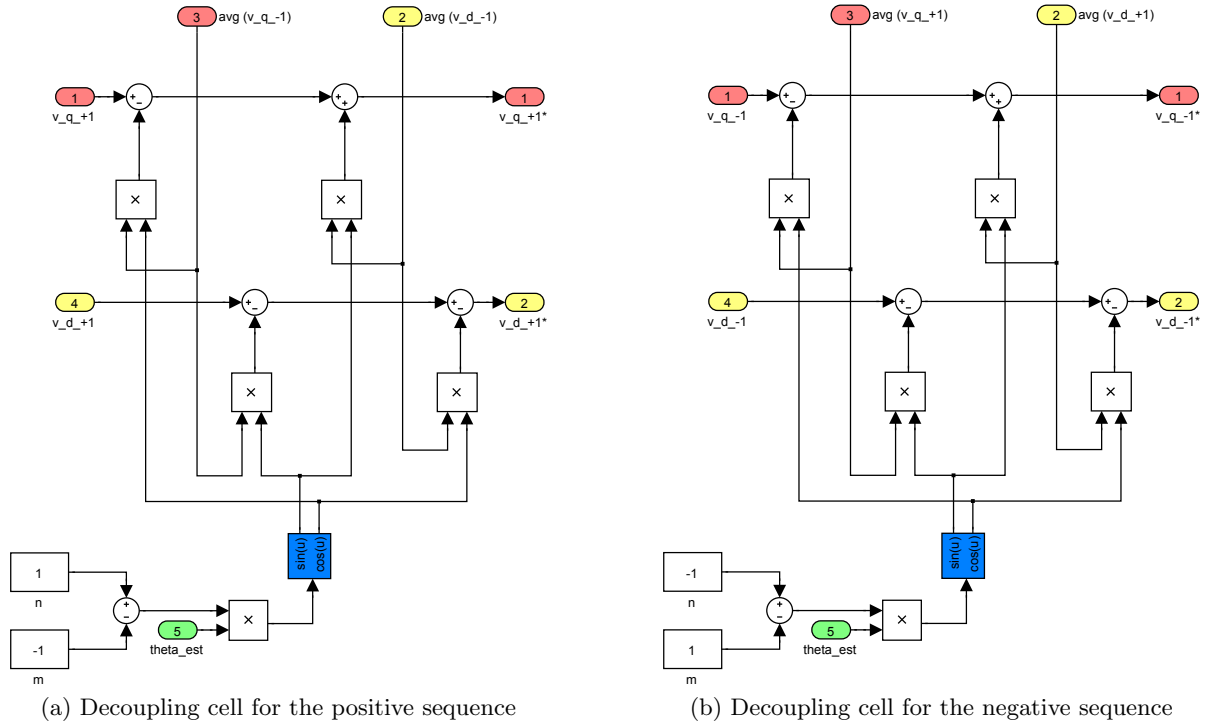


Figure 5.1.: Decoupling cells used in the decoupling network

5.2.2. Decoupling network

The decoupling network is developed by making use of the following two properties of (5.9) and (5.11):

1. The average of the positive sequence components (v_q^{+1} and v_d^{+1}) gives the fundamental positive sequence voltage. Similarly, the average of the negative sequence components (v_q^{-1} and v_d^{-1}) gives the fundamental negative sequence voltage.
2. The magnitude of oscillations in v_q^{+1} and v_d^{+1} is determined by V_m^{-1} . Also, the magnitude of oscillations in v_q^{-1} and v_d^{-1} is determined by V_m^{+1} .

5. Other PLLs in literature

If a mechanism is developed to compute the average values of v_q^{+1} , v_d^{+1} , v_q^{-1} and v_d^{-1} , denoted by \bar{v}_q^{+1} , \bar{v}_d^{+1} , \bar{v}_q^{-1} and \bar{v}_d^{-1} respectively, then the decoupled components (denoted by *) are given by

$$v_q^{+1*} = v_q^{+1} - \bar{v}_q^{-1} \cos(2\hat{\theta}) + \bar{v}_d^{-1} \sin(2\hat{\theta}) \quad (5.12a)$$

$$v_d^{+1*} = v_d^{+1} - \bar{v}_q^{-1} \sin(2\hat{\theta}) - \bar{v}_d^{-1} \cos(2\hat{\theta}) \quad (5.12b)$$

$$v_q^{-1*} = v_q^{-1} - \bar{v}_q^{+1} \cos(2\hat{\theta}) - \bar{v}_d^{+1} \sin(2\hat{\theta}) \quad (5.13a)$$

$$v_d^{-1*} = v_d^{-1} + \bar{v}_q^{+1} \sin(2\hat{\theta}) - \bar{v}_d^{+1} \cos(2\hat{\theta}) \quad (5.13b)$$

Equations (5.12) and (5.13) can be implemented in the form of a decoupling cell as shown in figure 5.1. To calculate the averages \bar{v}_q^{+1} , \bar{v}_d^{+1} , \bar{v}_q^{-1} and \bar{v}_d^{-1} , a cross-feedback network is used as shown in figure 5.2.

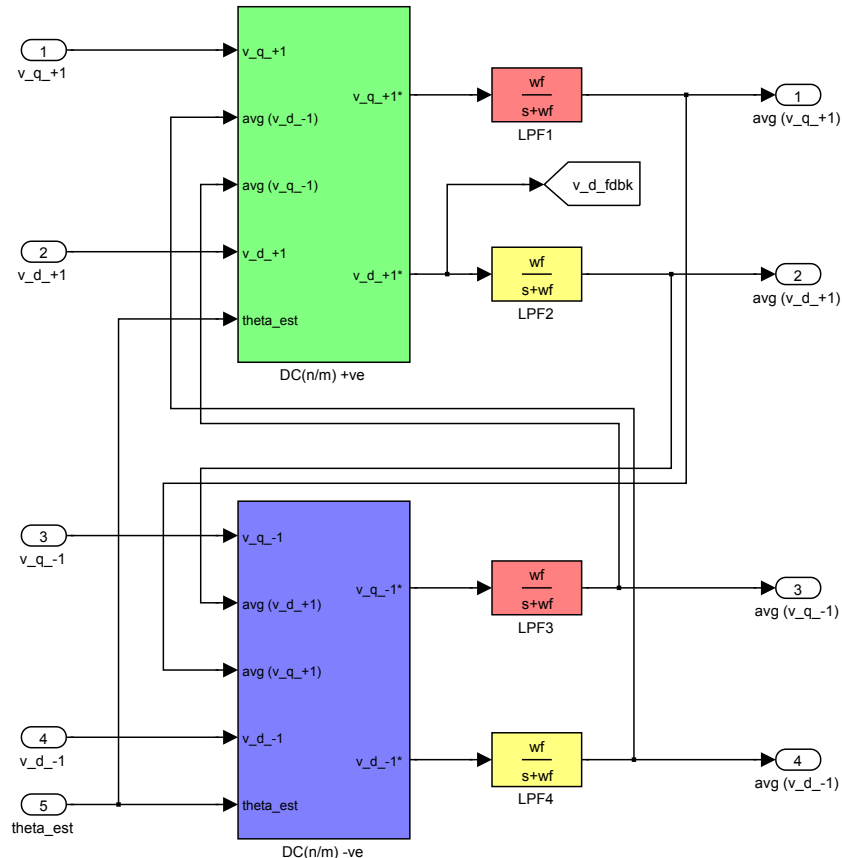


Figure 5.2.: Decoupling network

In this decoupling network, a first-order low pass filter is used. i.e.,

$$\text{LPF}(s) = \frac{s}{s + \omega_f} \quad (5.14)$$

5. Other PLLs in literature

The decoupling can be qualitatively understood as follows: Initially, the average values of the d-q components are zero, resulting in oscillating v_q^{+1*} , v_d^{+1*} , v_q^{-1*} and v_d^{-1*} . These oscillations are somewhat attenuated by the LPF. In the next iteration, the attenuated values are fed to the decoupling network. This in turn results in improved values (lesser magnitude of oscillations) of v_q^{+1*} , v_d^{+1*} , v_q^{-1*} and v_d^{-1*} . The process continues and eventually results in complete decoupling.

A detailed analysis of the decoupling network is beyond the scope of this report and is available in [1]. Moreover, [1] justifies the fact that choosing $\omega_f = \sqrt{2}\omega$ results in optimum dynamic performance.

The decoupled positive sequence fundamental d-component, v_d^{+1*} is fed to the loop filter. Then on, the working of DDSRF PLL is same as that of the conventional SRF PLL.

5.3. Dual Second Order Generalized Integrator based PLL (DSOGI PLL)

DSOGI PLL is another improvisation on the conventional SRF PLL. The objective of the second order generalized integrator is to extract the positive sequence fundamental component of the grid voltage in the stationary reference frame, before feeding it to the Park transformation block of SRF PLL.

To understand the construction and working of DSOGI PLL, it is important to know the method to extract the positive sequence component from a grid contaminated with both positive and negative sequence components. This is explained below.

From Fortescue's theory of symmetrical components, the positive sequence component is given by

$$v_a^+ = \frac{1}{3}(v_a + av_b + a^2v_c) \quad (5.15)$$

where v_a , v_b and v_c are the grid phase voltages and $a = e^{j\frac{2\pi}{3}}$. Also

$$v_b^+ = a^2v_a^+ \quad (5.16)$$

$$v_c^+ = av_a^+ \quad (5.17)$$

Substituting (5.15) in (5.16) and (5.17), we obtain

$$\underbrace{\begin{bmatrix} v_a^+ \\ v_b^+ \\ v_c^+ \end{bmatrix}}_{\mathbf{v}_{abc}^+} = \underbrace{\frac{1}{3} \begin{bmatrix} 1 & a & a^2 \\ a^2 & 1 & a \\ a & a^2 & 1 \end{bmatrix}}_{\mathbf{T}^+} \underbrace{\begin{bmatrix} v_a \\ v_b \\ v_c \end{bmatrix}}_{\mathbf{v}_{abc}} \quad (5.18)$$

5. Other PLLs in literature

i.e.,

$$\mathbf{v}_{\text{abc}}^+ = \mathbf{T}^+ \mathbf{v}_{\text{abc}} \quad (5.19)$$

Applying Clarke transformation,

$$\underbrace{\begin{bmatrix} v_\beta \\ v_\alpha \end{bmatrix}}_{\mathbf{v}_{\beta\alpha}} = \underbrace{\frac{2}{3} \begin{bmatrix} 1 & -\frac{1}{2} & -\frac{1}{2} \\ 0 & -\frac{\sqrt{3}}{2} & \frac{\sqrt{3}}{2} \end{bmatrix}}_{\mathbf{T}_{\beta\alpha}} \underbrace{\begin{bmatrix} v_a \\ v_b \\ v_c \end{bmatrix}}_{\mathbf{v}_{\text{abc}}} \quad (5.20)$$

i.e.,

$$\mathbf{v}_{\beta\alpha} = \mathbf{T}_{\beta\alpha} \mathbf{v}_{\text{abc}} \quad (5.21)$$

Similarly,

$$\mathbf{v}_{\beta\alpha}^+ = \mathbf{T}_{\beta\alpha} \mathbf{v}_{\text{abc}}^+ \quad (5.22)$$

Substituting (5.19) in (5.22),

$$\mathbf{v}_{\beta\alpha}^+ = \mathbf{T}_{\beta\alpha} \mathbf{T}^+ \mathbf{v}_{\text{abc}} \quad (5.23)$$

Substituting for \mathbf{v}_{abc} from (5.21) in (5.23),

$$\mathbf{v}_{\beta\alpha}^+ = \mathbf{T}_{\beta\alpha} \mathbf{T}^+ (\mathbf{T}_{\beta\alpha})^{-1} \mathbf{v}_{\beta\alpha} \quad (5.24)$$

Expanding and simplifying,

$$\begin{bmatrix} v_\beta^+ \\ v_\alpha^+ \end{bmatrix} = \frac{1}{2} \begin{bmatrix} 1 & q \\ -q & 1 \end{bmatrix} \begin{bmatrix} v_\beta \\ v_\alpha \end{bmatrix} \quad (5.25)$$

i.e.,

$$v_\beta^+ = \frac{1}{2} (v_\beta + q v_\alpha) \quad (5.26)$$

$$v_\alpha^+ = \frac{1}{2} (-q v_\beta + v_\alpha) \quad (5.27)$$

where $q = -j$ (short for ‘quadrature’).

Hence, from (5.26) and (5.27), it is clear that to calculate the positive sequence components, a quadrature signals generator is required. i.e., to compute v_β^+ , v_β and the quadrature of v_α are required, and to compute v_α^+ , v_α and the quadrature of v_β are required.

5. Other PLLs in literature

5.3.1. Second Order Generalized Integrator for Quadrature Signals Generation (SOGI-QSG)

SOGI-QSG contains two outputs; the fundamental component of the input voltage and its quadrature. Figure 5.3 shows SOGI-QSG for v_β and v_α .

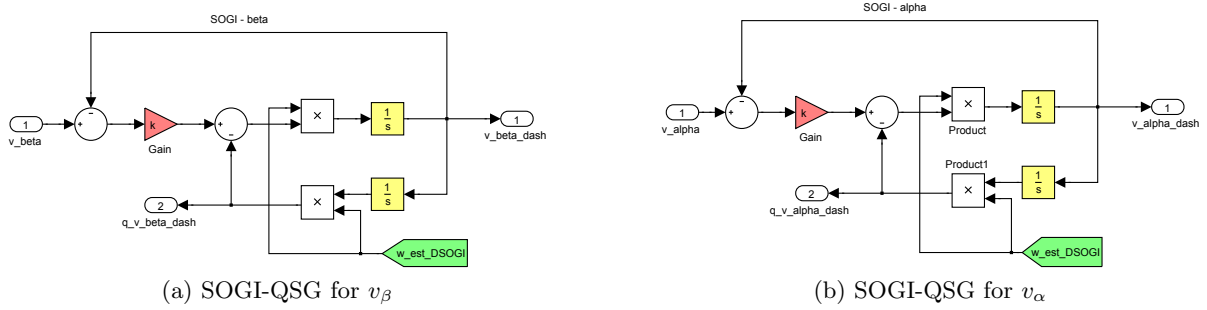


Figure 5.3.: SOGI - Quadrature Signals Generator

The transfer functions of the SOGI-QSG corresponding to the two output points are

$$D(s) = \frac{V'(s)}{V(s)} = \frac{k\omega' s}{s^2 + k\omega' s + \omega'^2} \quad (5.28)$$

$$Q(s) = \frac{qV'(s)}{V(s)} = \frac{k\omega'^2}{s^2 + k\omega' s + \omega'^2} \quad (5.29)$$

The magnitude and phase of $D(s)$ and $Q(s)$ are given by

$$|D| = \frac{k\omega\omega'}{\sqrt{(k\omega\omega')^2 + (\omega^2 - \omega'^2)^2}} \quad (5.30a)$$

$$\angle D = \tan^{-1} \left(\frac{\omega'^2 - \omega^2}{k\omega\omega'} \right) \quad (5.30b)$$

$$|Q| = \frac{\omega'}{\omega} |D| \quad (5.31a)$$

$$\angle Q = \angle D - \frac{\pi}{2} \quad (5.31b)$$

It is worth to remark from (5.31b) that qv' always lags v' by 90° . The Bode plot of $D(s)$ and $Q(s)$ for three different values of k are given in figure 5.4. $k = \sqrt{2}$ is chosen for a critically damped response [2].

5. Other PLLs in literature

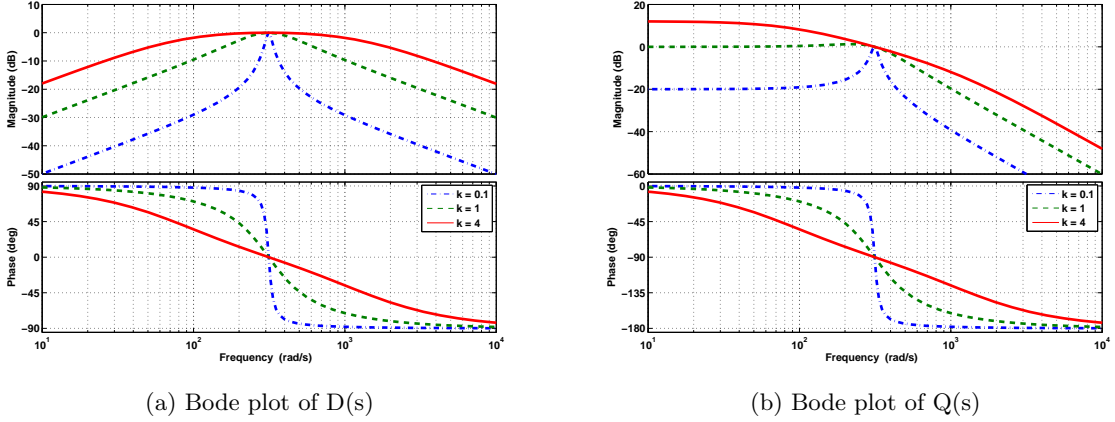


Figure 5.4.: Bode plots for SOGI - QSG

From the Bode plots it is clear that the SOGI-QSG scheme

- (i) attenuates the harmonics present in the grid voltage and filters out the fundamental component as one of its outputs, v'
- (ii) also generates the quadrature of v' , namely qv'

Since a method for quadrature signals generation is established, (5.26) and (5.27) can be used to calculate the positive sequence.

5.3.2. Positive Sequence Detector using a dual SOGI-QSG

Two SOGIs, one for v_β and v_α each, and a positive sequence calculator (PSC) (based on (5.26) and (5.27)) is used as shown in figure 5.5, to generate the positive sequence fundamental components, v_β^+ and v_α^+ . They are then fed to the Park transformation block of the conventional SRF PLL.

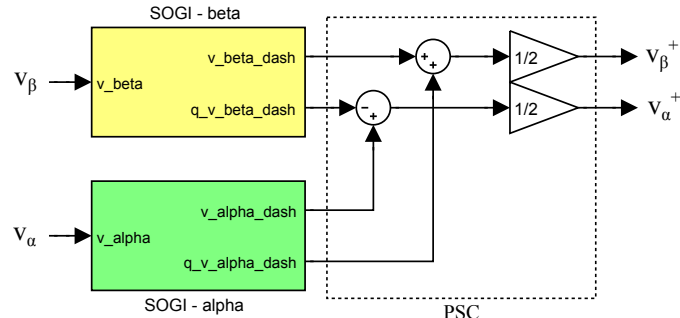


Figure 5.5.: DSOGI-QSG with Positive Sequence Calculator

5. Other PLLs in literature

It is important to note that a frequency adaptive DSOGI PLL is required for tracking frequency changes in the grid voltage. Hence, ω computed by SRF PLL is fed back to the DSOGI, thus adaptively changing ω' .

To sum up,

1. SOGI-QSG suppresses the harmonics present in the grid and generates the fundamental component and its quadrature
2. Dual SOGI and PSC are used to extract the positive sequence fundamental component
3. The computed frequency from SRF PLL is adaptively fed back to the DSOGI block to take care of frequency excursions in the grid

5.4. Multiple-Complex Coefficient-Filter based PLL (MCCF PLL)

MCCF based PLL, as the name suggests, makes use of many complex coefficient filters (CCFs) in parallel, to extract out the positive sequence fundamental component. The CCFs are placed in the stationary reference frame. To understand how MCCF PLL works, it is mandatory to know the filtering characteristics of a basic complex coefficient filter.

5.4.1. A basic CCF

All the real coefficient filters (RCFs) are frequency selective but not polarity selective. i.e., RCFs cannot distinguish between ' $+\omega$ ' and ' $-\omega$ '. In other words, RCFs are symmetric about the $\omega = 0$ axis. On the other hand, CCFs have the unique feature of both frequency and polarity selectivity. This is evident from figure 5.6, which compares the frequency response of RCF with that of CCF.

A typical first order CCF can be expressed as

$$\text{CCF}(s) = \frac{\omega_c}{s - j\omega_0 + \omega_c} \quad (5.32)$$

The magnitude of (5.32) is given by

$$M = \frac{\omega_c}{\sqrt{(\omega - \omega_0)^2 + \omega_c^2}} \quad (5.33)$$

5. Other PLLs in literature

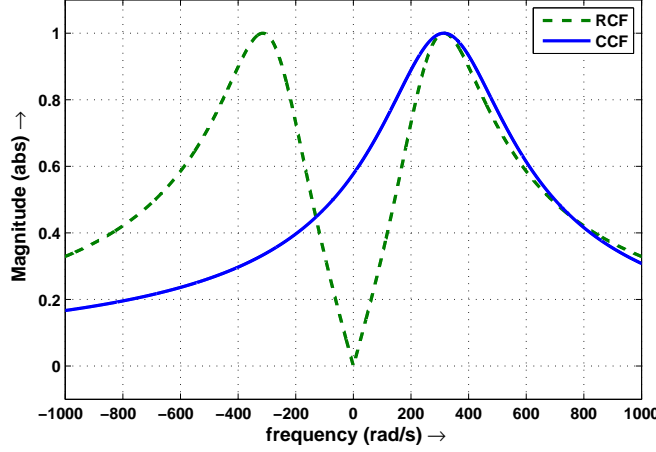


Figure 5.6.: Frequency response of Real and Complex Coefficient Filters

From (5.33), the following can be inferred:

$$(i) \quad M\Big|_{\omega=\omega_0} = 1$$

The frequency ω_0 is passed through the CCF as such, without any attenuation.

$$(ii) \quad M\Big|_{\omega=-\omega_0} = \frac{\omega_c}{\sqrt{4\omega_0^2 + \omega_c^2}}$$

The corresponding negative sequence component gets attenuated by a factor of $\frac{\omega_c}{\sqrt{4\omega_0^2 + \omega_c^2}}$.

$$(iii) \quad M\Big|_{\omega=\omega_0} \neq M\Big|_{\omega=-\omega_0}$$

CCFs are not symmetric about the $\omega = 0$ axis; i.e., the positive and negative sequence components can be distinguished.

Hence multiple CCFs can be used to extract out each positive and negative sequence n^{th} order component individually. A general CCF module that extracts the positive sequence n^{th} order component is given by

$$\text{CCF}_{n+}(s) = \frac{\omega_c}{s - jn\omega_0 + \omega_c} \quad (5.34)$$

To extract the negative sequence n^{th} order component,

$$\text{CCF}_{n-}(s) = \frac{\omega_c}{s + jn\omega_0 + \omega_c} \quad (5.35)$$

5. Other PLLs in literature

5.4.2. Building a CCF

The design of a CCF is a difficult task as it involves complex coefficients. The following property is employed to design a CCF.

$$\begin{bmatrix} v_\beta \\ v_\alpha \end{bmatrix} = \begin{bmatrix} V_m \cos \theta_{ef} \\ -V_m \sin \theta_{ef} \end{bmatrix} \quad (5.36)$$

$$= \begin{bmatrix} V_m \cos \theta_{ef} \\ V_m \cos(\frac{\pi}{2} + \theta_{ef}) \end{bmatrix} \quad (5.37)$$

which shows that

$$v_\alpha = jv_\beta \quad (5.38)$$

In general, for the positive sequence components,

$$v_\alpha^{n+} = jv_\beta^{n+} \quad (5.39)$$

Similarly for the negative sequence components,

$$v_\alpha^{n-} = jv_\beta^{n-} \quad (5.40)$$

Now consider a positive sequence n^{th} order CCF:

$$\frac{V_\beta^{n+}(s)}{V_\beta(s)} = \frac{\omega_c}{s - jn\omega_0 + \omega_c} \quad (5.41)$$

$$\Rightarrow sV_\beta^{n+}(s) - n\omega_0(jV_\beta^{n+}(s)) + \omega_c V_\beta^{n+}(s) = \omega_c V_\beta(s) \quad (5.42)$$

Substituting for $jV_\beta^{n+}(s)$ from (5.39),

$$sV_\beta^{n+}(s) - n\omega_0 V_\alpha^{n+}(s) + \omega_c V_\beta^{n+}(s) = \omega_c V_\beta(s) \quad (5.43)$$

$$\Rightarrow V_\beta^{n+}(s) = \frac{1}{s} \left[n\omega_0 V_\alpha^{n+}(s) - \omega_c V_\beta^{n+}(s) + \omega_c V_\beta(s) \right] \quad (5.44)$$

Similarly,

$$\frac{V_\alpha^{n+}(s)}{V_\alpha(s)} = \frac{\omega_c}{s - jn\omega_0 + \omega_c} \quad (5.45)$$

$$\Rightarrow sV_\alpha^{n+}(s) + n\omega_0(-jV_\alpha^{n+}(s)) + \omega_c V_\alpha^{n+}(s) = \omega_c V_\alpha(s) \quad (5.46)$$

5. Other PLLs in literature

Substituting for $-jV_\alpha^{n+}(s)$ from (5.39),

$$sV_\alpha^{n+}(s) + n\omega_0 V_\beta^{n+}(s) + \omega_c V_\alpha^{n+}(s) = \omega_c V_\alpha(s) \quad (5.47)$$

$$\Rightarrow V_\alpha^{n+}(s) = \frac{1}{s} \left[-n\omega_0 V_\beta^{n+}(s) - \omega_c V_\alpha^{n+}(s) + \omega_c V_\alpha(s) \right] \quad (5.48)$$

Equations (5.44) and (5.48) are implemented as shown in figure 5.7a. The negative sequence component filter, $\text{CCF}_{n-}(s)$ is obtained by replacing n by $-n$, and is shown in figure 5.7b.

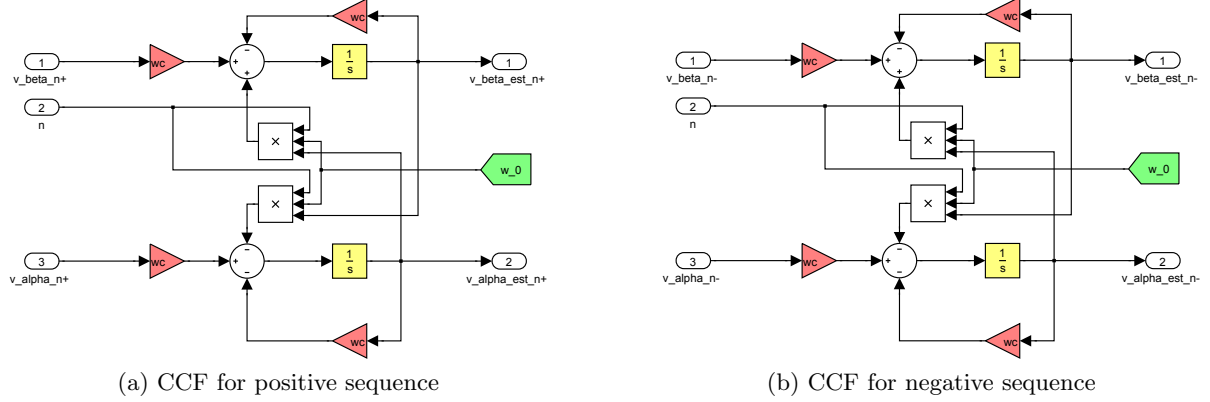


Figure 5.7.: Complex coefficient filter

5.4.3. MCCF structure

Multiple CCFs are connected in parallel to obtain the MCCF structure. Figure 5.8 shows 4 CCF modules for separating the positive and negative sequences of the fundamental and the 5th order harmonic respectively. The MCCF structure is self explanatory. A detailed analysis using state space modelling is done in [3]. The positive sequence fundamental component is then fed to SRF PLL. To track in case of frequency excursions, a frequency adaptive mechanism (similar to DSOGI PLL) is used, wherein, the calculated ω is fed back to the MCCF structure to adaptively change ω_0 .

5. Other PLLs in literature

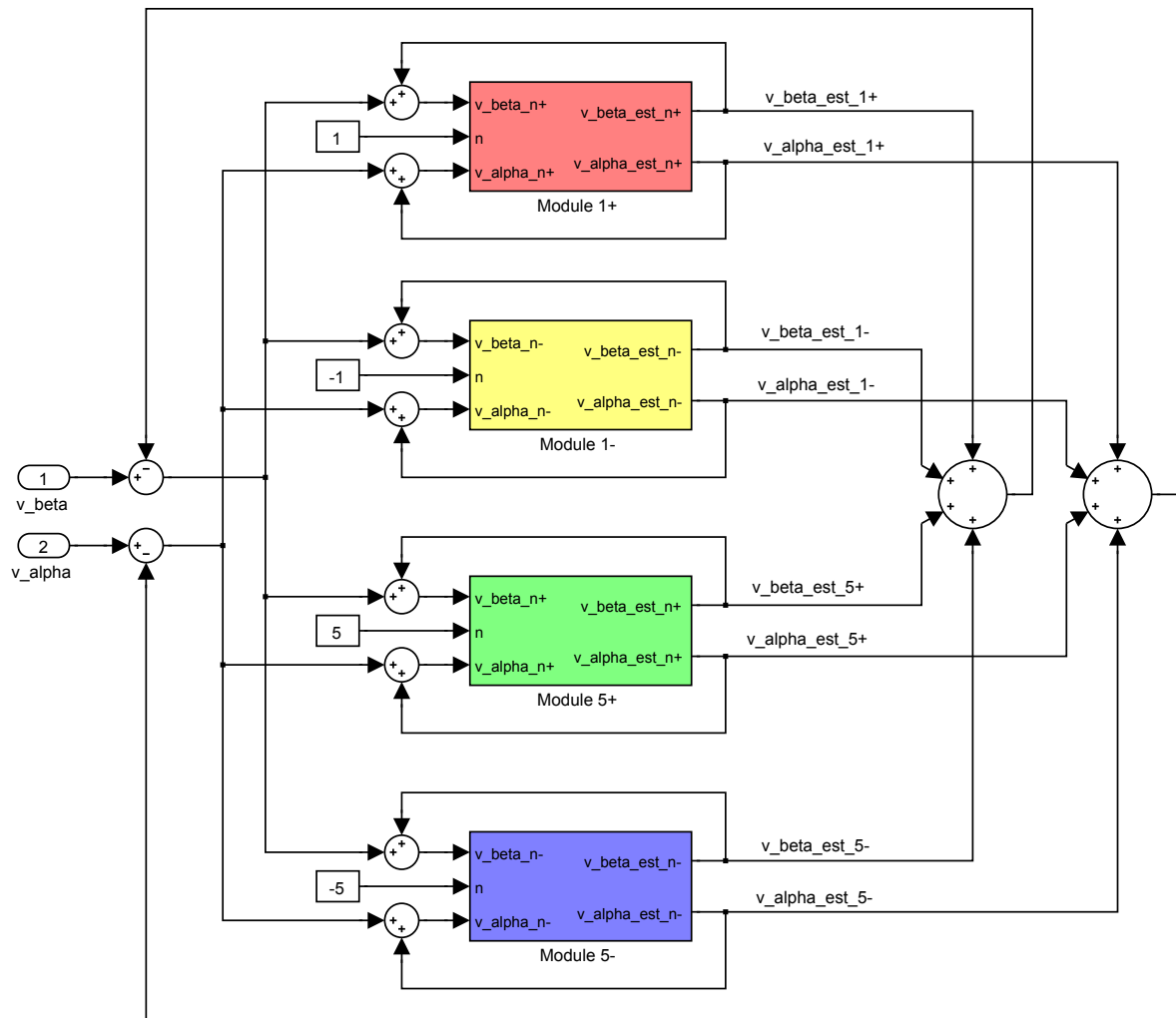


Figure 5.8.: MCCF structure

6. Simulation Models

This chapter elaborates on the simulations that were performed to establish the nature of the existing 3-phase PLL schemes in literature and to implement the proposed self-consistent model for optimizing the loop filter parameters of SRF PLL. The following PLL schemes were chosen for comparison:

1. Synchronous Reference Frame PLL (SRF PLL)
2. Decoupled Double Synchronous Reference Frame PLL (DDSRF PLL) [1]
3. Dual Second Order Generalized Integrator based PLL (DSOGI PLL) [2]
4. Multiple-Complex Coefficient-Filter based PLL (MCCF PLL) [3]

Conventional SRF PLL (as discussed in chapter 3) contains the Clarke and Park transformations, PI loop filter and an integrator as shown in figure 3.1. These blocks can be modelled in Simulink[®] to obtain SRF PLL as shown in figure 6.1. DDSRF PLL contains an added block called the decoupling network which decouples the positive and negative sequence components of the unbalanced grid voltages, in the synchronous reference frame. The Simulink model of DDSRF PLL is shown in figure 6.2. DSOGI PLL comprises of three fundamental blocks, namely, the quadrature-signals generator (QSG), the positive-sequence calculator (PSC) and SRF PLL. The function of QSG and PSC is to filter out the positive sequence fundamental component under unbalanced and distorted grid operating conditions. This is done in the stationary reference frame, before being fed to SRF PLL. The Simulink model of DSOGI PLL is shown in figure 6.3. MCCF PLL uses a multiple complex coefficient filter which has a unique property of being able to distinguish between positive and negative sequences of a particular frequency, unlike filters whose frequency response is symmetric about zero frequency. MCCF module operates in the stationary reference frame whose output is fed to the fundamental SRF PLL. The Simulink model of MCCF PLL is shown in figure 6.4.

To test the working of each of the above schemes, it is required to create a grid that is disturbed with

- unbalanced voltages
- harmonics
- frequency excursion
- phase jump

6. Simulation Models

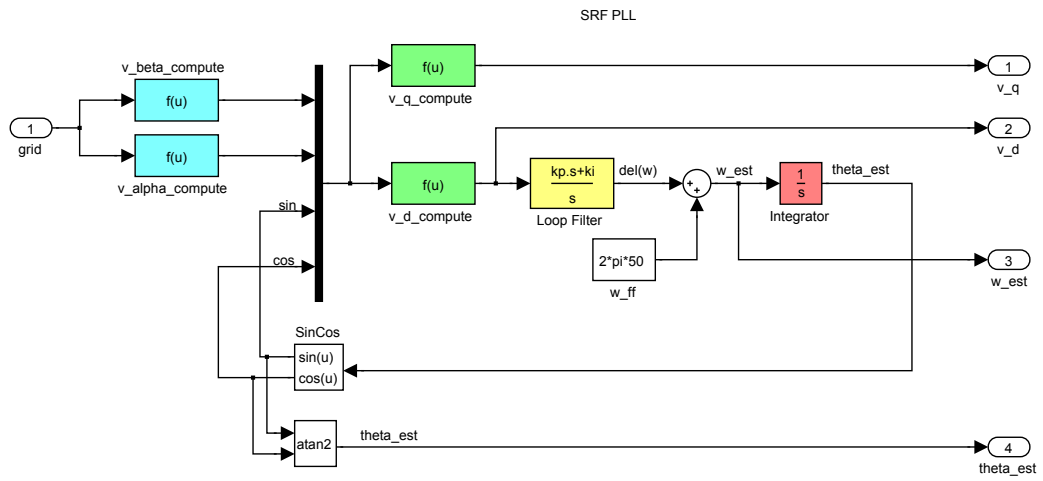


Figure 6.1.: Simulink model of SRF PLL

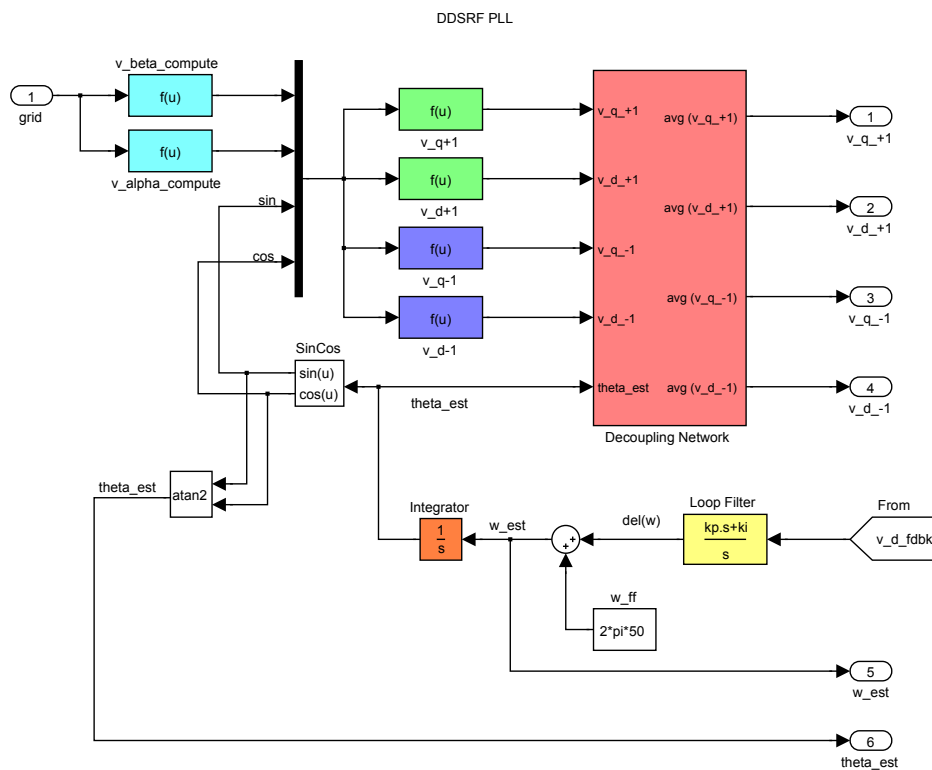


Figure 6.2.: Simulink model of DDSRF PLL

6. Simulation Models

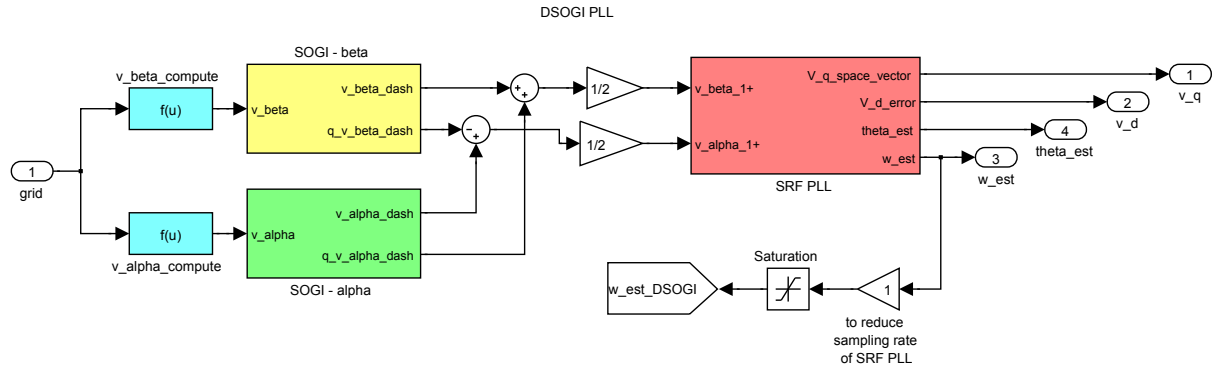


Figure 6.3.: Simulink model of DSOGI PLL

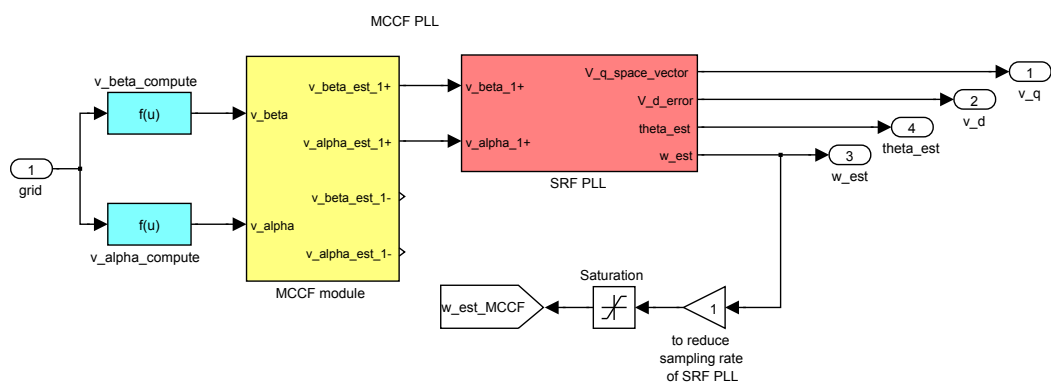


Figure 6.4.: Simulink model of MCCF PLL

6. Simulation Models

Hence a grid simulator (figure 6.5) is constructed in Simulink, which simulates each of the above grid imperfections.

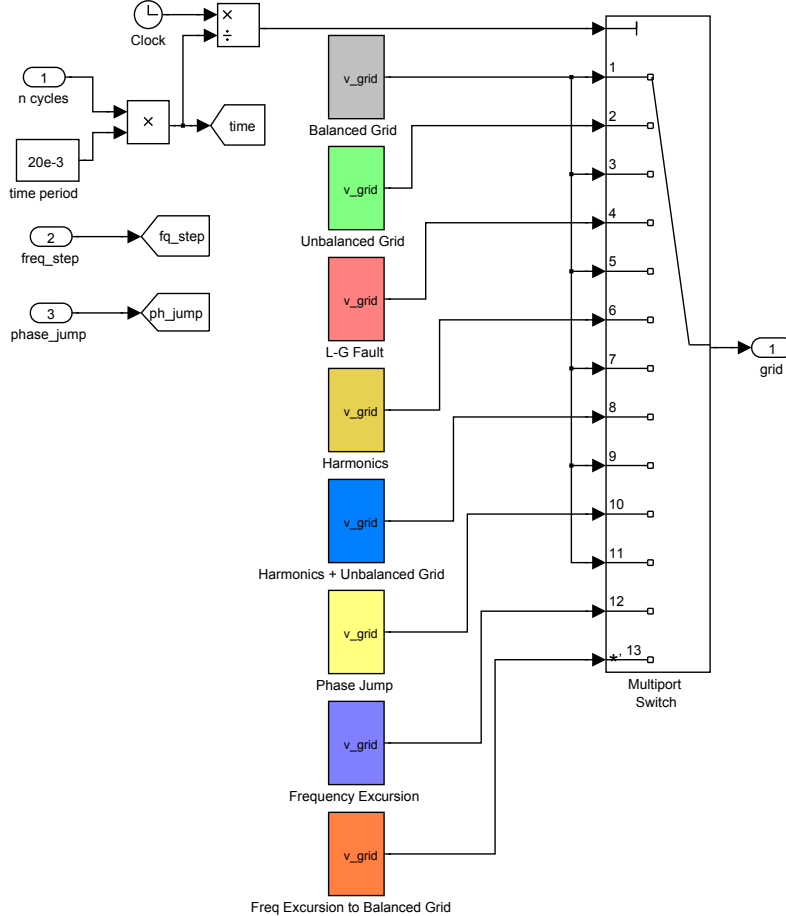


Figure 6.5.: The grid simulator used to create grid imperfections

To have a common platform for comparison, the four PLLs are combined in a single Simulink model and are run in parallel, as shown in figure 6.6.

An important block of each of these PLL models is the loop filter. The loop filter parameters, namely, the proportional gain k_p and the integral gain k_i , need to be designed and fed before the simulation is run. This can be done either using the Wiener optimization method (as discussed in section 3.5) or the proposed self-consistent model based method (as discussed in section 4.4.2).

Once the complete model is run, the following data is computed:

- Space vector, v_q
- Voltage error, v_d

6. Simulation Models

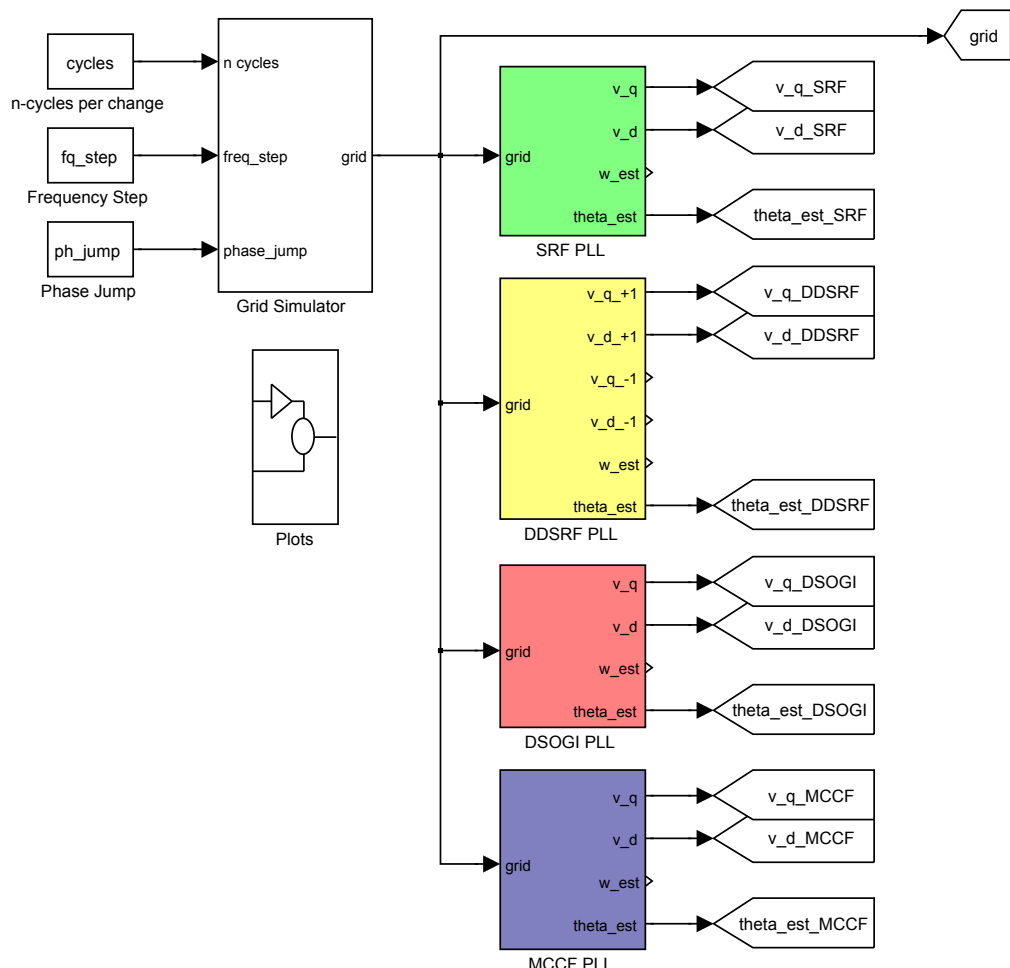


Figure 6.6.: Complete Simulink model for all the PLL schemes

6. Simulation Models

- Phase error, $e(t)$
- Estimated angle, $\hat{\theta}(t)$

The four PLL schemes can be compared in $2^4 - 1 = 15$ different ways. Each of these can be done for 4 imperfections and for 4 of the above outputs. This amounts to $15 \times 4 \times 4 = 240$ combinations! To resolve this complexity, an intuitive plot program is written which plots the data in a comprehensive manner based on the choice given by the user.

To sum up,

- a) Loop filter design using the proposed method
- b) Simulink models with PLL schemes
- c) Intuitive plot program

can be amalgamated into a software applet for easy comparisons. It also holds educational value by serving as an excellent learning tool that gives insights into the working of the PLLs.

7. Results and Discussions

The simulation models discussed in chapter 6 are run in the sequence mentioned before and the results are discussed in this chapter. These results were obtained through two methods of filter design, namely the Wiener optimization method and the proposed self-consistent model based design.

7.1. Results through the Wiener method

This is the method that is presently used in [2, 1, 3]. Simulations were carried out using this method to match the results obtained in literature. The values chosen for the loop filter design are $\delta = \frac{1}{\sqrt{2}}$ and $\omega_n = 100\pi \text{ rad s}^{-1}$.

As discussed in chapter 6, the intuitive plot program gives a choice of looking into four outputs of a PLL, namely, the space vector, the voltage error, the phase error and the estimated angle. Each of these outputs is shown in figure 7.1 for SRF PLL, when the grid voltages are subject to a frequency excursion of $\Delta\omega_{step} = 10 \text{ Hz}$. It is expected that the space vector, which denotes the magnitude of the positive sequence fundamental component of the grid, does not change under a frequency jump. This is observed in figure 7.1a. The voltage error and the phase error are expected to be zero when a PLL is in lock. This is seen in figures 7.1b and 7.1c. The estimated angle contains the phase information of the grid and is expected to be ‘closely clubbed’ for a positive frequency jump, as observed in figure 7.1d. Hence it can be said that SRF PLL tracks changes in frequency. Using Wiener method, the settling time (which is about one cycle in this case) is not fully under the designer’s control, and the design has to be done through trial and error to achieve the required performance.

Since there are many combinations involved in comparing the schemes (240 comparisons as seen in chapter 6), phase error is chosen as a reasonable standard for comparison.

The plot program also takes a choice from the user as to which of the four PLL schemes are to be compared. Figure 7.2a shows the tracking capability of the four PLL schemes discussed in chapter 6, for a frequency excursion of $\Delta\omega_{step} = 10 \text{ Hz}$. It can be seen that SRF PLL is the fastest of all, followed by DDSRF PLL. DSOGI PLL and MCCF PLL take a longer time to track. Similar tracking capability and characteristics are seen in figure 7.2b for the case of phase jump $\phi = \frac{\pi}{6} \text{ rad}$.

In case of voltage unbalance, SRF PLL does not track the fundamental positive sequence voltage, as seen in figure 7.2c. As discussed in section 3.2, it is expected to see oscillations

7. Results and Discussions

of double the grid frequency (100 Hz) when SRF PLL is subject to an unbalanced set of grid voltages, which can also be observed from this figure. DDSRF PLL, DSOGI PLL and MCCF PLL are able to track successfully within two cycles.

In case of harmonics, SRF fails. As discussed in section 3.3, it is expected to see oscillations of six times the grid frequency (300 Hz) when SRF PLL is subject to harmonics, as observed in figure 7.2d. DDSRF PLL, DSOGI PLL and MCCF PLL are able to track successfully within a cycle. It can be observed from figure 7.2e that MCCF PLL has the best performance of the four, in case of a grid affected by both harmonics and voltage unbalance.

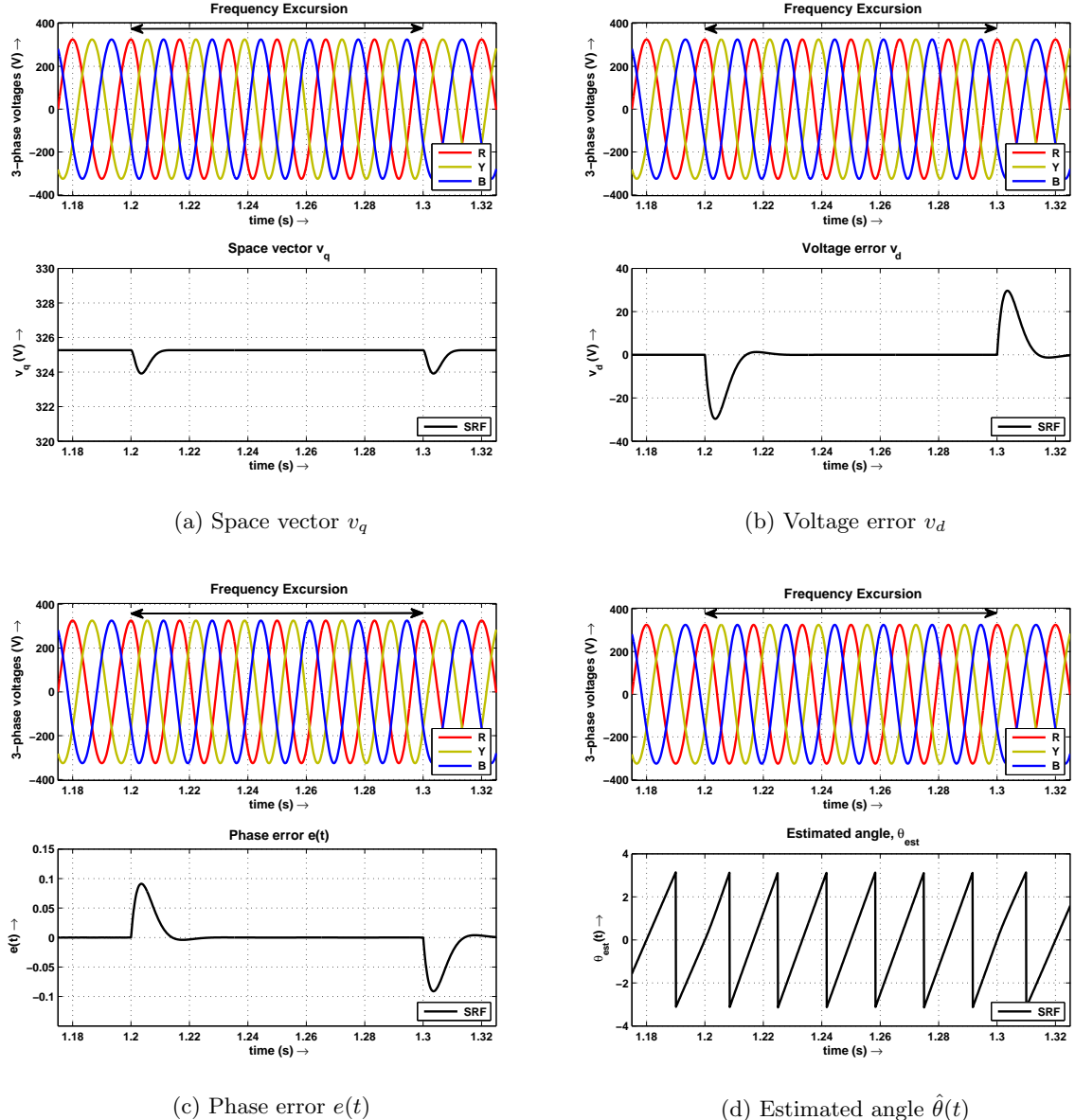


Figure 7.1.: SRF PLL under frequency excursion

7. Results and Discussions

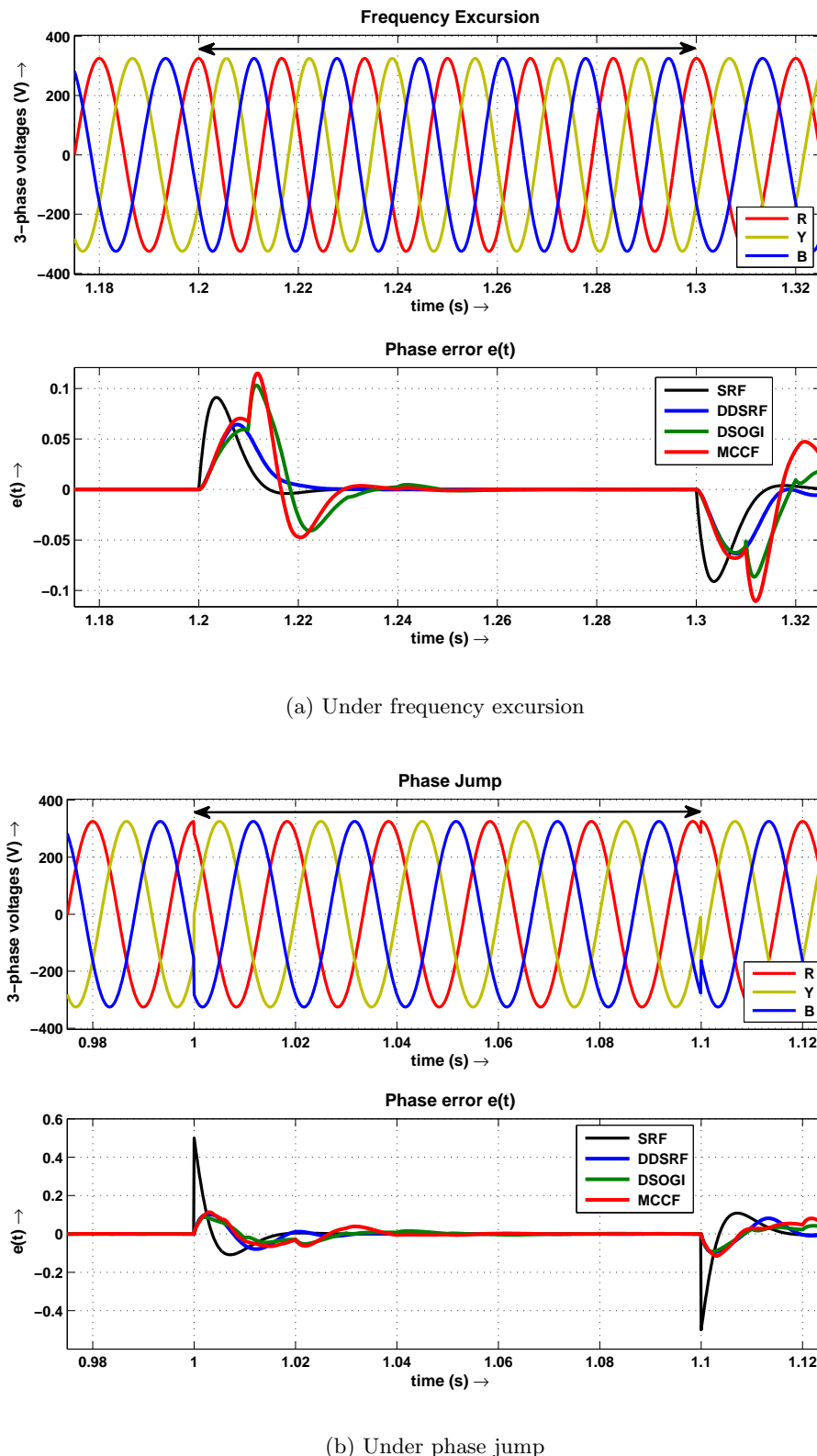


Figure 7.2.: Phase error of the four PLLs

7. Results and Discussions

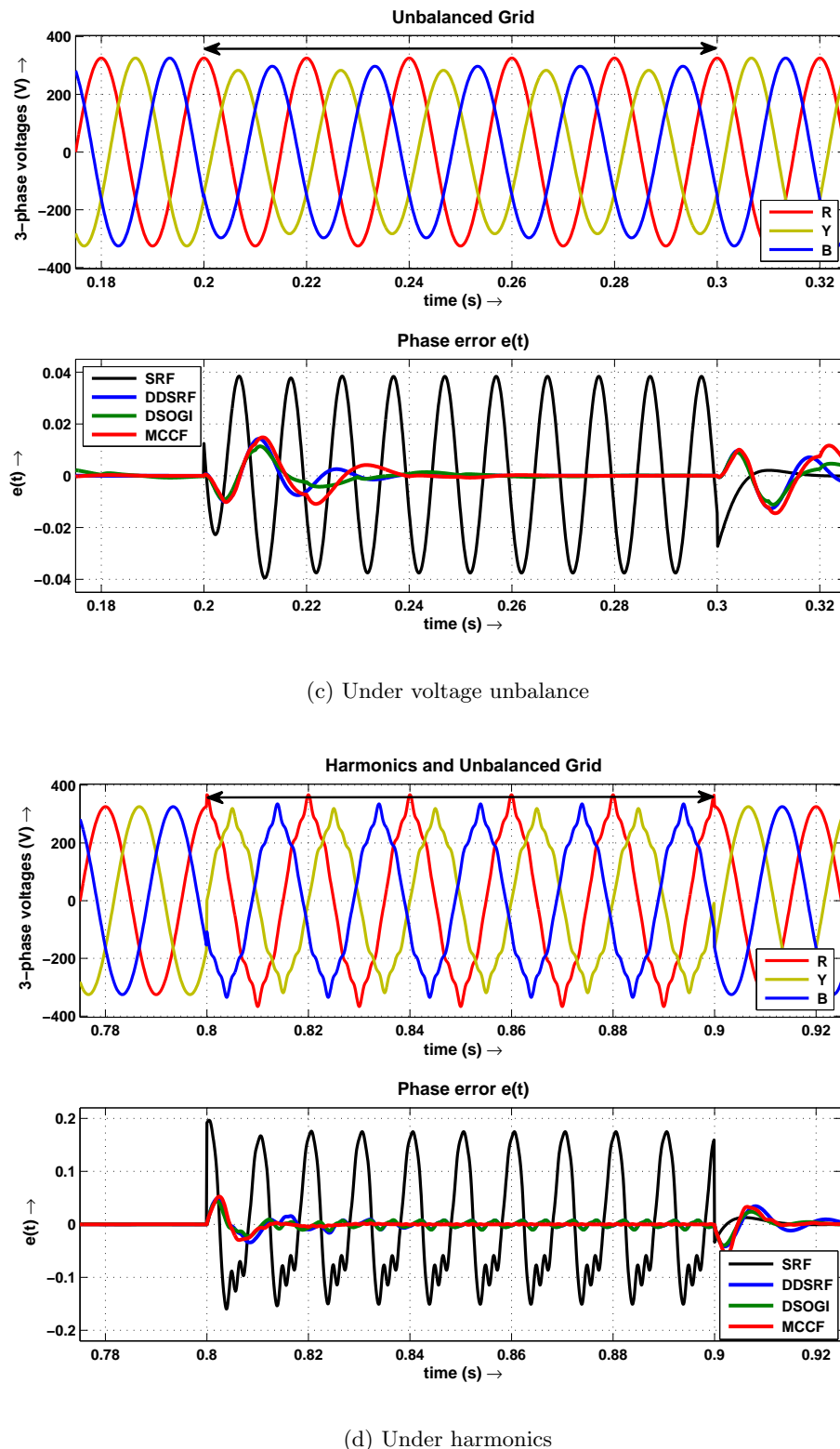
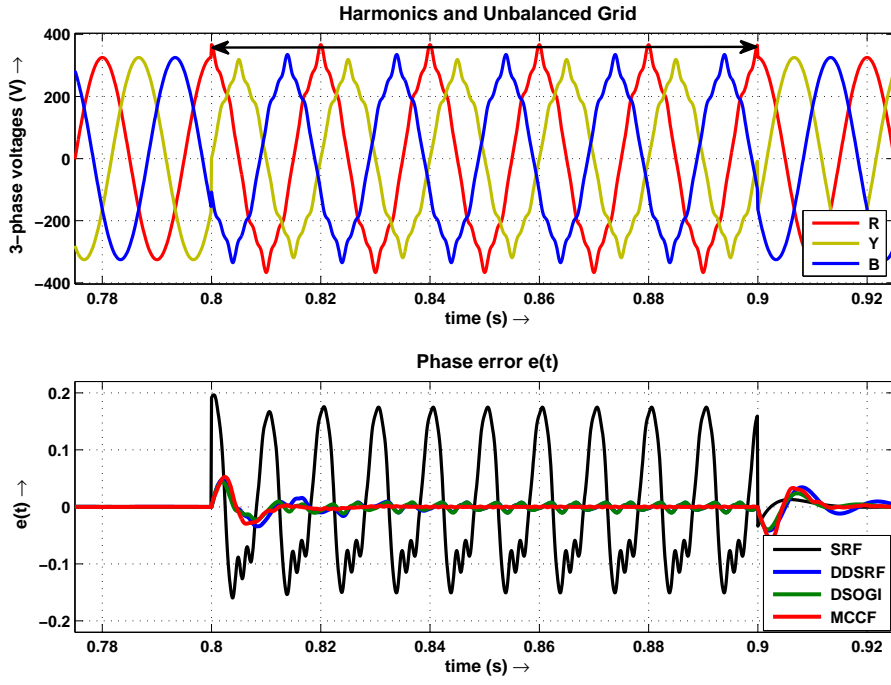


Figure 7.2.: Phase error of the four PLLs

7. Results and Discussions



(e) Under harmonics and voltage unbalance

Figure 7.2.: Phase error of the four PLLs

7.2. Comparisons between the Wiener method and the proposed method

It was seen in chapter 4 that for a fixed ω_n , there exists a unique value of δ for which the error band is minimum. This is basis for the proposed method and this property can be seen from figure 7.4.

Moreover, the proposed method quantizes the error band within the user specifications. Assume the design requirements are $E = 0.02$ rad at $t_0 = 0.01$ s. For a phase jump $\phi = \frac{\pi}{6}$ rad, the data-tip in figure 7.3 shows an instantaneous error of -0.0099 rad. Using symmetry about the time axis, the error band at this instant is approximately twice the instantaneous value, i.e., $0.0099 \times 2 \approx 0.02$ rad. This verifies that the proposed method meets the user's requirements. Clearly, the Wiener's method does not quantize the error as specified.

The Wiener method and the proposed method are compared for the case of frequency excursion $\Delta\omega_{step} = 10$ Hz in figure 7.5a. The design was done using the self-consistent model discussed in section 4.4.2. The values $\delta = 0.8823$, $\omega_n = 398.10 \text{ rad s}^{-1}$, $k_p = -2.159$, $k_i = -487.25$ and $\tau = 4.432$ ms for the user specifications of $E = 0.02$ rad at $t_0 = 0.01$ s are calculated using the proposed method. It is observed that the proposed method has a better dynamic performance.

7. Results and Discussions

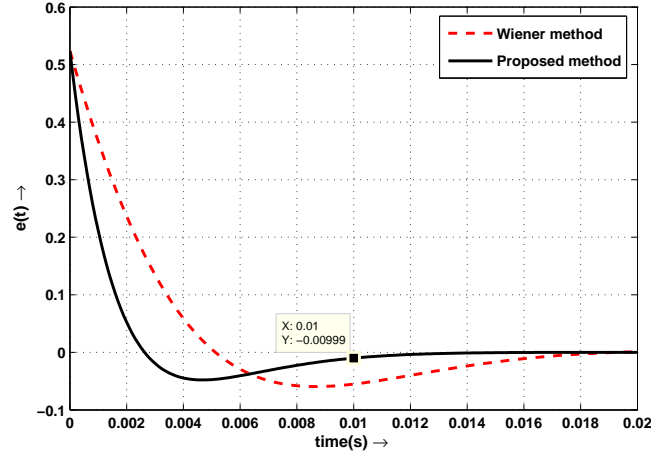


Figure 7.3.: Comparison of error between the Wiener method and the proposed method

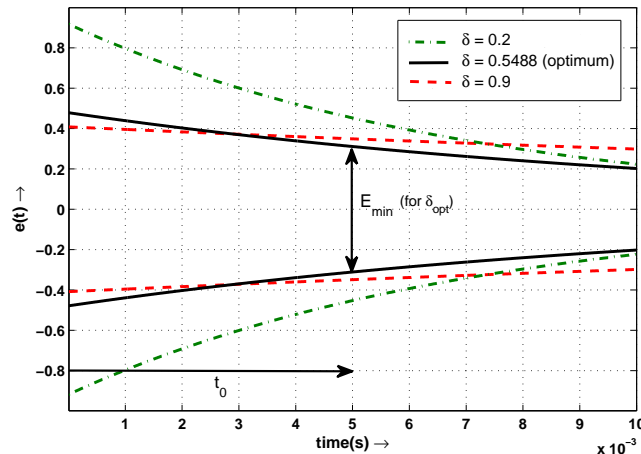


Figure 7.4.: Comparison of the error bands for three cases of δ

A similar comparison is done for the case of phase jump $\phi = \frac{\pi}{6}$ rad in figure 7.5b. The values $\delta = 0.9104$, $\omega_n = 531.71 \text{ rad s}^{-1}$, $k_p = -2.976$, $k_i = -869.17$ and $\tau = 3.424 \text{ ms}$ are obtained for the same user specifications. Clearly, the proposed method has faster tracking capability.

Figures 7.6a, 7.6b and 7.6c, 7.6d compare the results of the Wiener method with that of the proposed method for the four PLLs for the user specifications mentioned above. It can clearly be seen that in both these cases, the proposed method offers a faster tracking capability.

For the case of harmonics and voltage unbalance, the design of k_p and k_i is done for the worst practical case of $\Delta\omega_{step} = 10 \text{ Hz}$ and $\phi = -\frac{\pi}{6}$ rad. This is because opposite signs of frequency step and phase jump cause a larger strain on the design parameters, as discussed

7. Results and Discussions

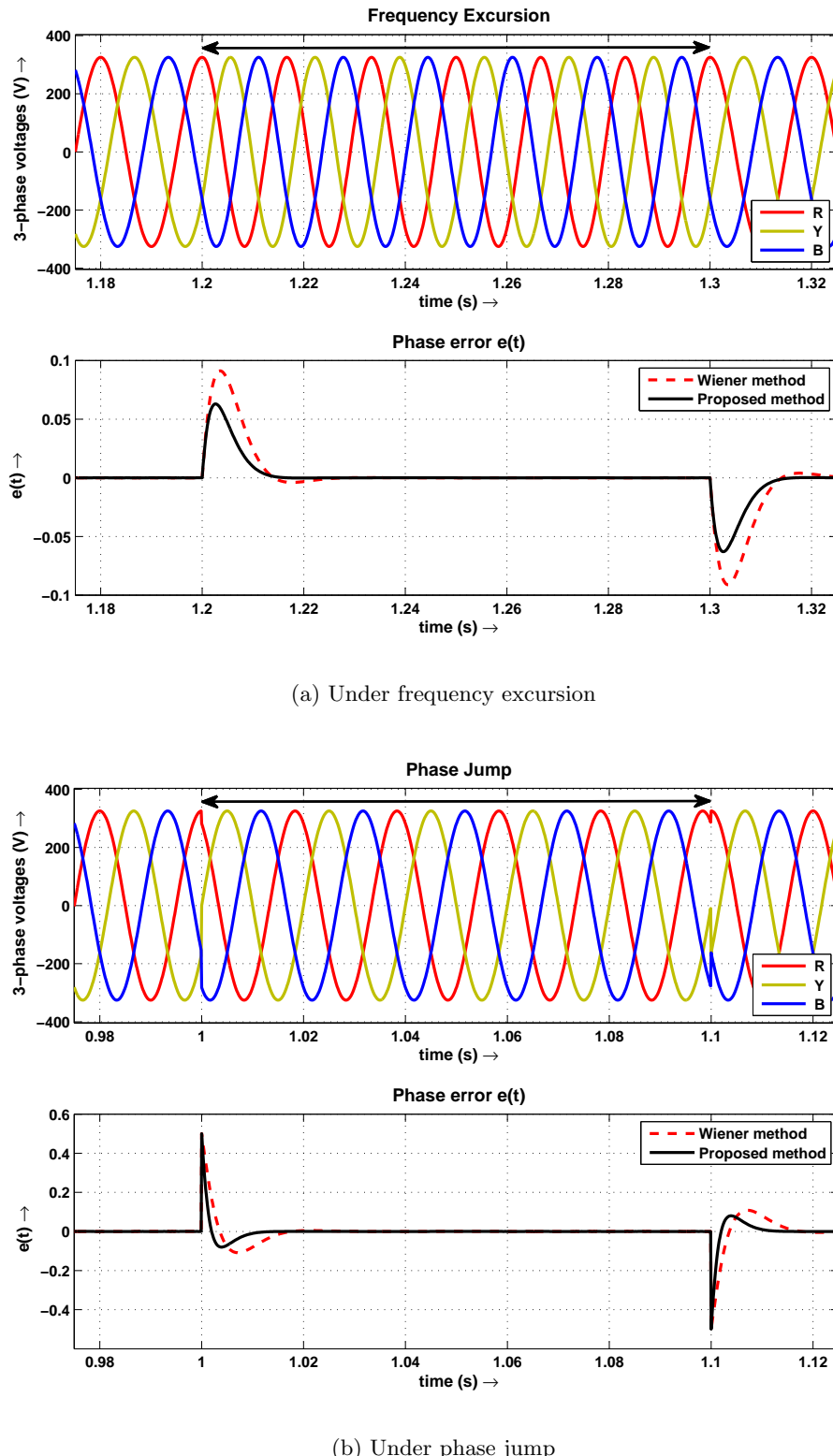


Figure 7.5.: Comparison of phase error in SRF PLL

7. Results and Discussions

in section 4.4.3. The designed values are $\delta = 0.9112$, $\omega_n = 551.86 \text{ rad s}^{-1}$, $k_p = -3.092$, $k_i = -936.29$ and $\tau = 3.302 \text{ ms}$. From figures 7.6e, 7.6f and 7.6g, 7.6h and 7.6i, 7.6j, it is seen that the proposed design yields a better performance even for voltage unbalance, harmonics or both.

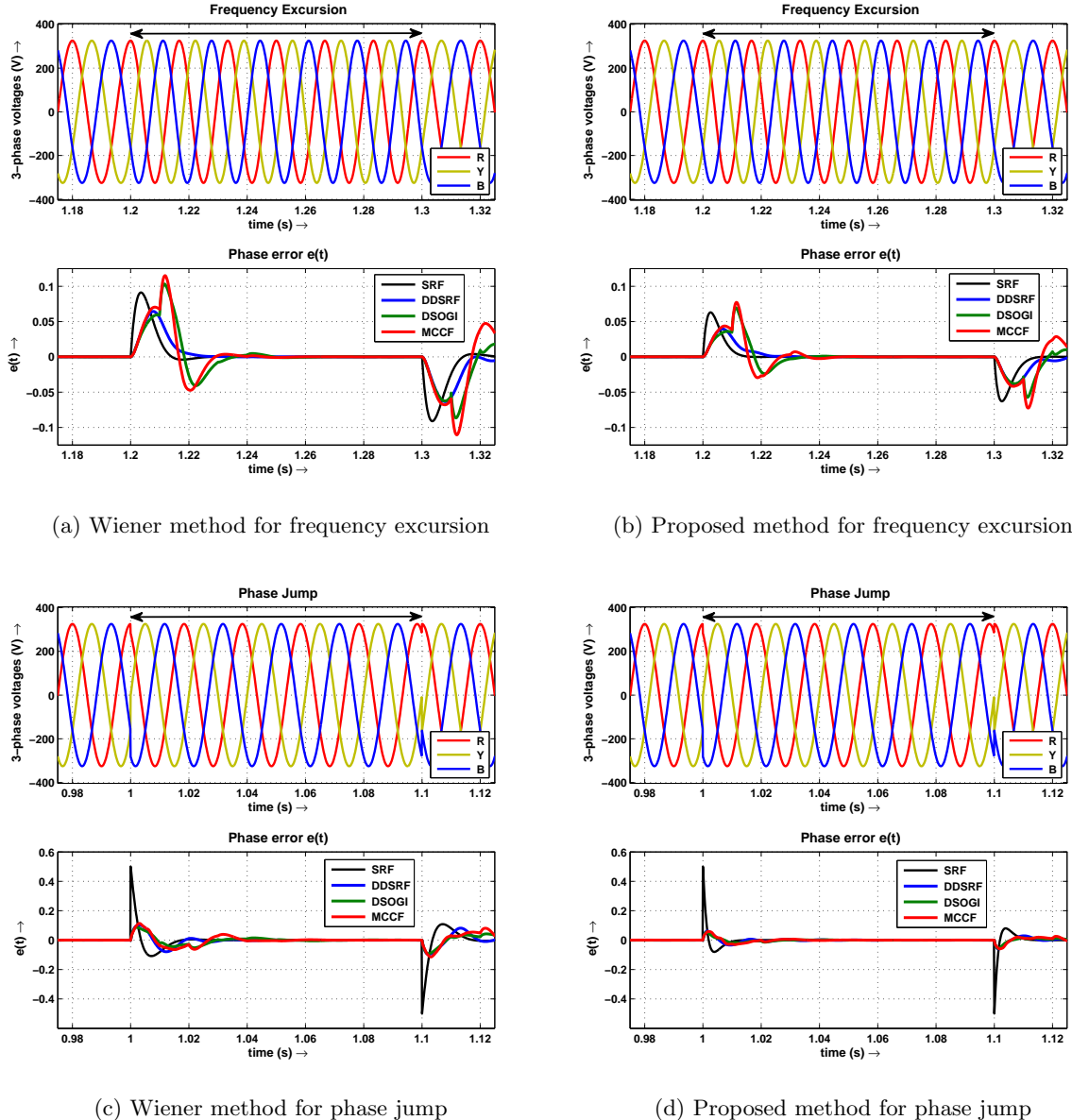
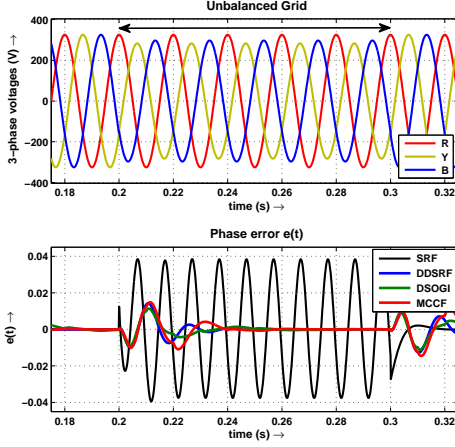


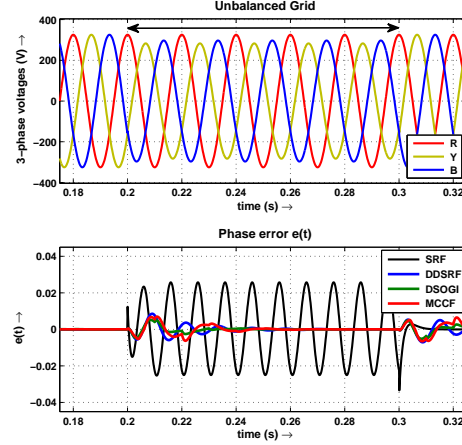
Figure 7.6.: Comparison between the Wiener method and the proposed method

To sum up, the self-consistent model based loop filter design is both convenient as it does not involve trial and error, and it meets the user specifications accurately.

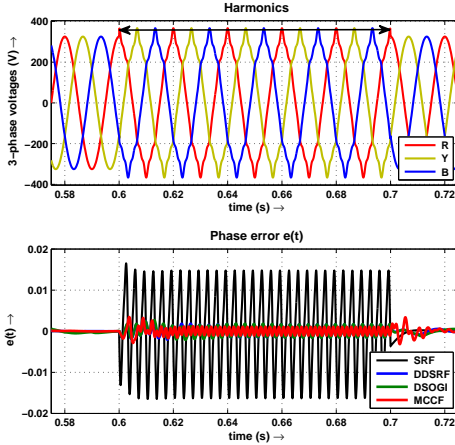
7. Results and Discussions



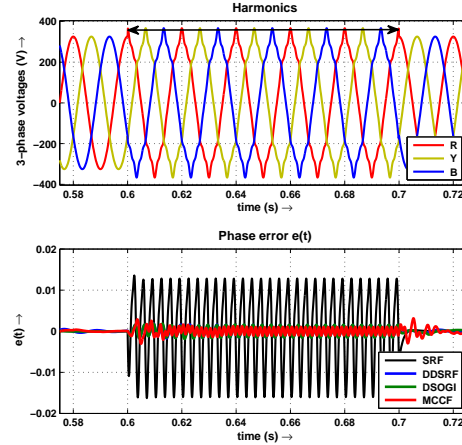
(e) Wiener method for voltage unbalance



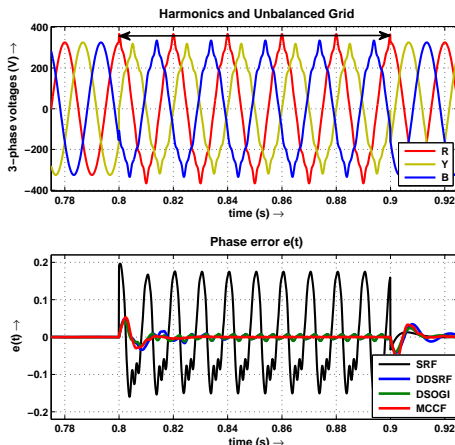
(f) Proposed method for voltage unbalance



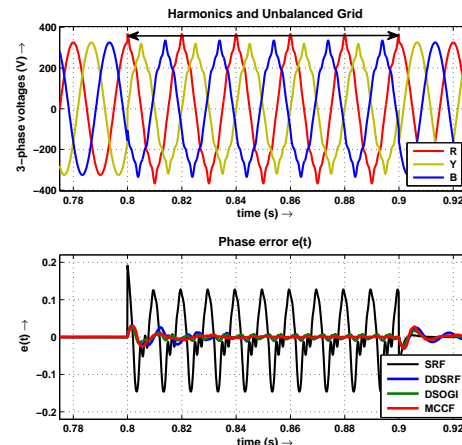
(g) Wiener method for harmonics



(h) Proposed method for harmonics



(i) Wiener method for harmonics and voltage unbalance



(j) Proposed method for harmonics and voltage unbalance

Figure 7.6.: Comparison between the Wiener method and the proposed method

8. Experimentation

It is evident from literature that most of the modified 3-phase PLLs for tracking disturbed grids are based on the conventional SRF PLL. This was the motivation behind devising an optimization algorithm (using the self-consistent model) to improve the dynamic performance of a conventional SRF PLL. Computer simulations are carried out to evaluate the integrity of the proposed design discussed in the previous chapters. The next step of evaluation is to implement a working model of the conventional SRF PLL on a practical setup.

For the practical setup, we need:

1. A 3-phase grid supply (415 V , 50 Hz)
2. Three voltage sensors and signal conditioning circuitry
3. A digital signal processor/microcontroller
4. A digital storage oscilloscope (DSO)

It will be shown in the following discussion that our choice of a microcontroller over a DSP is cleverly justified. The microcontroller that we shall use is MSP430TM by Texas Instruments. The details are given below:

- Variant: MSP430G2553
- Package: PDIP20 pin
- Development board: MSP-EXP430G2 Launchpad
- Price: \$4.50

Further on, MSP430G2553 shall be referred to as MSP430 itself. MSP430 is a powerful, low power¹, 16-bit microcontroller with up to 16 MHz internal DCO clock (figure 8.1c). It also includes peripherals like the 8-channel 10-bit SAR A/D, timers with PWM and capture capability, 16 kB on-chip flash memory, 512 B RAM, on-chip comparator and such.

The MSP-EXP430G2 Launchpad (figure 8.1a) is a low cost experimenter board which has an integrated USB-based emulator. It also includes an on-board flash emulation tool to interface with a PC for easy programming, debugging and evaluation.

These features of the MSP430 microcontroller make it a promising candidate for the practical

¹Ultra-fast 1 μ s DCO start-up allows MSP430 based systems to remain in low-power modes for the longest possible interval, hence extending the battery life (figure 8.1d)

8. Experimentation

implementation of the conventional SRF PLL shown in figure 3.1. For clarity, the SRF PLL structure is divided into the following segments:

- i. Transformation from abc to dq reference frame (Clarke+Park)
- ii. PI loop filter
- iii. VCO + feedback

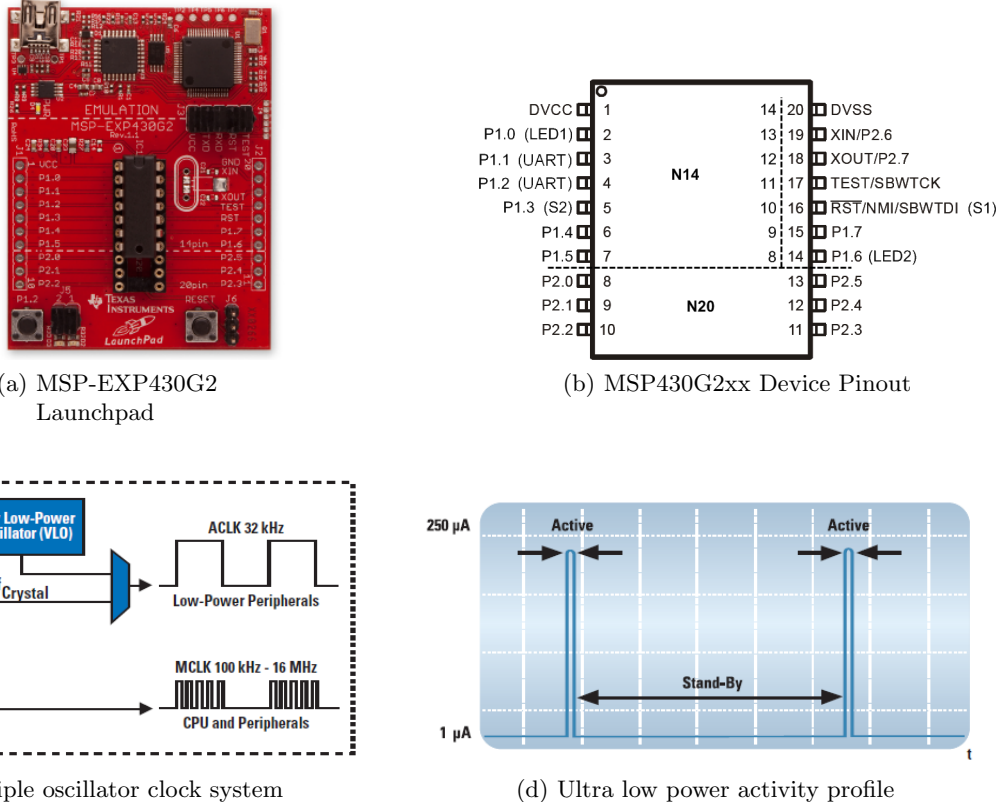


Figure 8.1.: MSP430 overview

8.1. Implementation of Clarke and Park Transformations

At this juncture, the following points deserve a mention:

Trigonometric lookup table: The transformation between reference frames requires trigonometric computations, as it can be seen from (2.2). For this purpose, a 64-point, 8-bit sine and cosine lookup tables are implemented. Owing to the on-chip memory limitations, a 64-point resolution is chosen. However, with external memory support, higher point lookup tables may be used, for higher accuracy.

8. Experimentation

A/D converter to sample the input: The three inputs to the transformation, namely v_a , v_b and v_c need to be sampled and be made available in digital form. The internal 10-bit SAR A/D is used for this purpose. It is configured to sample in ‘sequence of channels’ mode with a clock source, ADC10CLK=5 MHz. The inputs are connected to channels 0, 1 and 2 respectively. Internal reference (system GND and 2.5 V) is used. The conversion results are stored to a specified memory block in the on-chip RAM, using the in-built data transfer controller (DTC) module. The use of DTC makes the sampling process faster by avoiding any CPU intervention after every conversion.

Signal conditioning and clamping circuits: Since the A/D is configured to use an internal reference in the range 0 to 2.5 V, the inputs v_a , v_b and v_c to the MSP430 need to be scaled to fall in this range. The voltage sensors, after down-scaling and signal conditioning, provide an output of 3 V (peak to peak, bipolar). An op-amp based clamper (figure 8.2) is made use of to obtain an output of 3 V (peak to peak, unipolar). To obtain an output in the range 0 to 2.5 V, an amplifier with a gain of $2/3$ is used, leaving a safe band of 0.5 V in case of voltage swells.

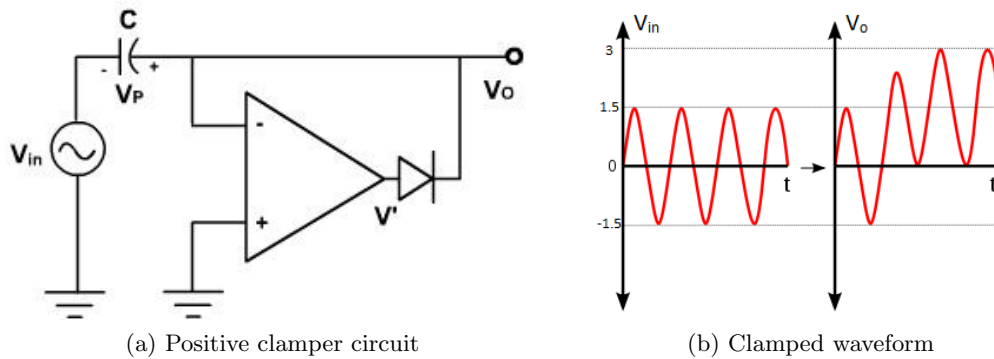


Figure 8.2.: Op-amp based positive clamper

8.2. Implementation of the PI loop filter as a digital filter

Since the microcontroller operates on digital signals (sampled and held), the loop filter needs to be transformed from the continuous s -domain to its equivalent discrete z -domain. For this, the bilinear transformation (BLT) is used (see Appendix A.4). This involves substituting

$$s = \frac{2}{T_s} \left(\frac{1 - z^{-1}}{1 + z^{-1}} \right) \quad (8.1)$$

where T_s is the sampling period.

8. Experimentation

Hence the PI loop filter transfer function in (4.2) becomes

$$K_f(z) = \frac{\Delta\hat{\omega}(z)}{V_d(z)} = \left[k_p + \frac{k_i T_s}{2} \left(\frac{1+z^{-1}}{1-z^{-1}} \right) \right] \quad (8.2)$$

$$= \frac{2k_p(1-z^{-1}) + k_i T_s(1+z^{-1})}{2(1-z^{-1})} \quad (8.3)$$

$$= \frac{\left(k_p + \frac{k_i T_s}{2} \right) + \left(\frac{k_i T_s}{2} - k_p \right) z^{-1}}{1-z^{-1}} \quad (8.4)$$

Expressing (8.4) in direct form, we obtain

$$\Delta\hat{\omega}(z) = \left(k_p + \frac{k_i T_s}{2} \right) V_d(z) + \left(\frac{k_i T_s}{2} - k_p \right) z^{-1} V_d(z) + z^{-1} \Delta\hat{\omega}(z) \quad (8.5)$$

Taking the inverse z-transform yields

$$\Delta\hat{\omega}(nT_s) = \left(k_p + \frac{k_i T_s}{2} \right) v_d(nT_s) + \left(\frac{k_i T_s}{2} - k_p \right) v_d((n-1)T_s) + \Delta\hat{\omega}((n-1)T_s) \quad (8.6)$$

8.3. Implementation of VCO+Feedback

The function of VCO (figure 3.4) is to add ω_{ff} to the output of the loop filter and to integrate the result. Hence the input to the integrator is given by

$$\hat{\omega}(t) = \Delta\hat{\omega}(t) + \omega_{ff} \quad (8.7)$$

In discrete domain, (8.7) becomes

$$\hat{\omega}(nT_s) = \Delta\hat{\omega}(nT_s) + \omega_{ff} \quad (8.8)$$

Integrator in z-domain

In s-domain, the integrator can be expressed as

$$\frac{\hat{\theta}(s)}{\hat{\omega}(s)} = \frac{1}{s} \quad (8.9)$$

Applying BLT (see Appendix A.4) to transform to z-domain,

$$\frac{\hat{\theta}(z)}{\hat{\omega}(z)} = \frac{T_s}{2} \left(\frac{1+z^{-1}}{1-z^{-1}} \right) \quad (8.10)$$

$$\Rightarrow \hat{\theta}(z) - z^{-1}\hat{\theta}(z) = \frac{T_s}{2} \left(\hat{\omega}(z) + z^{-1}\hat{\omega}(z) \right) \quad (8.11)$$

8. Experimentation

Taking the inverse z-transform, we obtain

$$\hat{\theta}(nT_s) = \frac{T_s}{2} [\hat{\omega}(nT_s) + \hat{\omega}((n-1)T_s)] + \hat{\theta}((n-1)T_s) \quad (8.12)$$

The computed angle, $\hat{\theta}(nT_s)$ is fed back to the Park transformation block.

8.4. Outputs using the PWM module

The two 16-bit timers, namely Timer0_A3 and Timer1_A3 are fed with a clock, SMCLK=16 MHz and configured to count in the up-mode, up to the clock ticks specified in the TxCRR0 register. ‘CCR’ stands for capture/compare register. The TxCRRx is set to PWM output mode 7 (PWM set/reset mode) to generate a PWM output with a duty cycle that varies with the stored value in the TxCRRx registers. Figure 8.3 explains the selected PWM mode in detail. Using this variant of MSP430, four PWM outputs can be achieved using the T0CCR1, T0CCR2, T1CCR1 and T1CCR2 capture/compare registers. The fundamental component of these PWM signals is the desired output, to be viewed on the oscilloscope.

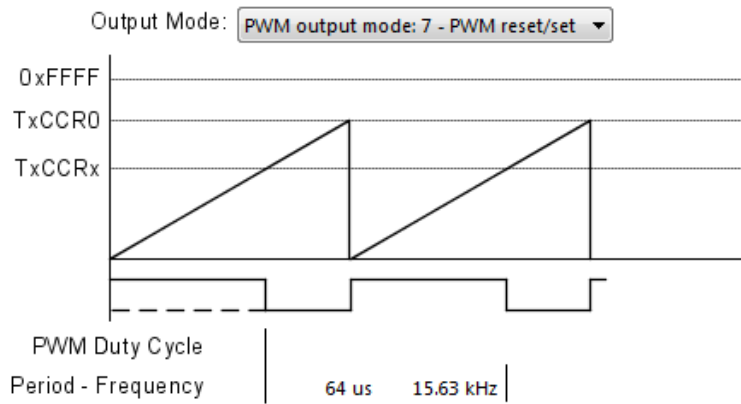


Figure 8.3.: PWM mode in the MSP430

8.5. Results

The above points are useful in implementing SRF PLL on the MSP430. It is observed that the MSP430 takes approximately 0.3 ms for each iteration. Hence it is important that the designed sampling time T_s be greater than 0.3 ms. The experimental results obtained are for $T_s = 0.3125$ ms.

The operation of SRF PLL is established in figure 8.4, which is shown to track the grid frequency of 50 Hz. Figure 8.4a shows the phase voltage (before clamping) and the estimated

8. Experimentation

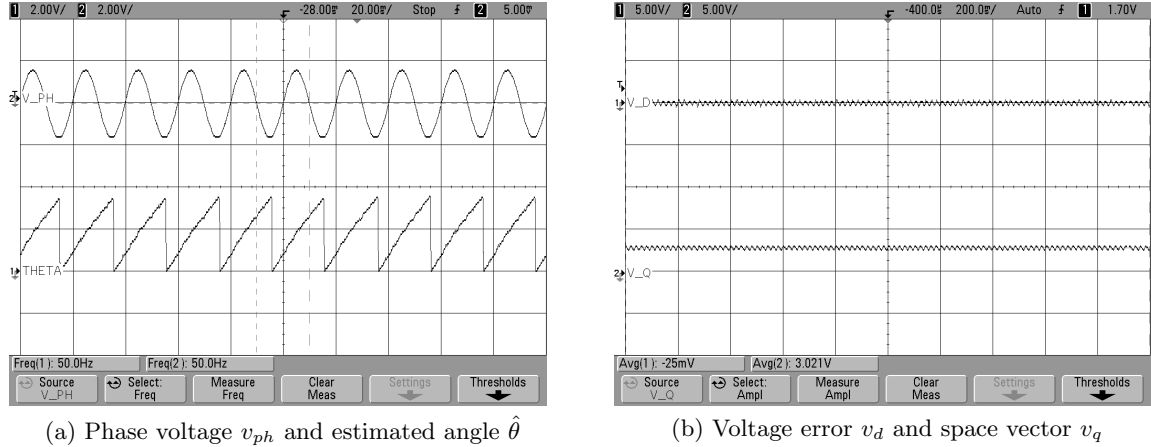


Figure 8.4.: SRF PLL tracking the 3-phase grid voltages at 50 Hz

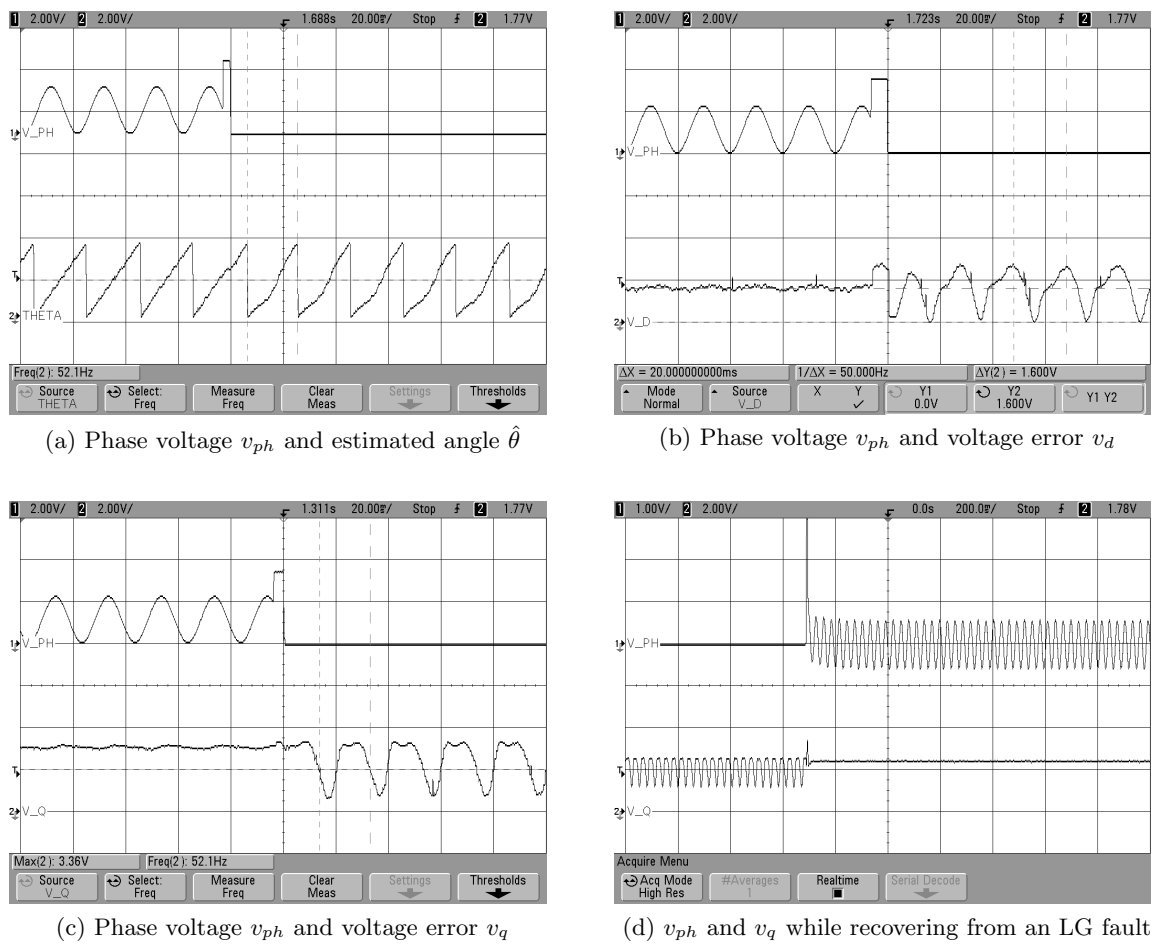


Figure 8.5.: SRF PLL during an LG fault

8. Experimentation

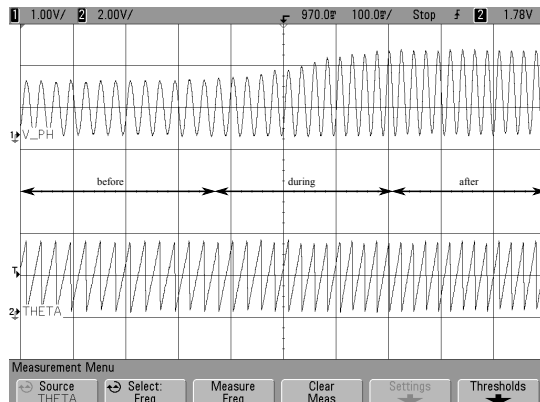
angle to be of the same frequency (50 Hz). The voltage error v_d and space vector v_q are shown in figure 8.4b. As expected, v_d is zero and v_q is the maximum magnitude of the phase voltage (after clamping).

Figures 8.5a, 8.5b and 8.5c show the phase voltage (after clamping) during a line to ground fault. Clearly, SRF PLL loses synchronism and this is evident from the oscillating nature of v_d and v_q . Also, $\hat{\theta}$ deviates from its linear behaviour. Figure 8.5d shows the phase voltage (before clamping) while the LG fault is cleared. Consequently, SRF PLL falls into lock again, which is evident from v_q .

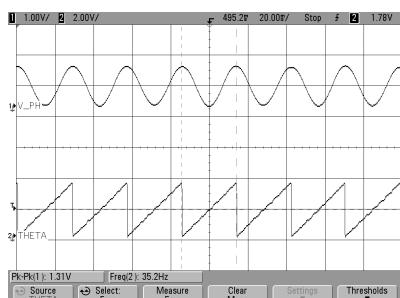
A 3-phase induction generator, which is mechanically coupled to a variable speed DC motor, is used for creating both frequency and voltage disturbance. The speed of the DC motor is varied by varying its armature rheostat, hence creating the disturbance. Figure 8.6a shows the clamped phase voltage, before, during and after the disturbance is created. Figure 8.6b shows a phase voltage of 1.31 V (peak to peak) and the angle tracking its frequency of 35.2 Hz. In figure 8.6c, a gradual transition of frequency and magnitude is shown and clearly, SRF PLL is trying to catch up with the grid frequency. Finally, figure 8.6d shows a phase voltage of 2.06 V (peak to peak) and the angle tracking its frequency of 42.7 Hz. This shows successful locking of SRF PLL under frequency excursion coupled with voltage swell. Figures 8.6e and 8.6f show the phase voltage (before clamping) under the same disturbance. The voltage error v_d continues to be zero. Figures 8.6g and 8.6h show the space vector tracking the voltage magnitude successfully.

Pictures of the hardware setup are shown in figure 8.7.

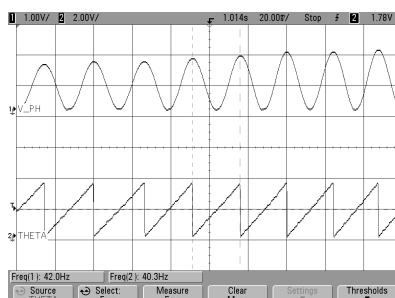
8. Experimentation



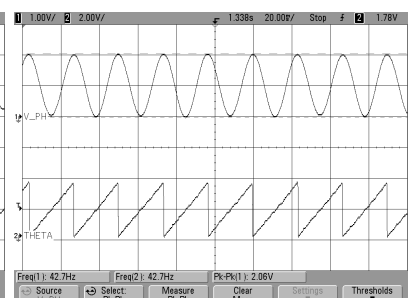
(a) v_{ph} and $\hat{\theta}$ - complete window



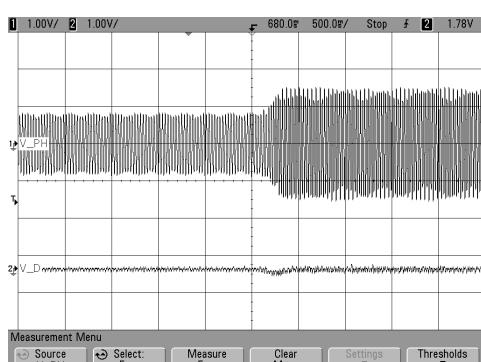
(b) v_{ph} and $\hat{\theta}$ - before disturbance



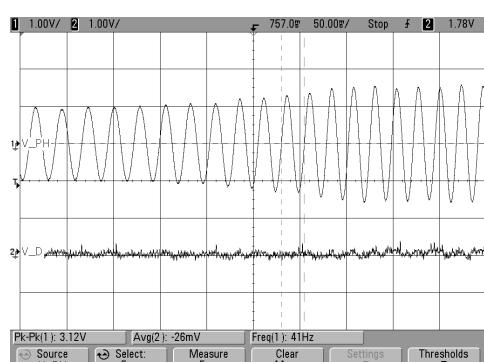
(c) v_{ph} and $\hat{\theta}$ - during disturbance



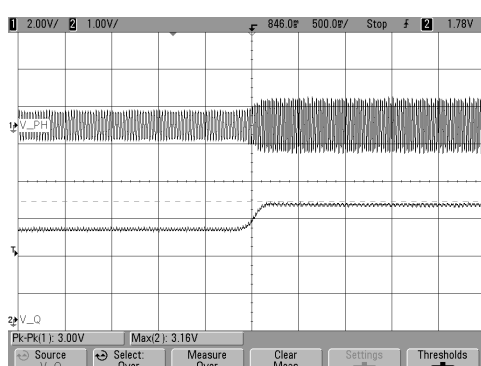
(d) v_{ph} and $\hat{\theta}$ - after disturbance



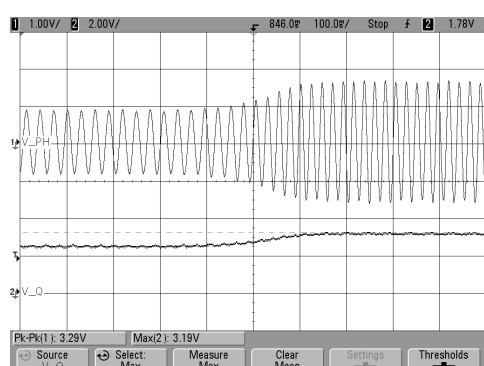
(e) v_{ph} and v_d - wide time band



(f) v_{ph} and v_d - narrow time band



(g) v_{ph} and v_q - wide time band



(h) v_{ph} and v_q - narrow time band

Figure 8.6.: SRF PLL under frequency excursion with voltage swell

8. Experimentation

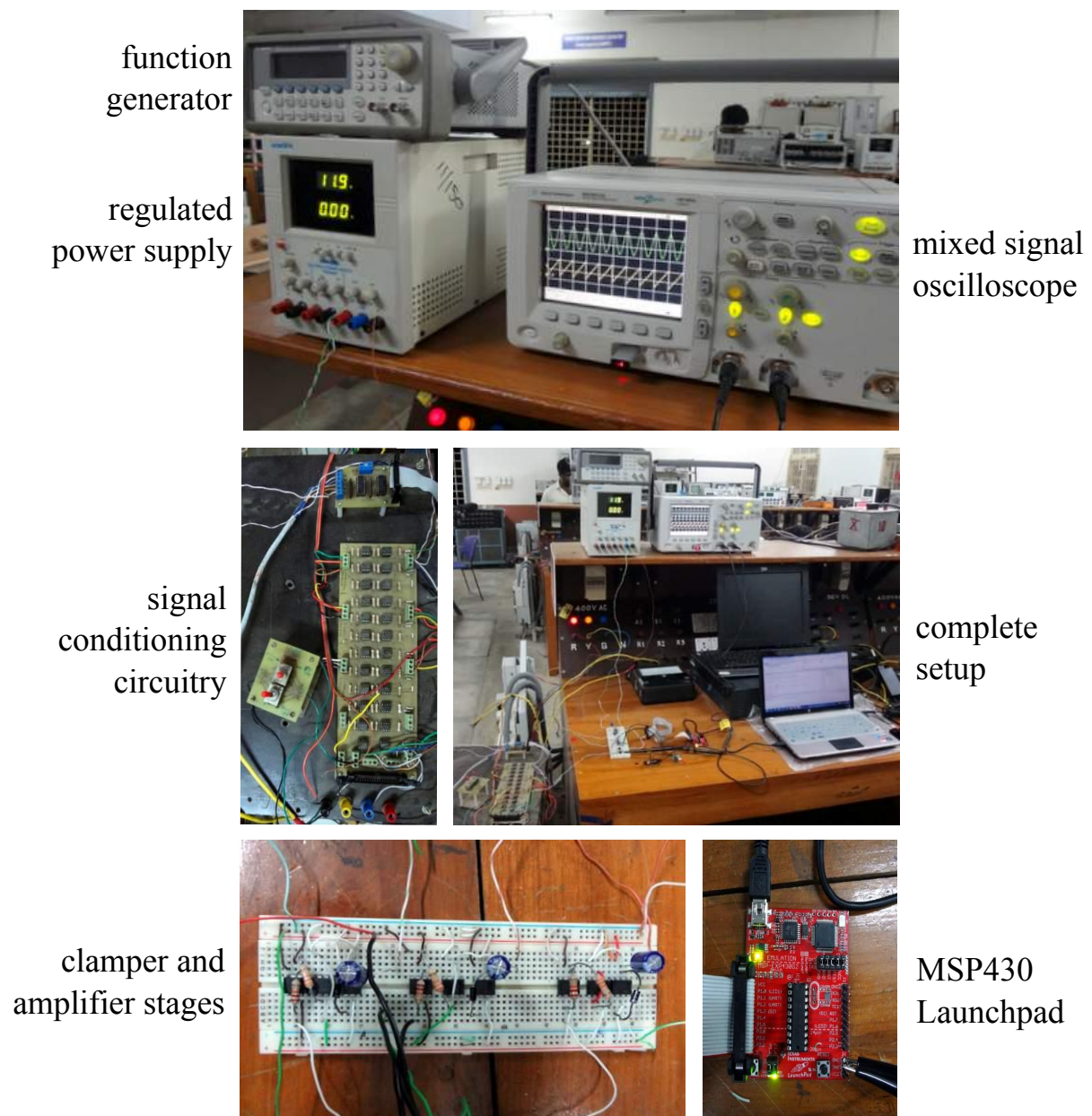


Figure 8.7.: Experimental Setup

9. Conclusions

Different PLL schemes, namely the conventional SRF PLL, DDSRF PLL [1], DSOGI PLL [2] and MCCF PLL [3] have been analysed in depth and each of these are simulated in Simulink[®]. The values of the loop filter parameters were taken as is from literature and the simulation results are matched to the results in [1, 2, 3]. Further, with the possibility of over 200 performance comparisons among the PLLs (due to the fact that each PLL had 4 output variables and was subject to 4 different grid imperfections), a software tool (applet) is developed which facilitates easy comparison and also produces the desired plots in a clear and intuitive manner. It is observed that SRF and DDSRF PLL have faster tracking compared to DSOGI and MCCF PLL in case of frequency excursion or phase jump. On the other hand, MCCF and DSOGI PLL deal with voltage unbalance and harmonics in a more efficient manner compared to DDSRF PLL; SRF PLL fails to track in this scenario. Moreover, the applet enables us to explore subtle insights like the ‘ 2ω ’ and ‘ 6ω ’ oscillations in phase error of SRF PLL when subject to voltage unbalance and harmonics respectively.

It is observed that the dynamic performance or speed of tracking of a PLL solely depends on the value of the loop filter parameters, proportional gain k_p and integral gain k_i . The design used in literature so far is mostly based on a trade-off between filtering and dynamic performance (called the Wiener method). Dynamic performance of a PLL is given more importance, leaving the task of filtering to the other augmented stages of the modified PLLs, therefore decoupling both. A self-consistent model for the design of the loop parameters is developed which generates a unique (k_p, k_i) pair for a given set of user specifications of maximum permissible error band E at settling time t_0 , maximum allowable frequency step $\Delta\omega_{step}$ and maximum allowable phase jump ϕ . A comparative study between the existing Wiener method and the proposed self-consistent model based method is carried out by simulating the different PLLs under the same grid imperfections, but different loop filter designs. The proposed method for loop filter design is shown to have superior dynamic performance.

The concept of the self-consistent model is further extended to obtain a 3D lookup table for all possible practical combinations of frequency excursions and phase jumps. From a learning perspective, several properties of the nature of the lookup table such as symmetry about origin, stress on the filter parameters based on the quadrant of operation etc. can be studied. Apart from the theoretical inferences, practical implementation is made feasible by eliminating the constraints on the speed and computing power of the micro-controller or DSP.

Hardware implementation of SRF PLL is achieved on a micro-controller (MSP430). The output waveforms are used to establish the successful locking of SRF PLL under frequency excursions and voltage swells. Yet, it is shown to fail in the case of line to ground fault.

9. Conclusions

Future work

Implementation of the 3D lookup table in a micro-controller or a DSP can be done for enabling re-configurable filter design for optimized performance on the part of PLL to cope with dynamically varying grid voltages on the fly. Hardware implementation can be extended to the modified PLL schemes mentioned in the previous chapters and the applicability of the proposed design method to these schemes can be verified.

10. Acknowledgements

We are grateful to our mentor and guide, Prof. Dr. C. Nagamani for her constant support and encouragement which drove our progress in this piece of research. She has been active and helping in every possible way, on both theoretical and motivational grounds. Her keen attention and willingness to hear our thoughts is greatly appreciated. She has always given us the drive to delve deeper into research, and the freedom to explore the unfamiliar. She stood with us in the long discussions we had almost each day, often resulting in many fruitful outcomes. We also acknowledge her patience to have read our report in detail and to have given many useful suggestions during the course of penning it down.

We greatly owe, G. Girish and V. Rama Raju, M. S. students, who selflessly devoted their time in helping us with the experimental setup. We especially thank Girish for the motivation behind using the MSP430 Launchpad and the insights into digital filter implementation. We also appreciate Rama Raju for helping us in generating frequency excursion and recording the waveforms systematically.

We thank our parents and friends without whose moral support we would not have achieved this. Finally, we thank God without whose grace this piece of work would not have materialized.

Sambhav R Jain
Pradhyumna Ravikirthi

Bibliography

- [1] P. Rodríguez, J. Pou, J. Bergas, J. I. Candela, R. P. Burgos, and D. Boroyevich, “Decoupled double synchronous reference frame PLL for power converters control,” *IEEE Transactions on Power Electronics*, vol. 22, pp. 584–592, March 2007.
- [2] P. Rodríguez, R. Teodorescu, I. Candela, A. Timbus, M. Liserre, and F. Blaabjerg, “New positive-sequence voltage detector for grid synchronization of power converters under faulty grid conditions,” in *Power Electronics Specialists Conference (PESC)*, no. 37, IEEE, June 2006.
- [3] X. Guo, W. Wu, and Z. Chen, “Multiple-complex coefficient-filter-based phase-locked loop and synchronization technique for three-phase grid-interfaced converters in distributed utility networks,” *IEEE Transactions on Industrial Electronics*, pp. 1194–1204, April 2011.
- [4] IEEE Std. 519-1992, “IEEE recommended practices and requirements for harmonic control in electrical power systems,” April 1993.
- [5] Z. Miao and L. Fan, “The art of modeling and simulation of induction generator in wind generation applications using high-order model,” *Simulation Modelling Practice and Theory*, vol. 16, no. 9, pp. 1239–1253, 2008.
- [6] M. R. Banaei, S. H. Hosseini, S. Khanmohammadi, and G. B. Gharehpetian, “Loss reduction of distribution system using APLC,” *Simulation Modelling Practice and Theory*, vol. 13, pp. 169–178, February 2005.
- [7] R. K. Varma, S. Audy, and Y. Semsedini, “Mitigation of subsynchronous resonance in a series-compensated wind farm using FACTS controllers,” *IEEE Transactions on Power Delivery*, vol. 23, pp. 1645–1654, July 2008.
- [8] A. Ajami, S. H. Hosseini, S. Khanmohammadi, and G. B. Gharehpetian, “Modeling and control of C-UPFC for power system transient studies,” *Simulation Modelling Practice and Theory*, vol. 14, pp. 564–576, July 2006.
- [9] R. Weidenbrug, F. P. Dawson, and R. Bonert, “New synchronization method for thyristor power converters to weak AC-systems,” *IEEE Transactions on Industrial Electronics*, vol. 40, pp. 505–511, October 1993.
- [10] M. H. J. Bollen, “Fast assessment methods for voltage sags in distribution systems,” *IEEE Transactions on Industry Applications*, vol. 32, pp. 1414–1423, November/December 1996.

Bibliography

- [11] K. Gulez, “Neural network based switching control of AC-AC converter with DC-AC inverter for voltage sags, harmonics and EMI reduction using hybrid filter topology,” *Simulation Modelling Practice and Theory*, vol. 16, pp. 597–612, July 2008.
- [12] I. Carugati, S. Maestri, P. G. Donato, D. Carrica, and M. Benedetti, “Variable sampling period filter PLL for distorted three-phase systems,” *IEEE Transactions on Power Electronics*, vol. 27, pp. 321–330, January 2012.
- [13] Y. Han, L. Xu, M. M. Khan, G. Yao, L.-D. Zhou, and C. Chen, “A novel synchronization scheme for grid-connected converters by using adaptive linear optimal filter based PLL,” *Simulation Modelling Practice and Theory*, vol. 17, pp. 1299–1345, May 2009.
- [14] J. L. Blackburn, *Symmetrical Components for Power Systems Engineering*. Marcel Dekker, Inc., 1993.
- [15] Wikipedia, “Bode plot.” http://en.wikipedia.org/wiki/Bode_plot.
- [16] F. M. Gardner, *Phaselock Techniques*. Wiley-Interscience, 3rd ed., 2005.
- [17] S.-K. Chung, “A phase tracking system for three phase utility interface inverters,” *IEEE Transactions on Power Electronics*, vol. 15, pp. 431–438, May 2000.

Appendix A.

Mathematical concepts

A.1. L' Hospital rule

L' Hospital's rule is applicable in the following two cases.

1. If $\left[\frac{\text{num}(0)}{\text{den}(0)} \right]$ is of the form $(\frac{0}{0})$, then

$$\lim_{t \rightarrow 0} \left[\frac{\text{num}(t)}{\text{den}(t)} \right] = \lim_{t \rightarrow 0} \left[\frac{\frac{d}{dt}(\text{num}(t))}{\frac{d}{dt}(\text{den}(t))} \right] \quad (\text{A.1})$$

2. If $\left[\frac{\text{num}(\infty)}{\text{den}(\infty)} \right]$ is of the form $(\frac{\infty}{\infty})$, then

$$\lim_{t \rightarrow \infty} \left[\frac{\text{num}(t)}{\text{den}(t)} \right] = \lim_{t \rightarrow \infty} \left[\frac{\frac{d}{dt}(\text{num}(t))}{\frac{d}{dt}(\text{den}(t))} \right] \quad (\text{A.2})$$

A.2. Properties of a cubic equation

Consider a cubic equation

$$x^3 + lx^2 + mx + n = 0 \quad (\text{A.3})$$

Let the roots of this equation be α_1 , α_2 and α_3 .

$$\Rightarrow (x - \alpha_1)(x - \alpha_2)(x - \alpha_3) = 0 \quad (\text{A.4})$$

$$\Rightarrow (x - \alpha_1)(x^2 - (\alpha_2 + \alpha_3)x + \alpha_2\alpha_3) = 0 \quad (\text{A.5})$$

$$\Rightarrow x^3 - (\alpha_1 + \alpha_2 + \alpha_3)x^2 + (\alpha_1\alpha_2 + \alpha_2\alpha_3 + \alpha_1\alpha_3)x - \alpha_1\alpha_2\alpha_3 = 0 \quad (\text{A.6})$$

Equations (A.3) and (A.6) are identical; hence comparing their respective coefficients, we get

$$(i) \text{ sum of roots} = \alpha_1 + \alpha_2 + \alpha_3 = -l$$

$$(ii) \text{ product of roots} = \alpha_1\alpha_2\alpha_3 = -n$$

Appendix A. Mathematical concepts

A.3. Newton Raphson iterative scheme

Any equation $f(x) = 0$ can be solved iteratively using the Newton Raphson technique, as listed below:

Step 1: Assume an initial value of $x = x_0$

Step 2: Find $f(x)$ and $f'(x)$ at $x^{(k)}$, where k indicates the iteration index

Step 3: The next iteration value, $x^{(k+1)}$ is given by

$$x^{(k+1)} = x^{(k)} - \frac{f(x^{(k)})}{f'(x^{(k)})} \quad (\text{A.7})$$

Step 4: Repeat steps 2 and 3 till the error $\Delta x = x^{(k+1)} - x^{(k)}$, is within the specified limit

In SRF PLL, while quantizing the error, ω_n is solved for, using the Newton Raphson scheme. In this case, the function of interest is given by

$$f(\omega_n) = \frac{2e^{-\delta\omega_n t_0}}{\omega_n \sqrt{1-\delta^2}} \underbrace{\sqrt{\Delta\omega_{step}^2 + \phi^2\omega_n^2 - 2\Delta\omega_{step}\phi\omega_n\delta}}_K - E \quad (\text{A.8})$$

Differentiating with respect to ω_n ,

$$f'(\omega_n) = \frac{2e^{-\delta\omega_n t_0}}{K\omega_n^2 \sqrt{1-\delta^2}} g(\omega_n) \quad (\text{A.9})$$

where

$$g(\omega_n) = (-\phi^2\delta t_0)\omega_n^3 + (2\Delta\omega_{step}\phi\delta^2 t_0)\omega_n^2 + (-\Delta\omega_{step}^2\delta t_0 + \Delta\omega_{step}\phi\delta)\omega_n - \Delta\omega_{step}^2 \quad (\text{A.10})$$

ω_n can be iteratively found out using the Newton Raphson scheme as follows:

$$\omega_n^{(k+1)} = \omega_n^{(k)} - \frac{f(\omega_n^{(k)})}{f'(\omega_n^{(k)})} \quad (\text{A.11})$$

A.4. Bilinear Transformation (BLT)

BLT is a tool which transforms an analog filter to a digital infinite impulse response (IIR) filter. Consider a first order differential equation,

$$\frac{dy(t)}{dt} = w(t) \quad (\text{A.12})$$

Appendix A. Mathematical concepts

Taking Laplace transform, we obtain

$$sY(s) = W(s) \quad (\text{A.13})$$

$$\implies \frac{W(s)}{Y(s)} = s \quad (\text{A.14})$$

Let T_s denote the sampling period. In discrete domain, (A.12) becomes

$$\frac{y(nT_s) - y((n-1)T_s)}{T_s} = \frac{w(nT_s) + w((n-1)T_s)}{2} \quad (\text{A.15})$$

$$\implies y(nT_s) - y((n-1)T_s) = \frac{T_s}{2} [w(nT_s) + w((n-1)T_s)] \quad (\text{A.16})$$

Taking z-transform on both sides, we obtain

$$Y(z)(1 - z^{-1}) = \frac{T_s}{2} W(z)(1 + z^{-1}) \quad (\text{A.17})$$

$$\implies \frac{W(z)}{Y(z)} = \frac{2}{T_s} \left(\frac{1 - z^{-1}}{1 + z^{-1}} \right) \quad (\text{A.18})$$

Comparing (A.14) and (A.18), the required transformation is obtained as

$$s = \frac{2}{T_s} \left(\frac{1 - z^{-1}}{1 + z^{-1}} \right) \quad (\text{A.19})$$

Appendix B.

Hyperbolic functions

The hyperbolic sine and cosine functions are given by

$$\sinh x = \frac{e^x - e^{-x}}{2} \quad (\text{B.1})$$

$$\cosh x = \frac{e^x + e^{-x}}{2} \quad (\text{B.2})$$

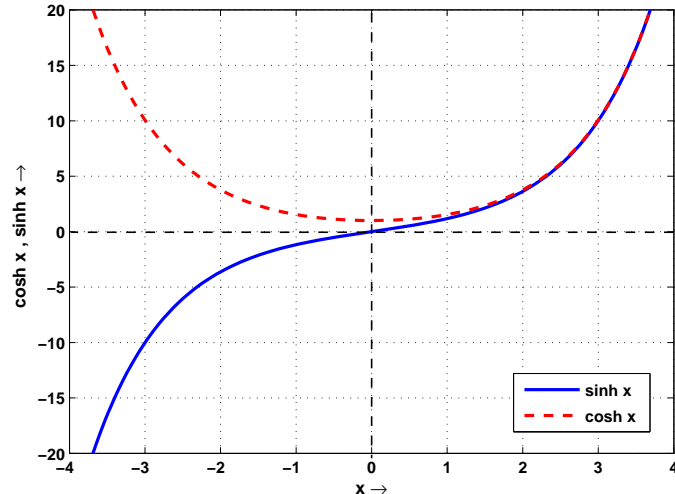


Figure B.1.: Hyperbolic sine and cosine functions

It can be noted from the plot in figure B.1 that

$$\sinh(-x) = -\sinh x \quad (\text{B.3})$$

$$\cosh(-x) = \cosh x \quad (\text{B.4})$$

B.1. Properties

A few other properties of hyperbolic sine and cosine functions that can also be deduced from the plot are

- (i) $\sinh x$ is an increasing function, $\forall x$ while $\cosh x$ has a point of minima at $x = 0$
- (ii) $\sinh x$ has a slope of 1 (45° with the x-axis) at $x = 0$
- (iii) $\cosh x$ has a slope of 0 at $x = 0$
- (iv) The rate of change of slope of $\sinh x$ changes from negative to positive at $x = 0$

Relation with trigonometric sine and cosine functions

Hyperbolic functions can be related to trigonometric functions as follows:

$$\sin(ix) = i \sinh x \quad (\text{B.5a})$$

$$\cos(ix) = \cosh x \quad (\text{B.5b})$$

where

$$i = \sqrt{-1}$$

B.2. Identities

$$\cosh^2 x - \sinh^2 x = 1 \quad (\text{B.6})$$

$$\sinh(x + y) = \sinh x \cosh y + \cosh x \sinh y \quad (\text{B.7})$$

$$\sinh(x - y) = \sinh x \cosh y - \cosh x \sinh y \quad (\text{B.8})$$

$$\cosh(x + y) = \cosh x \cosh y + \sinh x \sinh y \quad (\text{B.9})$$

$$\cosh(x - y) = \cosh x \cosh y - \sinh x \sinh y \quad (\text{B.10})$$

Proofs

We know

$$\sin(x + y) = \sin x \cos y + \cos x \sin y \quad (\text{B.11})$$

Appendix B. Hyperbolic functions

Replacing x by ix and y by iy ,

$$\sin(ix + iy) = \sin(ix)\cos(iy) + \cos(ix)\sin(iy) \quad (\text{B.12})$$

Using (B.5),

$$i\sinh(x + y) = i\sinh x \cosh y + i\cosh x \sinh y \quad (\text{B.13})$$

Hence proving

$$\sinh(x + y) = \sinh x \cosh y + \cosh x \sinh y \quad (\text{B.14})$$

On replacing y by $-y$,

$$\sinh(x - y) = \sinh x \cosh y - \cosh x \sinh y \quad (\text{B.15})$$

Now consider

$$\cos(ix + iy) = \cos(ix)\cos(iy) - \sin(ix)\sin(iy) \quad (\text{B.16})$$

Using (B.5),

$$\cosh(x + y) = \cosh x \cosh y - i^2 \sinh x \sinh y \quad (\text{B.17})$$

Hence proving

$$\cosh(x + y) = \cosh x \cosh y + \sinh x \sinh y \quad (\text{B.18})$$

On replacing y by $-y$,

$$\cosh(x - y) = \cosh x \cosh y - \sinh x \sinh y \quad (\text{B.19})$$

Substituting $x = y$,

$$\cosh(0) = \cosh^2 x - \sinh^2 x = 1 \quad (\text{B.20})$$

B.3. Inverse Hyperbolic Functions

$$\sinh^{-1} y = \log \left(y + \sqrt{y^2 + 1} \right) \quad (\text{B.21})$$

$$\cosh^{-1} y = \pm \log \left(y + \sqrt{y^2 - 1} \right) \quad (\text{B.22})$$

Appendix B. Hyperbolic functions

Proofs

Let

$$\sinh^{-1} y = x \quad (\text{B.23})$$

$$y = \sinh x \quad (\text{B.24})$$

$$y = \frac{e^x - e^{-x}}{2} \quad (\text{B.25})$$

$$2y = \frac{e^{2x} - 1}{e^x} \quad (\text{B.26})$$

$$e^{2x} - 2ye^x - 1 = 0 \quad (\text{B.27})$$

The roots of this equation are

$$e^x = y \pm \sqrt{y^2 + 1} \quad (\text{B.28})$$

Note that $y - \sqrt{y^2 + 1}$ is always negative. Hence

$$e^x = y - \sqrt{y^2 + 1} \quad (\text{B.29})$$

is not a valid root, as e^x cannot be negative.

Hence the only valid root is

$$e^x = y + \sqrt{y^2 + 1} \quad (\text{B.30})$$

i.e.,

$$x = \log \left(y + \sqrt{y^2 + 1} \right) \quad (\text{B.31})$$

Thus it is proved that

$$\sinh^{-1} y = \log \left(y + \sqrt{y^2 + 1} \right) \quad (\text{B.32})$$

Now consider

$$\cosh^{-1} y = x \quad (\text{B.33})$$

$$y = \cosh x \quad (\text{B.34})$$

$$y = \frac{e^x + e^{-x}}{2} \quad (\text{B.35})$$

$$2y = \frac{e^{2x} + 1}{e^x} \quad (\text{B.36})$$

$$e^{2x} - 2ye^x + 1 = 0 \quad (\text{B.37})$$

Appendix B. Hyperbolic functions

The roots of this equation are

$$e^x = y \pm \sqrt{y^2 - 1} \quad (\text{B.38})$$

The first root being

$$x = \log \left(y + \sqrt{y^2 - 1} \right) \quad (\text{B.39})$$

and the second root

$$x = \log \left(y - \sqrt{y^2 - 1} \right) \quad (\text{B.40})$$

$$= -\log \left(\frac{1}{y - \sqrt{y^2 - 1}} \right) \quad (\text{B.41})$$

$$= -\log \left(y + \sqrt{y^2 - 1} \right) \quad (\text{B.42})$$

Thus it is proved that

$$\cosh^{-1} y = \pm \log \left(y + \sqrt{y^2 - 1} \right) \quad (\text{B.43})$$

Appendix C.

Mathematical Simplifications

C.1. Section 2.1 Equation (2.4) to (2.5)

$$\begin{bmatrix} v_q \\ v_d \end{bmatrix} = \frac{2}{3} \begin{bmatrix} \cos \theta & \cos(\theta - \frac{2\pi}{3}) & \cos(\theta + \frac{2\pi}{3}) \\ \sin \theta & \sin(\theta - \frac{2\pi}{3}) & \sin(\theta + \frac{2\pi}{3}) \end{bmatrix} \begin{bmatrix} v_a \\ v_b \\ v_c \end{bmatrix} \quad (\text{C.1})$$

$$= \frac{2}{3} \begin{bmatrix} \cos \theta & \cos(\theta - \frac{2\pi}{3}) & \cos(\theta + \frac{2\pi}{3}) \\ \sin \theta & \sin(\theta - \frac{2\pi}{3}) & \sin(\theta + \frac{2\pi}{3}) \end{bmatrix} \begin{bmatrix} V_m \cos \theta_{ef} \\ V_m \cos(\theta_{ef} - \frac{2\pi}{3}) \\ V_m \cos(\theta_{ef} + \frac{2\pi}{3}) \end{bmatrix} \quad (\text{C.2})$$

Using the trigonometric identities

$$\cos A \cos B = \frac{1}{2} [\cos(A + B) + \cos(A - B)] \quad (\text{C.3})$$

$$\cos C + \cos D = 2 \cos \frac{C+D}{2} \cos \frac{C-D}{2} \quad (\text{C.4})$$

the q-component can simplified as

$$v_q = \frac{2}{3} V_m \left\{ \cos \theta \cos \theta_{ef} + \cos \left(\theta - \frac{2\pi}{3} \right) \cos \left(\theta_{ef} - \frac{2\pi}{3} \right) + \cos \left(\theta + \frac{2\pi}{3} \right) \cos \left(\theta_{ef} + \frac{2\pi}{3} \right) \right\} \quad (\text{C.5})$$

$$= \frac{1}{3} V_m \left\{ \cos(\theta + \theta_{ef}) + \cos \left(\theta + \theta_{ef} - \frac{4\pi}{3} \right) + \cos \left(\theta + \theta_{ef} + \frac{4\pi}{3} \right) + 3 \cos(\theta - \theta_{ef}) \right\} \quad (\text{C.6})$$

$$= \frac{1}{3} V_m \left\{ \cos(\theta + \theta_{ef}) - \cos(\theta + \theta_{ef}) + 3 \cos(\theta - \theta_{ef}) \right\} \quad (\text{C.7})$$

$$= V_m \cos(\theta - \theta_{ef}) \quad (\text{C.8})$$

Similarly, it can be shown that

$$v_d = -V_m \sin(\theta - \theta_{ef}) \quad (\text{C.9})$$

Appendix C. Mathematical Simplifications

C.2. Section 3.3 Equation (3.24) to (3.25)

When the Clarke transformation in (2.7) is applied to a n^{th} harmonic, we obtain

$$\begin{bmatrix} v_{\beta}^{+n} \\ v_{\alpha}^{+n} \end{bmatrix} = \frac{2}{3} V_m^{+n} \begin{bmatrix} 1 & -\frac{1}{2} & -\frac{1}{2} \\ 0 & -\frac{\sqrt{3}}{2} & \frac{\sqrt{3}}{2} \end{bmatrix} \begin{bmatrix} \cos(n\theta_{ef}) \\ \cos(n\theta_{ef} - \frac{2n\pi}{3}) \\ \cos(n\theta_{ef} + \frac{2n\pi}{3}) \end{bmatrix} \quad (\text{C.10})$$

Simplifying,

$$v_{\beta}^{+n} = \frac{2}{3} V_m^{+n} \left\{ \cos(n\theta_{ef}) - \frac{1}{2} \left[\cos\left(n\theta_{ef} - \frac{2n\pi}{3}\right) + \cos\left(n\theta_{ef} + \frac{2n\pi}{3}\right) \right] \right\} \quad (\text{C.11})$$

$$= \frac{2}{3} V_m^{+n} \left\{ \cos(n\theta_{ef}) - \frac{1}{2} \left[2 \cos(n\theta_{ef}) \cos\left(\frac{2n\pi}{3}\right) \right] \right\} \quad (\text{C.12})$$

$$= \frac{2}{3} V_m^{+n} \cos(n\theta_{ef}) \left\{ 1 - \cos\left(\frac{2n\pi}{3}\right) \right\} \quad (\text{C.13})$$

Similarly,

$$v_{\alpha}^{+n} = \frac{2}{3} V_m^{+n} \left\{ \frac{\sqrt{3}}{2} \left[\cos\left(n\theta_{ef} + \frac{2n\pi}{3}\right) - \cos\left(n\theta_{ef} - \frac{2n\pi}{3}\right) \right] \right\} \quad (\text{C.14})$$

$$= \frac{2}{3} V_m^{+n} \left\{ \frac{\sqrt{3}}{2} \left[-2 \sin(n\theta_{ef}) \sin\left(\frac{2n\pi}{3}\right) \right] \right\} \quad (\text{C.15})$$

$$= \frac{2}{3} V_m^{+n} \left\{ -\sqrt{3} \sin(n\theta_{ef}) \sin\left(\frac{2n\pi}{3}\right) \right\} \quad (\text{C.16})$$

Substituting $n = 1$, $n = 5$ and $n = 7$ in (C.13) and (C.16) yields

$$\begin{bmatrix} v_{\beta}^{+1} \\ v_{\alpha}^{+1} \end{bmatrix} = V_m^{+1} \begin{bmatrix} \cos \theta_{ef} \\ -\sin \theta_{ef} \end{bmatrix} \quad (\text{C.17})$$

$$\begin{bmatrix} v_{\beta}^{+5} \\ v_{\alpha}^{+5} \end{bmatrix} = V_m^{+5} \begin{bmatrix} \cos 5\theta_{ef} \\ +\sin 5\theta_{ef} \end{bmatrix} \quad (\text{C.18})$$

$$\begin{bmatrix} v_{\beta}^{+7} \\ v_{\alpha}^{+7} \end{bmatrix} = V_m^{+7} \begin{bmatrix} \cos 7\theta_{ef} \\ -\sin 7\theta_{ef} \end{bmatrix} \quad (\text{C.19})$$

C.3. Section 3.4.1.1 Equation (3.50) to (3.51)

$$\frac{dM}{d\omega} = 0 \quad (\text{C.20})$$

This would also mean

$$\frac{dM^2}{d\omega} = 0 \quad (\text{C.21})$$

Substituting for M from (3.39), we obtain

$$\frac{d}{d\omega} \left[\frac{\omega_n^4 + 4\delta^2\omega_n^2\omega^2}{(\omega_n^2 - \omega^2)^2 + 4\delta^2\omega_n^2\omega^2} \right] = 0 \quad (\text{C.22})$$

i.e.,

$$[(\omega_n^2 - \omega^2)^2 + 4\delta^2\omega_n^2\omega^2] [8\delta^2\omega_n^2\omega] - [\omega_n^4 + 4\delta^2\omega_n^2\omega^2] [4\omega^3 + 2\omega_n^2\omega(4\delta^2 - 2)] = 0 \quad (\text{C.23})$$

Expanding and simplifying yields

$$2\delta^2\omega^4 + \omega_n^2\omega^2 - \omega_n^4 = 0 \quad (\text{C.24})$$

Dividing throughout by ω_n and defining

$$p = \left(\frac{\omega}{\omega_n} \right)^2 \quad (\text{C.25})$$

(C.24) becomes

$$2\delta^2p^2 + p - 1 = 0 \quad (\text{C.26})$$

On solving,

$$p = \frac{-1 + \sqrt{1 + 8\delta^2}}{4\delta^2} \quad (\text{C.27})$$

Substituting for p from (C.25),

$$\frac{\omega}{\omega_n} = \left[\frac{-1 + \sqrt{1 + 8\delta^2}}{4\delta^2} \right]^{\frac{1}{2}} \quad (\text{C.28})$$

$$= \frac{1}{2\delta} \left[-1 + \sqrt{1 + 8\delta^2} \right]^{\frac{1}{2}} \quad (\text{C.29})$$

Hence the point of maxima is given by

$$\omega = \omega_{max} = \frac{\omega_n}{2\delta} \left[-1 + \sqrt{1 + 8\delta^2} \right]^{\frac{1}{2}} \quad (\text{C.30})$$

C.4. Section 4.1.2 Equation (4.79) to (4.80)

$$\frac{d}{dt} \left\{ \frac{e^{-\delta\omega_n t}}{\omega_u} \Delta\omega_{step} \sinh(\omega_u t) \right\} = 0 \quad (\text{C.31})$$

Hence

$$e^{-\delta\omega_n t} \omega_u \cosh(\omega_u t) + \sinh(\omega_u t) (-\delta\omega_n) e^{-\delta\omega_n t} = 0 \quad (\text{C.32})$$

Dropping the $e^{-\delta\omega_n t}$ term and substituting for ω_u from (4.58), we get

$$\omega_n \sqrt{\delta^2 - 1} \cosh(\omega_u t) - \delta\omega_n \sinh(\omega_u t) = 0 \quad (\text{C.33})$$

Using (4.67) and (4.68) and rearranging,

$$\cosh \gamma_u \sinh(\omega_u t) - \sinh \gamma_u \cosh(\omega_u t) = 0 \quad (\text{C.34})$$

Using the identity in (B.8), we obtain

$$\sinh(\omega_u t - \gamma_u) = 0 \quad (\text{C.35})$$

$$\omega_u t - \gamma_u = 0 \quad (\text{C.36})$$

Thus

$$t = t_{p1} = \frac{\gamma_u}{\omega_u} \quad (\text{C.37})$$

C.5. Section 4.1.3 Equation (4.103) to (4.104)

$$\frac{d}{dt} \left\{ \Delta\omega_{step} t e^{-\omega_n t} \right\} = 0 \quad (\text{C.38})$$

Implies

$$t e^{-\omega_n t} (-\omega_n) + e^{-\omega_n t} = 0 \quad (\text{C.39})$$

$$-\omega_n t + 1 = 0 \quad (\text{C.40})$$

Hence

$$t = t_{p2} = \frac{1}{\omega_n} \quad (\text{C.41})$$

C.6. Section 4.3.2 Equation (4.136) to (4.137)

$$\frac{dE_N}{d\delta} = 0 \quad (\text{C.42})$$

where

$$E_N = \frac{2 e^{-\delta\omega_n t_0}}{\omega_n \sqrt{1 - \delta^2}} \quad (\text{C.43})$$

Hence differentiating E_N with respect to δ ,

$$\frac{\omega_n \sqrt{1 - \delta^2} \left(-2 \omega_n t_0 e^{-\delta\omega_n t_0} \right) - 2 e^{-\delta\omega_n t_0} \left(\frac{-\delta\omega_n}{\sqrt{1 - \delta^2}} \right)}{\omega_n^2 (1 - \delta^2)} = 0 \quad (\text{C.44})$$

Upon simplification,

$$\omega_n \sqrt{1 - \delta^2} \left(-2 \omega_n t_0 e^{-\delta\omega_n t_0} \right) = 2 e^{-\delta\omega_n t_0} \left(\frac{-\delta\omega_n}{\sqrt{1 - \delta^2}} \right) \quad (\text{C.45})$$

$$\omega_n (1 - \delta^2) t_0 = \delta \quad (\text{C.46})$$

$$\omega_n t_0 \delta^2 + \delta - \omega_n t_0 = 0 \quad (\text{C.47})$$

Appendix D.

Error band as a function of Damping ratio

The error band at settling time t_0 , E is given by

$$E = \frac{2e^{-\delta\omega_n t_0}}{\omega_d} \sqrt{c_1 - 2c_2\delta} \quad (\text{D.1})$$

where

$$c_1 = \Delta\omega_{step}^2 + \phi^2\omega_n^2 \quad (\text{D.2})$$

$$c_2 = \Delta\omega_{step}\phi\omega_n \quad (\text{D.3})$$

$E'(\delta)$ is a good parameter to study the variation of error band E , with the damping ratio δ . Hence differentiating E partially with respect to δ yields

$$\frac{\partial E}{\partial \delta} = \frac{\partial}{\partial \delta} \left(\frac{2e^{-\delta\omega_n t_0}}{\omega_d} \sqrt{c_1 - 2c_2\delta} \right) \quad (\text{D.4})$$

$$= \frac{2}{\omega_n} \frac{\partial}{\partial \delta} \left(\frac{\sqrt{c_1 - 2c_2\delta}}{e^{\delta\omega_n t_0} \sqrt{1 - \delta^2}} \right) \quad (\text{D.5})$$

$$= \frac{2e^{-\delta\omega_n t_0}}{\omega_n (1 - \delta^2)^{\frac{3}{2}} \sqrt{c_1 - 2c_2\delta}} \left\{ -c_2(1 - \delta^2) - [\omega_n t_0(1 - \delta^2) - \delta] [c_1 - 2c_2\delta] \right\} \quad (\text{D.6})$$

$$= \frac{2e^{-\delta\omega_n t_0}}{\omega_n (1 - \delta^2)^{\frac{3}{2}} \sqrt{c_1 - 2c_2\delta}} \left\{ (-2\omega_n t_0 c_2)\delta^3 + (-c_2 + \omega_n t_0 c_1)\delta^2 + (c_1 + 2\omega_n t_0 c_2)\delta + (-c_2 - \omega_n t_0 c_1) \right\} \quad (\text{D.7})$$

Hence

$$E'(\delta) = \frac{2e^{-\delta\omega_n t_0}}{\omega_n (1 - \delta^2)^{\frac{3}{2}} \sqrt{c_1 - 2c_2\delta}} f(\delta) \quad (\text{D.8})$$

where

$$f(\delta) = (-2\omega_n t_0 c_2)\delta^3 + (-c_2 + \omega_n t_0 c_1)\delta^2 + (c_1 + 2\omega_n t_0 c_2)\delta + (-c_2 - \omega_n t_0 c_1) \quad (\text{D.9})$$

The following properties can be observed.

Appendix D. Error band as a function of Damping ratio

1. Substituting $\delta = 0$ in (D.8),

$$E'(0) = \frac{2}{\omega_n \sqrt{c_1}} \left[- (c_2 + \omega_n t_0 c_1) \right] \quad (\text{D.10})$$

2. The stationary points are given by $E'(\delta) = 0$. From (D.8), it is evident that $f(\delta) = 0$. i.e.,

$$(-2\omega_n t_0 c_2)\delta^3 + (-c_2 + \omega_n t_0 c_1)\delta^2 + (c_1 + 2\omega_n t_0 c_2)\delta + (-c_2 - \omega_n t_0 c_1) = 0 \quad (\text{D.11})$$

3. Substituting $\delta = 0$ in (D.9),

$$f(0) = -c_2 - \omega_n t_0 c_1 \quad (\text{D.12})$$

4. Substituting $\delta = 1$ in (D.9),

$$f(1) = -2\omega_n t_0 c_2 - c_2 + \omega_n t_0 c_1 + c_1 + 2\omega_n t_0 c_2 - c_2 - \omega_n t_0 c_1 \quad (\text{D.13})$$

$$= c_1 - 2c_2 \quad (\text{D.14})$$

5. Differentiating (D.9) with respect to δ , we get

$$f'(\delta) = 3(-2\omega_n t_0 c_2)\delta^2 + 2(-c_2 + \omega_n t_0 c_1)\delta + (c_1 + 2\omega_n t_0 c_2) \quad (\text{D.15})$$

6. Substituting $\delta = 0$ in (D.15),

$$f'(0) = c_1 + 2\omega_n t_0 c_2 \quad (\text{D.16})$$

7. Substituting $\delta = 1$ in (D.15),

$$f'(1) = -6\omega_n t_0 c_2 - 2c_2 + 2\omega_n t_0 c_1 + c_1 + 2\omega_n t_0 c_2 \quad (\text{D.17})$$

$$= c_1 - 2c_2 + 2\omega_n t_0(c_1 - 2c_2) \quad (\text{D.18})$$

$$= (c_1 - 2c_2)(1 + 2\omega_n t_0) \quad (\text{D.19})$$

Appendix E.

Nature of $f(\delta)$ in (0,1) when $E'(0) > 0$

The following points help in establishing the nature of $f(\delta)$ in (0,1) when $E'(0) > 0$:

1. $f(0) > 0$
2. $f(1) > 0$
3. $f'(0) > 0$
4. $f'(1) > 0$
5. None of the two stationary points of $f(\delta)$ lie in (0,1)

Combining these conditions, it can be said that $f(\delta)$ is an always increasing function in the interval (0,1) with no roots in this interval. The variation of $f(\delta)$ for $\omega_n = 100\pi \text{ rad s}^{-1}$, $\Delta\omega_{step} = 20\pi \text{ rad s}^{-1}$, $t_0 = 0.001 \text{ s}$ and $\phi = -0.1 \text{ rad}$ is shown in figure E.1.

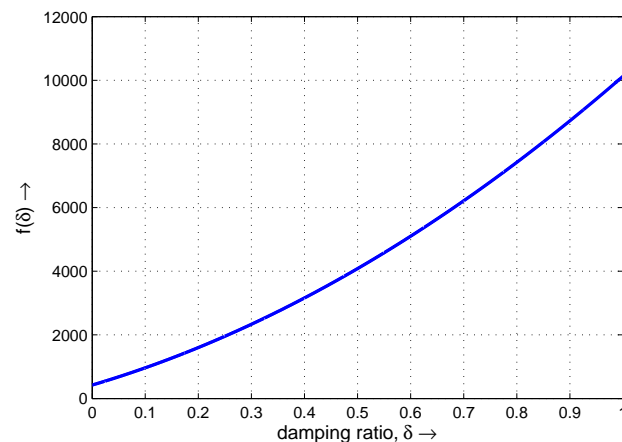


Figure E.1.: Variation of $f(\delta)$ with damping ratio in the interval [0, 1]

The above listed conditions are proved below.

From (D.12), we have

$$f(0) = -(c_2 + \omega_n t_0 c_1) \quad (\text{E.1})$$

Appendix E. Nature of $f(\delta)$ in (0,1) when $E'(\mathbf{0}) > \mathbf{0}$

Since $(c_2 + \omega_n t_0 c_1) < 0$ in this case,

$$f(0) > 0 \quad (\text{E.2})$$

which establishes point 1.

Moreover

$$f(1) = c_1 - 2c_2 \quad (\text{E.3})$$

$$\implies f(1) > 0 \quad (\text{E.4})$$

as $c_2 < 0$. This establishes point 2.

Also, from 4.199, we have

$$\omega_n t_0 < 1 \quad (\text{E.5})$$

$$\implies 2\omega_n t_0 c_2 > c_2 \quad (\text{E.6})$$

$$\implies c_1 + 2\omega_n t_0 c_2 > c_1 + c_2 \quad (\text{E.7})$$

But

$$c_1 + c_2 = \Delta\omega_{step}^2 + \phi^2 \omega_n^2 + \Delta\omega_{step} \phi \omega_n \quad (\text{E.8})$$

$$= \phi^2 \left[x^2 + x\omega_n + \omega_n^2 \right] \quad (\text{E.9})$$

$$= \underbrace{\phi^2 \left[\left(x + \frac{\omega_n}{2} \right)^2 + \frac{3\omega_n^2}{4} \right]}_{\text{always positive}} \quad (\text{E.10})$$

where

$$x = \frac{\Delta\omega_{step}}{\phi} \quad (\text{E.11})$$

Hence

$$c_1 + 2\omega_n t_0 c_2 > 0 \quad (\text{E.12})$$

Therefore from (D.16),

$$f'(0) > 0 \quad (\text{E.13})$$

which establishes point 3.

Since $c_1 - 2c_2 > 0$, from (D.19),

$$f'(1) = 0 \quad (\text{E.14})$$

which establishes point 4.

Appendix E. Nature of $f(\delta)$ in $(0,1)$ when $E'(\mathbf{0}) > \mathbf{0}$

The stationary points of $f(\delta)$ are given by

$$f'(\delta) = 0 \quad (\text{E.15})$$

i.e.,

$$\delta = \frac{\overbrace{-2(-c_2 + \omega_n t_0 c_1)}^{\text{-ve}} \pm \sqrt{4(-c_2 + \omega_n t_0 c_1)^2 + 24(\omega_n t_0 c_2)(c_1 + 2\omega_n t_0 c_2)}}{\underbrace{-6\omega_n t_0 c_2}_{\text{+ve}}} \quad (\text{E.16})$$

Clearly, one of the values of δ is negative (not lying in $(0,1)$). And since $f'(0) > 0$ and $f'(1) > 0$, the existence of one stationary point of $f(\delta)$ in $(0,1)$ is also ruled out. Hence there cannot be any stationary points in $(0,1)$, thus establishing point 5.

Appendix F.

Cardan's analytical method to solve Cubic equations

The general form of a cubic equation can be written as

$$ax^3 + bx^2 + cx + d = 0 \quad (\text{F.1})$$

where $a \neq 0$. Dividing throughout by a , we have

$$x^3 + lx^2 + mx + n = 0 \quad (\text{F.2})$$

where $l = \frac{b}{a}$, $m = \frac{c}{a}$ and $n = \frac{d}{a}$

On substituting

$$y = x + \frac{l}{3} \quad (\text{F.3})$$

we get

$$\left(y - \frac{l}{3}\right)^3 + l\left(y - \frac{l}{3}\right)^2 + m\left(y - \frac{l}{3}\right) + n = 0 \quad (\text{F.4})$$

Simplifying further,

$$y^3 + py + q = 0 \quad (\text{F.5})$$

where

$$p = m - \frac{l^2}{3} \quad (\text{F.6})$$

$$q = \frac{2l^3}{27} - \frac{lm}{3} + n \quad (\text{F.7})$$

Let

$$y = u + v \quad (\text{F.8})$$

$$\Rightarrow y^3 = (u + v)^3 \quad (\text{F.9})$$

$$\Rightarrow y^3 = u^3 + v^3 + 3uv(u + v) \quad (\text{F.10})$$

$$\Rightarrow y^3 = u^3 + v^3 + 3uvy \quad (\text{F.11})$$

Appendix F. Cardan's analytical method to solve Cubic equations

i.e.,

$$y^3 - 3uvy - (u^3 + v^3) = 0 \quad (\text{F.12})$$

Equation (F.5) and (F.12) are identical. On comparing their coefficients, we get

$$uv = -\frac{p}{3} \quad (\text{F.13})$$

$$u^3 + v^3 = -q \quad (\text{F.14})$$

On cubing (F.13), we obtain

$$u^3v^3 = -\frac{p^3}{27} \quad (\text{F.15})$$

Solving (F.14) and (F.15),

$$u^3 = \frac{-q + \sqrt{q^2 + \frac{4p^3}{27}}}{2} \quad (\text{F.16})$$

From (F.13)

$$v = -\frac{p}{3u} \quad (\text{F.17})$$

Defining

$$\lambda = \left[\frac{-q + \sqrt{q^2 + \frac{4p^3}{27}}}{2} \right]^{\frac{1}{3}} \quad (\text{F.18})$$

the roots of (F.16) are given by

$$u = \left\{ \lambda, \lambda\omega, \lambda\omega^2 \right\} \quad (\text{F.19})$$

where

$$\omega = e^{j\frac{2\pi}{3}} = \frac{-1 + \sqrt{3}j}{2} \quad (\text{F.20})$$

$$\omega^2 = e^{-j\frac{2\pi}{3}} = \frac{-1 - \sqrt{3}j}{2} \quad (\text{F.21})$$

Substituting (F.19) in (F.17),

$$v = \left\{ -\frac{p}{3\lambda}, -\frac{p}{3\lambda\omega}, -\frac{p}{3\lambda\omega^2} \right\} \quad (\text{F.22})$$

Hence from (F.8),

$$y = \left\{ \left(\lambda - \frac{p}{3\lambda} \right), \left(\lambda\omega - \frac{p}{3\lambda\omega} \right), \left(\lambda\omega^2 - \frac{p}{3\lambda\omega^2} \right) \right\} \quad (\text{F.23})$$

Appendix F. Cardan's analytical method to solve Cubic equations

Therefore, from (F.3), the roots of any general cubic equation are given by

$$x = \left\{ \left(\lambda - \frac{p}{3\lambda} - \frac{l}{3} \right), \left(\lambda\omega - \frac{p}{3\lambda\omega} - \frac{l}{3} \right), \left(\lambda\omega^2 - \frac{p}{3\lambda\omega^2} - \frac{l}{3} \right) \right\} \quad (\text{F.24})$$

So far, the Cardan's analytical technique is explained for obtaining the roots of a cubic equation. However, it is of interest to know if all the three roots of the cubic equation in (4.151) are real or only one of them turns out to be real. The following two cases illustrate this aspect.

Case 1: Only one root is real

Only one real root turns up if $\left(q^2 + \frac{4p^3}{27} \right) > 0$. This is because

$$\lambda = \left[\frac{-q + \sqrt{q^2 + \frac{4p^3}{27}}}{2} \right]^{\frac{1}{3}} \quad \text{is real.} \quad (\text{F.25})$$

Hence $x = \left(\lambda - \frac{p}{3\lambda} - \frac{l}{3} \right)$ corresponds to the real root of the cubic equation.

To sum up, if $\left(q^2 + \frac{4p^3}{27} \right) > 0$, then

(i) Only one real root exists

(ii) This real root is given by

$$x = \left(\lambda - \frac{p}{3\lambda} - \frac{l}{3} \right) \quad (\text{F.26})$$

where

$$\lambda = \left[\frac{-q + \sqrt{q^2 + \frac{4p^3}{27}}}{2} \right]^{\frac{1}{3}} \quad (\text{F.27})$$

Case 2: All roots are real

All roots are real if $\left(q^2 + \frac{4p^3}{27} \right) \leq 0$. This is proved as follows:

Appendix F. Cardan's analytical method to solve Cubic equations

1. If $\left(q^2 + \frac{4p^3}{27}\right) < 0$

Let

$$\lambda^3 = \frac{-q + \sqrt{q^2 + \frac{4p^3}{27}}}{2} \quad (\text{F.28})$$

Defining

$$jX = \sqrt{q^2 + \frac{4p^3}{27}} \quad (\text{F.29})$$

we get

$$\lambda = re^{j\theta} = \left(\frac{-q + jX}{2}\right)^{\frac{1}{3}} \quad (\text{F.30})$$

The magnitude of λ is given by

$$r = \left(\frac{q^2 + X^2}{4}\right)^{\frac{1}{6}} \quad (\text{F.31})$$

$$= \left(\frac{q^2 - \left[q^2 + \frac{4p^3}{27}\right]}{4}\right)^{\frac{1}{6}} \quad (\text{F.32})$$

$$= \left(\frac{-p}{3}\right)^{\frac{1}{2}} \quad (\text{F.33})$$

The phase angle of λ is given as

$$\theta = \frac{1}{3} \tan^{-1} \left(\frac{X}{-q} \right) \quad (\text{F.34})$$

Consider the first root of the set in (F.24). i.e.,

$$x_1 = \lambda - \frac{p}{3\lambda} - \frac{l}{3} \quad (\text{F.35})$$

$$= re^{j\theta} + \left(\frac{-p}{3}\right) \frac{1}{re^{j\theta}} - \frac{l}{3} \quad (\text{F.36})$$

Appendix F. Cardan's analytical method to solve Cubic equations

Substituting for $\frac{-p}{3}$ from (F.33),

$$x_1 = re^{j\theta} + r^2 \frac{1}{re^{j\theta}} - \frac{l}{3} \quad (\text{F.37})$$

$$= r \left(e^{j\theta} + e^{-j\theta} \right) - \frac{l}{3} \quad (\text{F.38})$$

$$= 2r \cos \theta - \frac{l}{3} \quad \text{which is real.} \quad (\text{F.39})$$

Consider the second root of the set in (F.24). i.e.,

$$x_2 = \lambda\omega - \frac{p}{3\lambda\omega} - \frac{l}{3} \quad (\text{F.40})$$

Substituting $\lambda = re^{j\theta}$ and $\omega = e^{j\frac{2\pi}{3}}$,

$$x_2 = re^{j(\theta+\frac{2\pi}{3})} + \left(\frac{-p}{3} \right) \frac{1}{re^{j(\theta+\frac{2\pi}{3})}} - \frac{l}{3} \quad (\text{F.41})$$

Substituting for $\frac{-p}{3}$ from (F.33),

$$x_2 = re^{j(\theta+\frac{2\pi}{3})} + r^2 \frac{1}{re^{j(\theta+\frac{2\pi}{3})}} - \frac{l}{3} \quad (\text{F.42})$$

$$= r \left[e^{j(\theta+\frac{2\pi}{3})} + e^{-j(\theta+\frac{2\pi}{3})} \right] - \frac{l}{3} \quad (\text{F.43})$$

$$= 2r \cos \left(\theta + \frac{2\pi}{3} \right) - \frac{l}{3} \quad \text{which is also real.} \quad (\text{F.44})$$

Similarly, the third root of the set in (F.24) is given by

$$x_3 = 2r \cos \left(\theta - \frac{2\pi}{3} \right) - \frac{l}{3} \quad \text{which is again real.} \quad (\text{F.45})$$

To sum up, if $\left(q^2 + \frac{4p^3}{27} \right) < 0$, then

(i) All roots are real

(ii) The roots are given by the set

$$x = \left\{ \left(2r \cos \theta - \frac{l}{3} \right), \left(2r \cos \left(\theta + \frac{2\pi}{3} \right) - \frac{l}{3} \right), \left(2r \cos \left(\theta - \frac{2\pi}{3} \right) - \frac{l}{3} \right) \right\} \quad (\text{F.46})$$

Appendix F. Cardan's analytical method to solve Cubic equations

where

$$r = \left(\frac{-p}{3} \right)^{\frac{1}{2}} \quad (\text{F.47})$$

$$\theta = \frac{1}{3} \tan^{-1} \left(\frac{X}{-q} \right) \quad (\text{F.48})$$

2. If $\left(q^2 + \frac{4p^3}{27} \right) = 0$

Equation (F.18) becomes

$$\lambda = \left(\frac{-q}{2} \right)^{\frac{1}{3}} \quad (\text{F.49})$$

Moreover

$$q^2 + \frac{4p^3}{27} = 0 \quad (\text{F.50})$$

implies

$$p = -3 \left(\frac{-q}{2} \right)^{\frac{2}{3}} \quad (\text{F.51})$$

Substituting for $\frac{-q}{2}$ from (F.49),

$$p = -3\lambda^2 \quad (\text{F.52})$$

Hence the first root of the set in (F.24) becomes

$$x_1 = \lambda - \frac{p}{3\lambda} - \frac{l}{3} \quad (\text{F.53})$$

$$= \lambda + \frac{3\lambda^2}{3\lambda} - \frac{l}{3} \quad (\text{F.54})$$

$$= 2\lambda - \frac{l}{3} \quad (\text{F.55})$$

Appendix F. Cardan's analytical method to solve Cubic equations

Consider the second root of the set in (F.24). i.e.,

$$x_2 = \lambda\omega - \frac{p}{3\lambda\omega} - \frac{l}{3} \quad (\text{F.56})$$

$$= \lambda\omega + \frac{3\lambda^2}{3\lambda\omega} - \frac{l}{3} \quad (\text{F.57})$$

$$= \lambda(\omega + \omega^2) - \frac{l}{3} \quad (\text{F.58})$$

$$= -\lambda - \frac{l}{3} \quad (\text{F.59})$$

(using the property $\frac{1}{\omega} = \omega^2$ and $1 + \omega + \omega^2 = 0$)

Similarly, the third root of the set in (F.24) is given by

$$x_3 = -\lambda - \frac{l}{3} \quad \text{which is same as } x_2. \quad (\text{F.60})$$

To sum up, if $\left(q^2 + \frac{4p^3}{27}\right) = 0$, then

(i) All roots are real with two repeated roots

(ii) The roots are given by the set

$$x = \left\{ \left(2\lambda - \frac{l}{3}\right), \left(-\lambda - \frac{l}{3}\right), \left(-\lambda - \frac{l}{3}\right) \right\} \quad (\text{F.61})$$

where

$$\lambda = \left(\frac{-q}{2}\right)^{\frac{1}{3}} = \left(\frac{-p}{3}\right)^{\frac{1}{2}} \quad (\text{F.62})$$

The condition for the existence of one real root or three real roots of (4.151) can be arrived at, through calculus also (however the roots cannot be found by this method).

Let

$$f(y) = y^3 + py + q = 0 \quad (\text{F.63})$$

It can be seen that

$$\lim_{y \rightarrow -\infty} f(y) = -\infty \quad (\text{F.64})$$

$$\lim_{y \rightarrow \infty} f(y) = +\infty \quad (\text{F.65})$$

Appendix F. Cardan's analytical method to solve Cubic equations

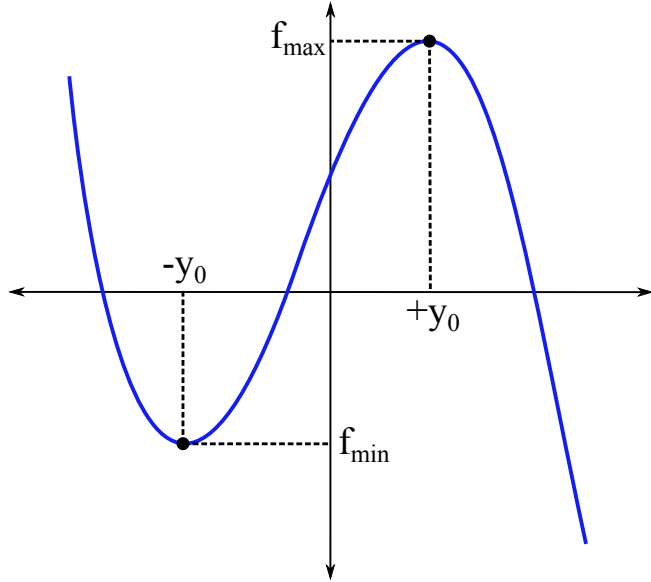


Figure F.1.: A cubic function $f(y)$ with three real roots

When three real roots exist, a rough sketch of $f(y)$ looks as shown in figure F.1

The stationary points are given by

$$f'(y) = 0 \quad (\text{F.66})$$

$$\implies 3y^2 + p = 0 \quad (\text{F.67})$$

i.e.,

$$y = \pm \sqrt{\frac{-p}{3}} = \pm y_0 \quad (\text{say}) \quad (\text{F.68})$$

For existence of three real roots, the stationary points in (F.68), should be real. i.e.,

$$p < 0 \quad (\text{F.69})$$

Moreover, for the existence of three real roots, it is mandatory that the maxima and minima lie as shown in figure F.1. i.e.,

$$f_{\min} f_{\max} < 0 \quad (\text{F.70})$$

$$\implies (-y_0^3 - py_0 + q)(y_0^3 + py_0 + q) < 0 \quad (\text{F.71})$$

$$\implies (y_0^3 + py_0)^2 - q^2 > 0 \quad (\text{F.72})$$

$$\implies y_0^2(y_0^2 + p)^2 - q^2 > 0 \quad (\text{F.73})$$

Appendix F. Cardan's analytical method to solve Cubic equations

Substituting for y_0^2 from (F.68) and simplifying, we obtain

$$q^2 + \frac{4p^3}{27} < 0 \quad (\text{F.74})$$

Conditions (F.69) and (F.74) are thus necessary for the existence of three real roots. However, (F.69) is absorbed in (F.74). Therefore (F.74) becomes the necessary and sufficient condition for three real roots to exist.

Appendix G.

Errata

Page 70. Change table 4.4 to this one:

Possibility	Inference
1. All real roots fall in $[0, 1]$	This statement is disproved through contradiction. It is impossible to have all real roots in $[0, 1]$.
2. $E'(0) < 0$ (or $c_2 + c_1\omega_n t_0 > 0$)	<p>(i) $c_1 - 2c_2 \neq 0$ The error band has a negative slope at $\delta = 0$ and $E \rightarrow \infty$ as $\delta \rightarrow 1$. This leaves the possibility of only one stationary point in $[0, 1]$; Only one real root in $[0, 1]$ of Cardan's 3 real roots.</p> <p>(ii) $c_1 - 2c_2 = 0$ The error band has a negative slope at $\delta = 0$ and E is finite as $\delta \rightarrow 1$. Also, E is a decreasing function in $[0, 1]$, thus eliminating the possibility of any stationary point in $[0, 1]$; No real root in $[0, 1]$. Choose optimum $\delta = 0.999$ i.e., $\delta \rightarrow 1$</p>
3. $E'(0) \geq 0$ (or $c_2 + c_1\omega_n t_0 \leq 0$)	The error band has a positive slope at $\delta = 0$ and $E \rightarrow \infty$ as $\delta \rightarrow 1$. Also, E is an increasing function in $[0, 1]$, thus eliminating the possibility of any stationary point in $[0, 1]$; No real root in $[0, 1]$. Choose optimum $\delta = 0$

Table G.1.: Choice of an optimum damping ratio, δ

Page 71. Before: The value of ω_n obtained in step 3 is fed to step 4 and the process is repeated till a unique (δ, ω_n) is obtained.

After: The value of ω_n obtained in step 3 is fed to step 2 and the process is repeated till a unique (δ, ω_n) is obtained.

Page 72. Add this point to the theoretical perspective: When $c_1 - 2c_2 = 0$, $\delta = 1$ is optimum. From section 4.4.1.3.3, this happens only when $c_2 > 0$. i.e., when both $\Delta\omega_{step}$ and ϕ are of the same polarity. This can be seen from the peaks of δ in the 3D lookup table in

Appendix G. Errata

figure 4.18, which only occur in the 1st and 3rd quadrant.

- Page 72. Append this to the first point (Symmetry about origin): This can also be corroborated from the sign of c_2 in (4.205). While c_1 is polarity independent, c_2 is not.
- Page 72. Append this to the third point under theoretical perspective: The mountain-like profile denotes regions of lower strain and the valley-like profile shows regions of higher strain, in terms of the physical realization of the loop filter. Interestingly, this is governed by (4.205). The error band E is always less when c_2 is positive, which is the case when both frequency excursion and phase jump are positive, or when both are negative.
- Page 75. Add this as a design note (footnote): While designing for δ and ω_n , only consider the magnitude of maximum permissible frequency step and maximum permissible phase jump, as inputs from the designer. But the design needs to be done with respect to the worst combination of $\Delta\omega_{step}$ and ϕ , which is when both are of opposite polarities. Hence in all cases, when the instantaneous $\Delta\omega_{step}$ and ϕ occurring in the grid are of the same polarity, the design would suppress the error band to much less than for the case when they are of the opposite polarity. Further, since the design is now made for the worst-case, error would always be limited within the specification for any combination of instantaneous $\Delta\omega_{step}$ and ϕ within the specified maxima.

Page 104. Missing closing bracket ')' in footnote.

Sambhav R Jain



Pradhyumna Ravikirthi

